



HAL
open science

Hydrogen production from steam reforming of ethanol over an Ir/ceria-based catalyst : catalyst ageing analysis and performance improvement upon ceria doping

Fagen Wang

► **To cite this version:**

Fagen Wang. Hydrogen production from steam reforming of ethanol over an Ir/ceria-based catalyst : catalyst ageing analysis and performance improvement upon ceria doping. Other. Université Claude Bernard - Lyon I; Dalian Institute of Chemical Physics, Chinese academy of sciences, 2012. English. NNT : 2012LYO10188 . tel-00967128

HAL Id: tel-00967128

<https://theses.hal.science/tel-00967128>

Submitted on 25 Nov 2014

HAL is a multi-disciplinary open access archive for the deposit and dissemination of scientific research documents, whether they are published or not. The documents may come from teaching and research institutions in France or abroad, or from public or private research centers.

L'archive ouverte pluridisciplinaire **HAL**, est destinée au dépôt et à la diffusion de documents scientifiques de niveau recherche, publiés ou non, émanant des établissements d'enseignement et de recherche français ou étrangers, des laboratoires publics ou privés.

N° d'ordre: 188-2012

Année :2012

THESE

présentée devant

l'UNIVERSITE CLAUDE BERNARD-LYON1

Spécialité : Chimie-Catalyse

pour l'obtention du

DIPLOME DE DOCTORAT EN CO-TUTELLE

(Arrêté du 01 Octobre 2008)

avec l'Institut de Chimie Physique de Dalian

Académie Chinoise des Sciences

Présentée et soutenue publiquement le 23 Octobre 2012 par

Fagen WANG

TITRE

**Hydrogen production from steam reforming of ethanol over an
Ir/ceria-based catalyst: catalyst ageing analysis and performance
improvement upon ceria doping**

Directeurs de thèse:

Claude MIRODATOS et Wenjie SHEN

JURY :

M. Jean-Marc CLACENS (rapporteur)

M. Claude DESCORME

M. Claude MIRODATOS

Mme Hélène PROVENDIER

M. Wenjie SHEN

M. Yujiang SONG

M. Anjie WANG (rapporteur)

Mme Anne-Cécile ROGER (rapporteur)

Contents

Contents.....	2
Chapter I Introduction and literature survey.....	1
I.1. Importance of hydrogen production	1
1.1.1. Overviews of hydrogen production technologies	1
1.1.2. Advantages of hydrogen from bio-ethanol.....	6
I.2. Catalysts for hydrogen from steam reforming of ethanol.....	7
I.2.1. Oxide catalysts.....	8
I.2.2. Supported metal catalysts	10
I.2.3. Concluding remarks on catalyst formulations	16
I.3. Mechanistic aspects of the steam reforming of ethanol.....	17
I.3.1. Thermodynamic studies.....	17
I.3.2. Reaction pathways.....	18
I.3.3. TPD and infrared investigations.....	22
I.3.4. Kinetic studies	24
I.4. Catalyst deactivation investigations	25
I.4.1. Deactivation studies over Ni and Co catalysts	27
I.4.2. Deactivation studies over noble metal catalysts.....	28
I.5. Objectives of the present thesis	30
References	32
Chapter II Experimental: catalysts preparation and characterization techniques.....	37
II.1. Catalysts preparation.....	37
II.1.1. Preparation of the 2 wt.% Ir/CeO ₂ catalyst.....	37
II.1.2. Preparation of the 2 wt.% Ir/Ce _{0.9} Pr _{0.1} O ₂ catalyst.....	38

II.1.3.	Preparation of the 2 wt.% Ir/CeO ₂ -nanorods catalyst.....	38
II.2.	Catalytic measurements and set-ups	38
II.2.1.	Catalytic performance	38
II.2.2.	Calculations	39
II.2.3.	Kinetic experiments.....	40
II.3.	Catalyst characterizations	42
II.3.1.	Chemical analysis (ICP).....	42
II.3.2.	Specific surface area (BET).....	42
II.3.3.	X-ray diffraction (XRD).....	42
II.3.4.	X-ray photoelectron spectroscopy (XPS).....	43
II.3.5.	Raman spectra	43
II.3.6.	Temperature-programmed reduction (TPR).....	43
II.3.7.	Oxygen storage capacity (OSC).....	43
II.3.8.	Hydrogen chemisorption	44
II.3.9.	Temperature-programmed desorption of oxygen (O ₂ -TPD)	44
II.3.10.	Temperature-programmed oxidation (TPO) on aged catalysts.....	45
II.3.11.	Transmission electron microscopy (TEM).....	45
	References	46
Chapter III Kinetic studies of steam reforming of ethanol over an Ir/CeO₂ catalyst		47
III.1.	Introduction	47
III.2.	Preliminary kinetic investigation of steam reforming of ethanol.....	48
III.2.1.	Gas phase mass transfer resistance.....	48
III.2.2.	Intra-particle mass transfer resistance	49
III.2.3.	Temperature gradient of the catalyst bed	49

III.2.4. Time on stream study	50
III.3. Influence of reaction conditions on the kinetics.....	51
III.3.1. Effects of temperature and space velocity.....	51
III.3.2. Effect of water/ethanol (S/E) molar ratio	54
III.3.3. Effect of the partial pressure of the products.....	55
III.4. Kinetic modelling.....	57
III.5. Summary	59
References	61
Chapter IV Ageing analysis of a model Ir/CeO₂ catalyst in steam reforming of ethanol	63
IV.1. Physical and chemical properties of the model Ir/CeO ₂ catalyst	65
IV.1.1. BET specific surface area characterization	65
IV.1.2. XRD characterization	65
IV.1.3. HRTEM characterization.....	66
IV.1.4. H ₂ -TPR characterization.....	67
IV.2. Ageing analysis under steam reforming of ethanol conditions	68
IV.2.1. Catalytic performance and ageing tests.....	69
IV.2.2. Origin of the ageing phenomena	80
IV.3. Summary	83
References	85
Chapter V Enhancing catalyst performance by PrO_x-doping in an Ir/Ce_{0.9}Pr_{0.1}O₂ system	88
.....	
V.1. Physical and chemical properties of the oxide supports and of the catalysts	89
V.1.1. The oxide supports characterizations	89
V.1.2. The Ir catalysts characterizations	92
V.2. Catalytic performances and stability of the Ir/CeO ₂ and Ir/Ce _{0.9} Pr _{0.1} O ₂ catalysts	97

V.2.1.	Catalytic performances of the Ir/CeO ₂ and Ir/Ce _{0.9} Pr _{0.1} O ₂ catalysts.....	97
V.2.2.	Stability tests of the Ir/CeO ₂ and Ir/Ce _{0.9} Pr _{0.1} O ₂ catalysts	99
V.3.	Characterization of the aged Ir/CeO ₂ and Ir/Ce _{0.9} Pr _{0.1} O ₂ catalysts	101
V.3.1.	OSC of the aged catalysts.....	101
V.3.2.	XRD of the aged catalysts	101
V.3.3.	Temperature-programmed oxidation (TPO).....	102
V.3.4.	High Resolution Transmission Electron Microscopy (HRTEM)	104
V.4.	Summary.....	106
	References	107
Chapter VI Influence of CeO₂ shape and structure on Ir/CeO₂ catalyst for hydrogen production from steam reforming of ethanol.....		110
VI.1.	Physical and chemical properties of the fresh nanomaterials (supports) and the catalysts (after Ir loading).....	112
VI.2.	Steam reforming of ethanol over the nano-shaped Ir/CeO ₂ catalysts.....	116
VI.2.1.	Effects of reaction temperature.....	116
VI.2.2.	Origin of the differences in activity and product selectivity for ethanol steam reforming between the Ir/CeO ₂ nano-shaped catalysts.....	118
VI.3.	Summary	119
	References	120
Chapter VII General conclusions and perspectives		124
Chapter VIII Hydrogen production from steam reforming of ethanol over Ni and Ni-Cu catalysts		132
VIII.1.	Experimental.....	133
VIII.1.1.	Catalyst preparation.....	133
VIII.1.2.	Catalyst characterization	134

VIII.1.3. Catalytic evaluation.....	135
VIII.2. Results and discussion.....	135
VIII.2.1. Physical and chemical properties of the Ni catalysts.....	135
VIII.2.2. Steam reforming of ethanol.....	138
VIII.2.3. Ageing analysis.....	140
VIII.3. Summary.....	145
References.....	146
List of Publications.....	148
Acknowledgements.....	151

Chapter I Introduction and literature survey

1.1. Importance of hydrogen production

Within the frame of limited fossil energy and environmental concerns, clean and renewable energy is worldwide concerned for its sustainability. Solar, wind, and hydro energies are promising renewable resources but generally site-specific, intermittent and thus not steadily available to meet the entire economy. Hydrogen, as an energy carrier and a strategic feedstock in chemical industries and refineries, has been identified as an ideal sustainable resource for a near future. The worldwide hydrogen production has been estimated to be about 12 trillion standard cubic feet (SCF)/year, including about 1.7 trillion SCF/year of merchant hydrogen [1].

Hydrogen has a very high energy density. 1 kg of hydrogen contains the same amount of energy as 2.6 kg of natural gas or 3.1 kg of gasoline. This makes it a potential fuel for electronic industry, engine and other H₂-demanding application fields. In chemical industry, hydrogen is consumed for the synthesis of ammonia and methanol. It is also used in refineries for upgrading crude oils, by hydro-cracking and hydro-treating to produce gasoline and diesel for engines and machines. Processing of heavier and sulfur-containing crude oils also requires large amounts of hydrogen. Within the perspective of non nuclear and/or non fossil based electricity generation, hydrogen fuel cells, either for industrial or even more for domestic applications, are also attracting considerable attention due to the potential advantages of their efficiency and to the expected environmental benefits. As a result, the development of science and technology for hydrogen production at various scales and places remains a major challenge in the near future for more efficient chemical processing and other applications.

1.1.1. Overviews of hydrogen production technologies

Hydrogen can be produced from a variety of feedstocks, including fossil fuels such as natural gas, oil, and coal and renewable sources like biomass. Nearly 50% of the hydrogen produced worldwide is derived from natural gas, primarily by steam reforming, as shown in

Figure I-1. The remaining hydrogen is produced from oil (30%), coal (19%) and water electrolysis (4%).

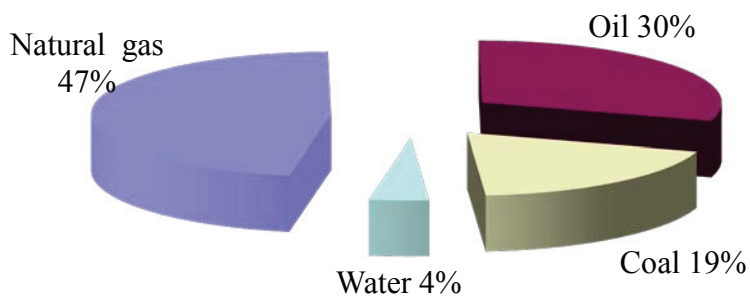


Figure I-1 Feedstock contributions to hydrogen production [2].

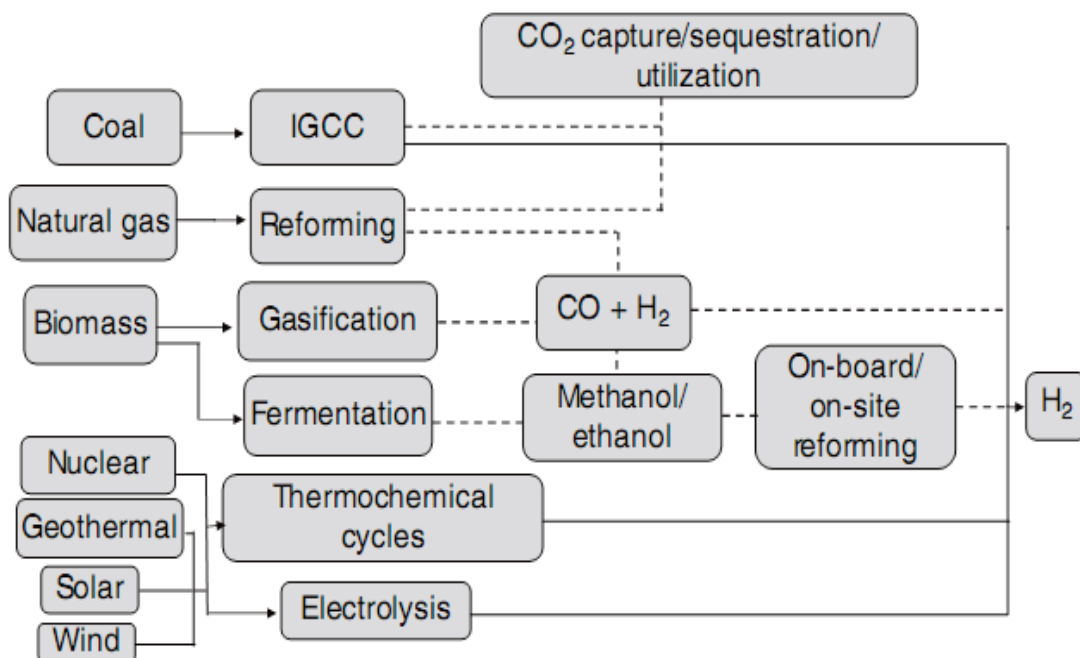


Figure I-2 Technological options for the production of hydrogen from various carbon - containing or carbon-free feedstocks [3]. (IGCC is Integrated Gasification Combined Cycle).

Figure I-2 shows the general options of technologies for hydrogen production from various hydrogen-containing feedstocks. Fossil and renewable feedstocks would undergo a reforming (natural gas) or gasification (biomass) process to produce syngas, respectively. The latter can

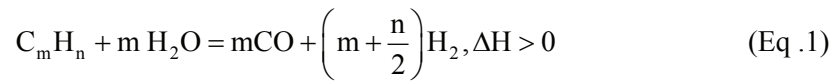
be used to synthesize liquid fuels by F-T synthesis or by a downstream treatment such as water gas shift reaction (WGS), eventually followed by a CO preferential oxidation to produce high purity hydrogen. Hydrogen could be produced directly from water, the most abundant source of hydrogen in the world, by electrolysis, thermochemical cycles or photocatalytic splitting, although this process is in the early stage of laboratory research.

In the following, the main hydrogen production technologies will be introduced and compared in details.

1.1.1.1. Hydrocarbon reforming

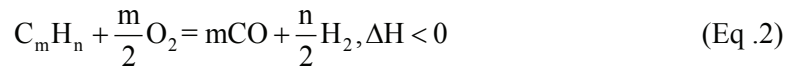
Three primary techniques can be applied to produce hydrogen from hydrocarbons: steam reforming (SR), partial oxidation (POX), and autothermal reforming (ATR).

Steam reforming is the most studied and used in industry since it has the highest hydrogen yield [4-7], and a H₂/CO ratio of about 3/1 would be produced. The steam reforming of hydrocarbon can be represented as:



Being an endothermic reaction, it requires external heat supply, especially when the molar ratio of water/hydrocarbon is high. Moreover, formation of coke (graphite, filament-like) or accumulation of by-products like acetaldehyde and acetone might lead to catalyst deactivation.

Partial oxidation (POX) which converts hydrocarbons to hydrogen in the presence of oxygen can be represented as:



This process is exothermic depending on the amount of oxygen added and does not require any external heat supply. Consequently, POX systems allow a fast start up and have short response time, which make them attractive for applications involving frequent transient operations. The POX reactor is more compact than the steam reformer, since it does not need heat exchangers. The produced H₂/CO ratio is in the range of 1/1 to 2/1, and the concentration of CH₄ is lower than that for steam reforming due to the combustion of methane with oxygen.

Although the coke formation is much less favoured than that in the SR process, the catalyst deactivation may occur as well because of hot-spots that induce active phase sintering [8].

Autothermal reforming combines POX to provide heat and SR to increase the hydrogen production. By feeding hydrocarbon, water and oxygen in a proper ratio, the overall reaction can be operated in close to thermo neutral state. Although external heat supply is not needed, an expensive and complex oxygen separation unit is required in order to feed pure oxygen to the reactor to avoid the produced gas to be diluted in nitrogen. H₂/CO ratio by ATR is about 2/1 to 3/1, which is less than SR, and the concentration of methane is lower. The catalyst would also be deactivated due to the oxygen addition favouring sintering, without fully discarding coke formation [8]. The ATR process can be depicted as:

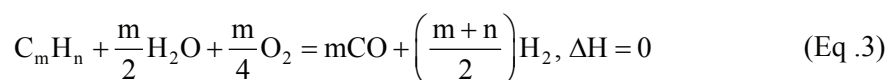


Table I-1 compares advantages and disadvantages of the above three reforming technologies.

Table I-1 Comparison of reforming technologies [9, 10].

Technology	Advantages	Disadvantages
Steam reforming	Most extensive industrial experiences	Highest air emissions
	Oxygen not required	Higher methane concentration
	Highest H ₂ concentration	Most coke formation
Partial oxidation	Low methane concentration	Low H ₂ /CO ratio
	Short response time	Soot formation
	Fast start up	Active phase sintering
Autothermal reforming	Lower process temperature	Limited commercial experience
	Low methane concentration	Requires air or oxygen
	No external heat supply	Deactivation still possible

1.1.1.2. Gasification

The second major route for hydrogen production involves gasification processes, as depicted in Figure I-3, which can be either proven technologies like coal gasification or still under development sustainable technology such as biomass gasification. They require high temperatures from 1073 to 1273 K. The feedstocks are converted in the gasifier with steam

and/or oxygen to produce syngas. Depending on the gasification employed, H_2O , CO_2 and CH_4 can be present in the syngas, as well as trace components such as tars, oils and phenolics. After the raw syngas is cleaned up, the WGS reaction is applied for hydrogen enrichment [11].

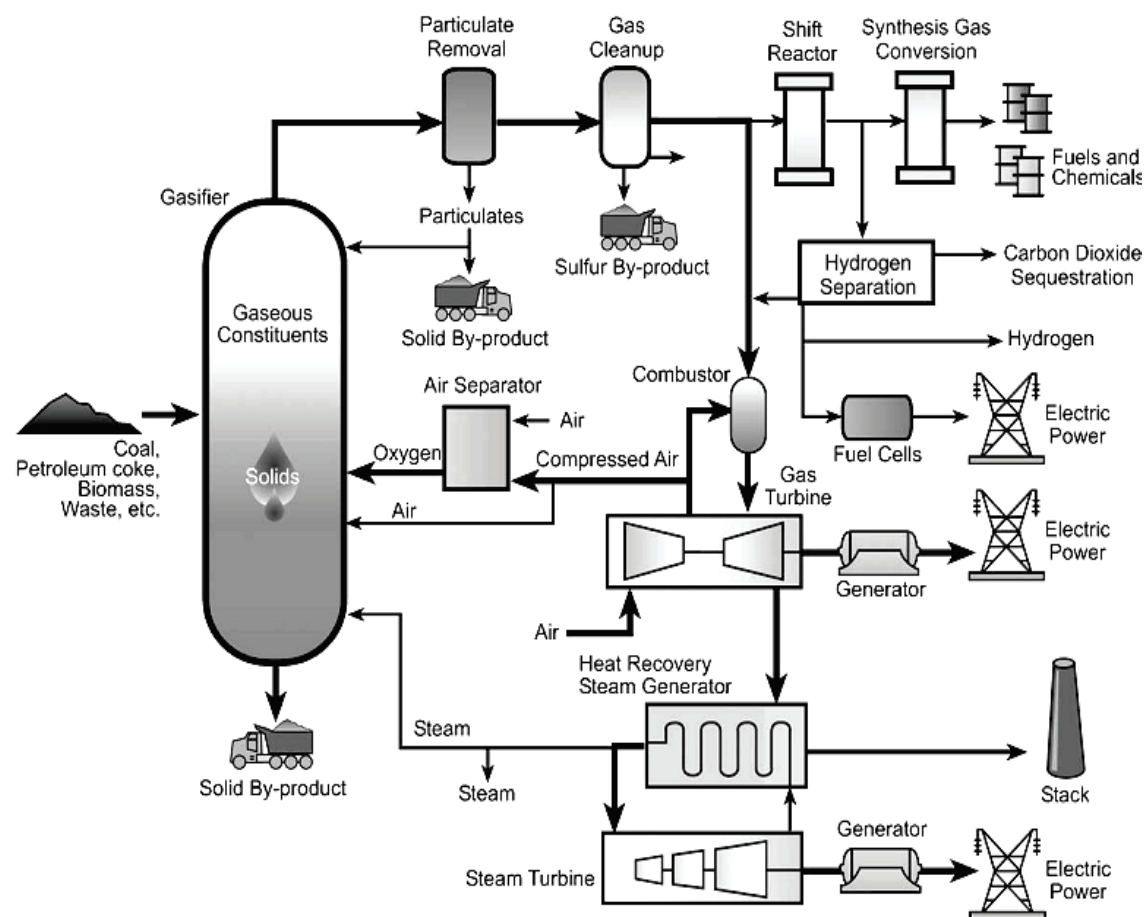


Figure I-3 Process flow diagram of a gasification option [2].

Biomass catalytic gasification can be performed in fixed or fluidized bed reactors. Although the process is performed at high temperatures, significant amounts of tar would be produced. Catalytic cracking, thermal cracking and plasma methods have been suggested to decrease the tar formation [12]. For example, $Rh/CeO_2/M$ ($M = SiO_2, Al_2O_3$ and ZrO_2) have been used to reduce the tar formation in the gasification process [13]. Zhang et al. [14] investigated tar catalytic destruction on a tar conversion system. Three Ni-based catalysts (ICI46-1 (NiO/CaO-K₂O-not reduced), Z409 (NiO/MgO-K₂O-FeO_x-not reduced) and RZ409 (NiO/MgO-K₂O-FeO_x-reduced)) were proven to be effective in eliminating heavy tars.

Coal gasification is a matured technology to produce syngas. Coal gasifiers use oxygen/air for heat providing by combustion of coal, and steam/ CO_2 for gasification reaction. Hydro-gasification and catalytic gasification processes can produce large quantities of synthetic natural gas and yield clean-burning fuel. Steam-oxygen and steam-air gasification processes produce a carbon monoxide- and hydrogen-rich syngas.

Although technologies have been developed over several decades to process petroleum-based feedstock to produce hydrogen, its production from biomass resources remains a major challenge [15]. Thus, if steam reforming of hydrocarbons is the most commonly used and the most economically competitive method for hydrogen production [16, 17], ethanol has been identified as one of the most important and potential feedstocks among the various renewable alternatives; it can easily be produced from biomass fermentation process, and is safe to handle, transport and store.

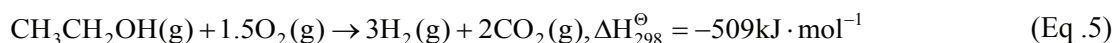
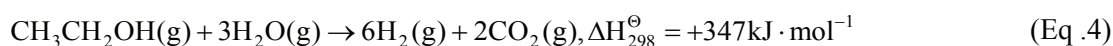
1.1.2. Advantages of hydrogen from bio-ethanol

Bio-ethanol, produced from biomass fermentation, such as sugar, starch, agro-industrial wastes, forestry residues and the organic fraction of municipal solid wastes can be sustainably utilized for sustainable hydrogen production. After distillation and purification, a mixture of 50% ethanol and water (molar ratio of ethanol/water close to 1/3) can be obtained [18, 19], which can directly be used for hydrogen production by SR:

- (i) As seen before, hydrogen production from natural gas steam reforming requires temperatures between 1000 and 1373 K, implying a large energy supply. In turn, the steam reforming of ethanol can be operated at lower temperature, e.g., in the range 673 - 923 K;
- (ii) Ethanol can be produced from biomass fermentation, which is renewable and sustainable. The CO_2 produced can be converted back to biomass by plants, as part of the carbon cycle, and reduce the green-house gas emissions;
- (iii) The price of bio-ethanol has been markedly reduced after the development of mature fermentation technologies. It is beneficial for ethanol utilization at large scales;
- (iv) Ethanol displays a lower toxicity than methanol, and is easy to transport and store;
- (v) Ethanol is free of sulfur, which is a well-known poison of metallic catalysts and so beneficial for the lifetime of the catalysts.

However, in balance with the advantages mentioned above, many limitations have to be considered. The ethanol production requires large planting areas and water resources. A strong debate related to bio-ethanol production routes competing with the food resources is permanently addressed. In this sense, bio-ethanol production might be less relevant using growing resources like sugar cane or maize than starting from agro-industrial wastes, forestry residue materials and organic fraction of municipal solid waste. Though such a debate is out of the scope of the present thesis, we might consider that for domestic and low power application such as small PEMFC units, the reforming of ethanol remains a valuable option, without excessive ILUC (indirect land use change) impact.

Ethanol can be converted to hydrogen through three processes: SR, POX and OSR. These techniques are described as:



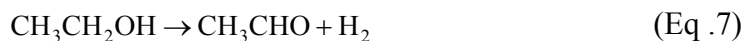
Compared with POX and OSR, SR has received more attention due to its relative higher conversion efficiency and higher hydrogen concentration in the dry gas product [20]. In the following, we focus on the SR of ethanol and the latest developments are reviewed.

1.2. Catalysts for hydrogen from steam reforming of ethanol

For the above mentioned reactions, catalysts play crucial roles in the activity toward complete conversion of ethanol (predicted by thermodynamics) and the selectivity towards hydrogen and CO_x production. Under non equilibrated conditions, each catalyst displays its own characteristics for catalytic activity and selectivity of products. Moreover, its stability and ageing are also strongly depending on the selected formula and sometimes shaping. Therefore, the selection of a suitable catalyst is somehow a challenge.

Though still highly controversial, the mechanism of steam reforming of ethanol is generally presented in an over simplified way, partly speculative, involving the following reactions [21]:

(i) dehydrogenation of ethanol to C_2 intermediates like acetaldehyde:



(ii) breaking the C-C bond of C_2 intermediates to CO_x and CH_x , which gives for the case of acetaldehyde :



(iii) reforming of CH_x (or CH_4) and WGS reaction to generate H_2 :



Indeed, in such a simplified scheme, the real adsorbed intermediates are not considered and a process without formation of the above mentioned molecules is much likely to occur on the catalytic surface. In addition, various side-reactions may also be involved. At low temperature, methanation of the syngas into methane could be considered as the reverse reaction of methane reforming occurring at high temperature. Ethylene can be formed by ethanol dehydration, especially on acidic supports (such as Al_2O_3 [22]). It is then easily polymerized and transformed into coke, potentially leading to catalyst deactivation. Another by-product, acetone, could also be produced from aldol condensation of acetaldehyde to butan-1-al-3-ol, further dehydrogenated and cleaved into acetone and formic acid [23]. All these mechanistic aspects will be deeply analyzed throughout the present work.

Let us consider now the main materials reported in the literature for the steam reforming of ethanol reaction: oxide and metal supported catalysts.

I.2.1. Oxide catalysts

In early studies, steam reforming of ethanol was performed over oxide catalysts. The advantage of oxide catalysts was the low concentration of CO in the outlet, while the disadvantages were the large yield of by-products and the low concentration of H_2 .

Llorca et al. [24,25] studied various metal oxides, such as MgO, Al_2O_3 , V_2O_5 , ZnO, La_2O_3 , CeO_2 and Sm_2O_3 , as catalysts in the steam reforming of ethanol at 573-723 K with an ethanol/water molar ratio of 1/13. The ethanol conversion increased with the temperature increase in all the cases. However, significant differences were observed in term of activity,

stability and selectivity. Al_2O_3 and V_2O_5 showed high conversion of ethanol at low temperatures but high selectivity of ethylene because of the acidity of these oxides. MgO showed low conversion of ethanol and high selectivity of acetaldehyde due to its basicity. CeO_2 gave an ethanol conversion of 25% at 723 K, but ethylene and acetone were formed. Sm_2O_3 showed deactivation, and ZnO showed high selectivity of H_2 . The performances of these oxides at 723 K are shown in Table I-2. The above results reveal that the nature of oxide catalyst, especially its acidity or basicity, markedly influences the catalytic performances.

Table I-2 Catalytic performances in the steam reforming of ethanol ($\text{C}_2\text{H}_5\text{OH}:\text{H}_2\text{O}$ molar ratio = 1:13) at 723 K under atmospheric pressure

Sample	GHSV /h ⁻¹	Con. /%	Selectivity (%)				
			H ₂	CO	C ₂ H ₄	CH ₃ CHO	CH ₃ COCH ₃
MgO	5000	6.9	45.9	--	6.8	44.3	--
Al ₂ O ₃	5000	100	--	--	100	--	--
V ₂ O ₅	5000	100	36.7	1.1	33.3	8.2	--
ZnO(1)	5000	100	61.4	--	1.7	10.2	6.6
ZnO(2)	5000	100	64.6	--	0.6	0.2	12.5
La ₂ O ₃	5000	19.9	44.4	--	33.0	--	--
CeO ₂	5000	24.4	52.4	0.2	18.9	--	11.4
Sm ₂ O ₃	5000	37.9	32.0	--	53.3	--	1.4
ZnO(2)	9900	100	65.0	--	1.1	5.9	5.8
ZnO(2)	22000	100	73.4	--	1.0	0.4	0.3

Wang et al. [26] studied the steam reforming of ethanol over cobalt oxides in a fixed-bed reactor. Fresh CoO_x precursors were converted to Co_3O_4 oxide upon thermal treatment. The complete conversion of ethanol was achieved around 598 K for the fresh CoO_x and C300 catalysts (calcined at 300°C), while it occurred at 648 K for C500 and C700 catalysts (calcined at 500 and 700°C), respectively, at a gas hourly space velocity (GHSV) of 22000 h⁻¹ and a water/ethanol molar ratio of 13. At low temperature, large amounts of CH_3CHO were present, indicating that the dehydrogenation of ethanol to acetaldehyde was predominant. In all the cases, the concentration of CH_4 was very low, indicating a low methanation activity over the oxides. The effects of temperature on the conversion of ethanol and the yield of

hydrogen confirmed that the activities of CoO_x and C300 are better than C500 and C700, indicating that the catalytic activity decreased when the catalyst crystallite size increased.

In a recent study, Liu et al. [27] studied nickel-lanthanum composite oxide catalysts in the steam reforming of ethanol. The activity of the 1La-1Ni (H) catalyst reduced at 473 K was found higher than the non-reduced one. The decomposition of acetaldehyde promoted the selectivity of H_2 , and the promotion effect of the reduced catalyst was more pronounced than the non-reduced one. The catalytic performances compared for various La/Ni ratios showed that the 1La-1Ni (H) catalyst displayed a much better activity at low temperature, while the 3La-1Ni (H) and 1La-3Ni (H) catalysts presented higher yields of H_2 at higher temperature. The composition in H_2 , CO, CO_2 and CH_4 were 72%, 0.5%, 20% and 7% over the 1La-1Ni catalyst at 648 K, respectively. The low concentration of CO at the outlet offers an obvious advantage to use the gas produced in fuel cells after only a minor post-treatment.

To summarize, it comes clear that most oxide catalysts present a reasonable activity towards steam reforming of ethanol. The concentration of CO remains very low and the concentrations of H_2 close to the equilibrium value. However, many by-products such as acetaldehyde, acetone, and ethylene are produced because of the poor capacity for C-C breaking of these oxides, which in turn decreases the selectivity to hydrogen. Within these by-products, coke precursors have to be considered, leading to catalyst deactivation. In contrast with the oxides, metals are expected to favor C-C breaking, and thus, supported metal catalysts have been widely investigated in the steam reforming of ethanol over the last decades.

1.2.2. Supported metal catalysts

For a number of metal supported catalysts, the support was found to activate primarily ethanol and water, producing C_2 intermediates and mobile surface OH groups, while the metal phase is used to break the C-C bond to C_1 intermediates. Following this bi-functional scheme, the metal supported catalysts display in general a much better catalytic activity than the pure oxide catalysts. In the literature, base and noble metals are generally considered for the steam reforming reaction.

1.2.2.1. Supported base metal catalysts

Base metal catalysts have been extensively investigated in the steam reforming of ethanol not only because of their lower price, but also because they demonstrated comparable catalytic performances to noble metals.

Among the most commonly used base metals, Ni is selected in a number of chemical industrial processes, especially for hydrogenation and dehydrogenation reactions as low cost and performing material. In the steam reforming of ethanol reaction, Ni causes bond breaking of ethanol in the following order: O-H > -CH₂- > C-C > -CH₃ [28]. Ni possesses hydrogenation, dehydrogenation, hydrogen exchange activity and hence adsorbed H atoms on the catalyst surface can easily combine into molecular hydrogen [29]. Frusteri et al. [30] got a 95% H₂ selectivity over a Ni/MgO catalyst upon steam reforming of ethanol at GHSV of 4×10⁴ h⁻¹ and 923 K. Fatsikostas et al. [31] compared the activity of Ni catalysts supported on La₂O₃, Al₂O₃, YSZ and MgO supports. The Ni/La₂O₃ exhibited the highest activity and stability, attributed to the formation of lanthanum oxy-carbonate species (La₂O₂CO₃), which scavenged the coke deposition. The activity of Ni/Al₂O₃ was comparable to that of Ni/La₂O₃, but the hydrogen selectivity was lower in the former case. In the case of Ni/YSZ, the selectivity towards CO and CO₂ decreased with time on stream. Ni/MgO catalyst was very stable, but the selectivity of products was poorer than for the other catalysts. Sun et al. [32] compared the catalytic activity of Ni/Y₂O₃, Ni/La₂O₃ and Ni/Al₂O₃ for steam reforming of ethanol at temperatures of 523-623 K. The catalytic activity, stability and selectivity of hydrogen followed the order of Ni/La₂O₃ > Ni/Y₂O₃ > Ni/Al₂O₃. The reported selectivity of hydrogen was relatively low, probably due to the low water/ethanol molar ratio of 3:1 and the low temperature. Comas et al. [33] demonstrated that increasing the water/ethanol ratio and the temperature would significantly increase the selectivity of hydrogen.

In order to improve the activity of Ni catalysts, other supported oxides or dopants have been tested as supports or catalyst modifiers. Yang et al. [34] showed that the selectivity of hydrogen ranked in the order : Ni/ZnO = Ni/La₂O₃ > Ni/ MgO > Ni/Al₂O₃ with almost 100% conversion of ethanol at 923 K. Frusteri et al. [35] investigated the effect of alkali addition (Li, Na and K) on the catalytic activity of a Ni/MgO catalyst in the steam reforming reaction. It

was found that Li and K enhanced the catalyst stability by depressing long term sintering of Ni. Recently, Zhou et al. [36] tuned the catalytic performances of $Ce_{1-x}Ni_xO_{2-y}$ catalysts in the steam reforming of ethanol by modifying the metal-support interactions. Below 673 K, the reforming activity of $Ce_{0.8}Ni_{0.2}O_{2-y}$ and $Ce_{0.9}Ni_{0.1}O_{2-y}$ was nearly identical, but the former showed almost twice higher hydrogen production than the latter, and was much more performing than the Rh/CeO₂ catalyst at 673 K and above. XRD results suggested that half of the Ni atoms were present as NiO, and the rest of the Ni atoms formed a $Ce_{0.8}Ni_{0.2}O_{2-y}$ solid solution, which induced strain in the oxide lattice and favored the formation of O vacancies. The O vacancies and related defects enhanced the dispersion of Ni on the oxide surface and facilitated the cleavage of the O-H bonds in water and ethanol.

Akande et al. [37] investigated the effects of catalyst preparation method and of Ni loading for ethanol steam reforming. 10-20 wt% Ni/Al₂O₃ catalysts were prepared by precipitation (PT), co-precipitation (CP) and impregnation (IM) method, and evaluated in reforming of crude ethanol for hydrogen production. The PT catalysts exhibited lower crystallite size of NiO and were more reducible than the CP and IM catalysts, resulting in higher ethanol conversion. Catalysts with 15 wt% Ni loading gave the best ethanol conversion for all the preparation methods. Ni-Cu supported over silica catalysts were also found as performing systems for on board reformers by Klouz et al. [38].

Cobalt, having properties close to Ni, was also investigated in recent years. Llorca et al. [25] studied the supported 1.1-1.2wt% Co catalysts in 573-723 K at atmospheric pressure. CO-free hydrogen was produced over the ZnO-, La₂O₃-, Sm₂O₃- and CeO₂-supported catalysts. ZnO-supported samples showed the best catalytic performances. The selectivity of H₂ and CO₂ were 73.8% and 24.2%, respectively, at 100% conversion of ethanol at 723 K. For the other catalysts, it was observed that the dehydration of ethanol to ethylene was the main reaction over the Co/Al₂O₃ catalyst due to the acidity of Al₂O₃. Co/MgO and Co/SiO₂ catalysts showed lower conversions of ethanol and the main reaction was dehydrogenation to acetaldehyde. Song et al. studied steam reforming of ethanol over several modified Co-based catalysts [39]. They found that the addition of CeO₂ promoted the activity and stability of Co/ZrO₂ significantly. The high oxygen storage capacity (OSC) and high oxygen mobility of the mixed oxide supports were thought to contribute to the higher activity and stability of the

Co/10%CeO₂-ZrO₂ catalyst, due to carbon deposit oxidation as soon as formed, therefore maintaining the catalyst surface clean and active.

The effect of cobalt precursors on the activity of ceria-supported cobalt catalysts was studied by Song et al. [40]. The results obtained from steady-state reaction experiments showed significantly better catalytic activity over the samples prepared using organometallic Co precursors. It was suggested that the organic ligands bound to the cobalt species facilitated the dispersion of Co on the surface of ceria, resulting in improved activity and stability.

The nature of the support and the preparation method were also found to determine the catalytic activity and stability of Co-based catalysts [41]. Co/SiO₂ and Co/Al₂O₃ catalysts were prepared by different methods including incipient wetness technique, impregnation and sol-gel methods. The catalysts exhibited different surface areas, compositions and metal dispersions, resulting in major differences in catalytic performances. It was found that the highest hydrogen selectivity (67%) was obtained over the 8 wt.% Co/Al₂O₃ catalyst prepared by impregnation method, which could be due to a higher metal dispersion.

Cu-based catalysts are the most frequently studied systems in steam reforming of methanol due to their high selectivity and activity [10, 42], and were also tested in steam reforming of ethanol. Cavallaro and Freni [43] investigated the steam reforming of ethanol over CuO/ZnO/Al₂O₃ catalyst and found a good catalytic activity above 630 K. The formation of by-products, like acetaldehyde and acetic acid, was favoured only at temperatures below 600 K. Nishiguchi et al. [23] reported that acetaldehyde was the most abundant product over CuO and CuO/SiO₂ catalysts in the temperature range of 473-673 K, indicating that ethanol could be almost selectively converted to acetaldehyde over the Cu-based catalysts at low temperature. It was found that H₂ and acetone were produced over the Cu/CeO₂-MgO catalyst at 623 K due to the aldol condensation of acetaldehyde, as already mentioned. A recent investigation [44] over Cu/ZnO-based catalysts revealed that different co-precipitation procedures were not influencing the catalytic behaviours. However, acetone was observed at temperatures above 673-723 K, which was not described by Cavallaro et al. [43]. The presence of a second metal (Ni or Co) in the Cu-based catalyst improved the activity and stability significantly [38]. On the Co/Cu/ZnO/Al₂O₃ catalyst, ethanol conversion was significant above 473 K, while the conversion started above 573 K on the Co/ZnO/Al₂O₃

catalyst. In the stability test, the initial activity could be maintained for 20 h over the Cu/ZnO/Al₂O₃ catalyst, but a slow deactivation was observed after this time. In comparison, no alteration of activity was observed over the catalyst after Co addition.

1.2.2.2. Noble metal based catalysts

Noble metal based catalysts are widely used for their high catalytic activities in reactions involving hydrocarbon activation and reforming. For steam reforming of ethanol, Rh, Pt, Pd, Ir and Ru have extensively been studied, as illustrated in Table I-3.

Liguras et al. [45] studied the influence of noble metals and supports for steam reforming of ethanol in 873-1073 K and metal loading of 0-5 wt.%. The ethanol conversion followed the order Rh >> Pt > Pd > Ru over the Al₂O₃-supported catalysts. Ru was less active at low temperature, but showed comparable activity with Rh at higher loading. At 1073 K, ethanol was completely converted and selectivity of hydrogen was above 95% over the 5 wt.% Ru/Al₂O₃ catalyst. The support was shown to play also an important role. The activity of Ru on different supports was found to vary in the order: Ru/Al₂O₃ > Ru/MgO > Ru/TiO₂.

Auprêtre et al. [46] studied the steam reforming of ethanol reaction over Rh and Pt catalysts supported on Al₂O₃, Al₂O₃-CeO₂, CeO₂ and Ce_{0.63}Zr_{0.37}O₂. The results revealed that the activity of the catalysts increased with increasing the OH group mobility at the surface, and the selectivity of CO₂ decreased with the increasing activity of reverse water gas shift reaction. They also investigated two series of Rh/Mg_xNi_{1-x}Al₂O₃ catalysts [47] prepared by two different methods and Rh precursors. The performances obtained at 973 K under 1 to 11 atm (ethanol/water molar ratio of 4 and GHSV of 24000 h⁻¹) demonstrated that the acidic and basic properties of the materials are crucial parameters to determine the selectivity of ethylene or acetaldehyde. The effect of Rh precursors revealed that the catalytic activity of the catalyst prepared from a nitrate precursor was much lower than the one prepared from an acetate or chloride precursors, because of the differences in the acidity of the catalysts.

Cai et al. [48] compared hydrogen production through steam reforming, partial oxidation and oxidative steam reforming of ethanol over Ir/CeO₂ catalysts. This material showed an outstanding catalytic activity towards SR, POX and OSR. Acetaldehyde was the primary product below 673 K, which further decomposed to methane and carbon monoxide at higher

temperatures. Methane steam reforming and WGS were also involved above 773 K. The catalyst showed rather high stability between 823 and 923 K without apparent deactivation after 60 h on stream. The strong Ir-ceria interaction was thought to prevent the sintering of Ir and to inhibit the carbon deposition.

Yamazaki et al. [49] studied the steam reforming of ethanol and biomass-derived ethanol over a Pt/ZrO₂ catalyst. At 673 K, the partial steam reforming of ethanol ($C_2H_5OH + H_2O \rightarrow CO_2 + CH_4 + 2H_2$) and the ethanol decomposition ($C_2H_5OH \rightarrow CH_4 + CO + H_2$) were occurring competitively over the catalyst. H₂ production decreased rapidly with time on stream, which was attributed to a faster decrease of the steam reforming of ethanol compared to the ethanol decomposition. On the other hand, the activity and stability were lower upon steam reforming of biomass-based ethanol at 773 K. The faster deactivation was assigned to a larger amount of carbon deposition and a poisoning effect by impurities.

Other noble catalysts supported on MgO, CeO₂ and CeZrO₂ were also studied[50-53]. The catalysts also showed high ethanol conversion and hydrogen selectivity even at low temperature. Ethanol conversion could be more than 90% over Ru and Rh supported on CeO₂ catalysts at 723 K, but with a rather limited stability [51]. While with a low steam/ethanol molar ratio (water/ethanol molar ratio = 2:1, i.e., below the stoichiometric ratio of 3:1), the ethanol conversion could reached 100% over the Pt supported on CeO₂ catalyst[53], although the hydrogen selectivity was slightly lower.

The following table I-3 summarizes the most representative cases where noble catalysts were used for ethanol steam reforming.

Table I-3 Review of representative noble metal catalysts for steam reforming of ethanol.

Catalyst (wt.%)	Support	Temp. (K)	S/E ratio	Ethanol conversion (%)	H ₂ sel. /Concen. (%)	Ref.
Rh (1)				100	95	
Ru (1)	Al ₂ O ₃	1073	3:1	42	55	[45]
Pt (1)				60	65	
Pd (1)				50	55	
Rh(1)	Al ₂ O ₃	973	3:1	100	72	[46]
Rh(1-2)	Mg _x Ni _{1-x} Al ₂ O ₃	973	4:1	100	70.2	[47]
Ir (2)	CeO ₂	923	3:1	100	72	[48]
Rh (3)	MgO	923	8.5:1	99 (10 h)	91	[50]
Pd (3)				10 (10 h)	70	
Ru (1)	CeO ₂	723	3:1	> 90	57 (20 min)	[51]
					25 (100 min)	
Rh (1)					82 (20 min)	
					56 (80 min)	
Ru (2.5)	Al ₂ O ₃	773	3:1	100	90	[52]
	ZrO ₂			75	60	
Pt (1.5)	CeO ₂	773	2:1	100	45	[53]
	CeZrO ₂			65	40	

1.2.3. Concluding remarks on catalyst formulations

From the above literature survey, the most performing base metal catalysts in the steam reforming of ethanol were found to be Ni and Co. However, they both lead to significant deactivation due to carbon deposition and/or metal sintering. The use of appropriate supports, like MgO, ZnO, CeO₂, La₂O₃ or mixed oxides, tends to limit the carbon deposition to some extent. The preparation method was also found to play a key role in catalytic activity. Note however that a number of these studies were essentially descriptive, without providing a deep understanding of the related catalytic phenomena.

Among the noble metals, Rh and Ir supported on ceria-based catalysts exhibit the best performances in terms of ethanol conversion and selectivity of hydrogen. These catalytic performances (activity, stability and selectivity) seem related to the strong capacity of the metal phase towards C-C bond breaking, the enhanced OH group mobility at the ceria surface, and the strong metal-support interactions inhibiting both coke deposition and metal sintering.

I.3. Mechanistic aspects of the steam reforming of ethanol reaction

I.3.1. Thermodynamic studies

Many thermodynamic studies have shown the feasibility of hydrogen production from steam reforming of ethanol for fuel cell applications, though the coke deposition remains a matter of discussion [54-56]. In the present study, we used the HSC software V4 to calculate the equilibrium composition upon steam reforming of ethanol based on the Gibbs energy minimization under different operating conditions. The main products considered were H₂, H₂O, CO, CO₂ and CH₄, but CH₃CHO, CH₃COCH₃, C₂H₄ and solid carbon were included as well in the list of potential products.

Figure I-4 shows the evolution of the dry gas composition upon steam reforming of ethanol (stoichiometric feed). Ethanol is fully converted and no coke nor C₂ products are formed within the temperature range considered (673-1273 K). The concentrations of H₂ and CO increase while the concentrations of CH₄ and CO₂ decreased with the temperature, indicating that methane steam reforming and RWGS were thermodynamically favored at higher temperatures (and inversely that methanation and WGS are favoured at low temperature). These results well illustrate the general agreement reported in previous studies [54-56]. It can be deduced from this thermodynamic analysis that the hydrogen production is maximized above 900 K and that the ethanol and the C₂ intermediates conversion is complete under equilibrium conditions. On the opposite, a too high temperature will favor the sintering of the catalyst and lead to deactivation. So, a compromise should be found.

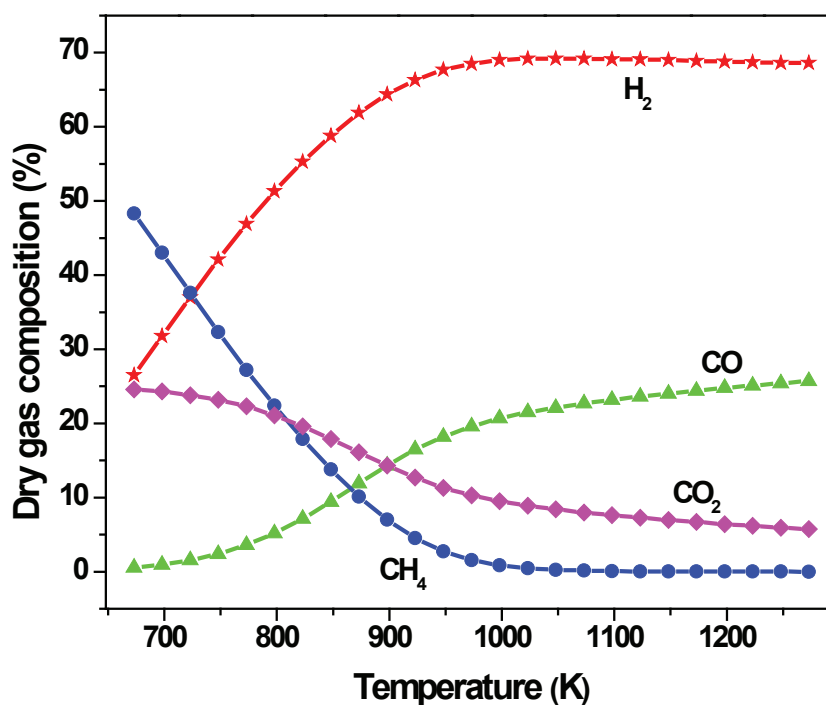


Figure I-4 Effect of temperature on equilibrium dry gas concentrations for steam reforming of ethanol (EtOH/H₂O = 1/3; pressure: 1 atm).

I.3.2. Reaction pathways

As already pointed out, the reaction pathways involved in steam reforming of ethanol process are very complex, depending on the catalyst formulation. Figure I-5 shows a possible reaction network over metal catalysts, as proposed by Adhikary et al. [20].

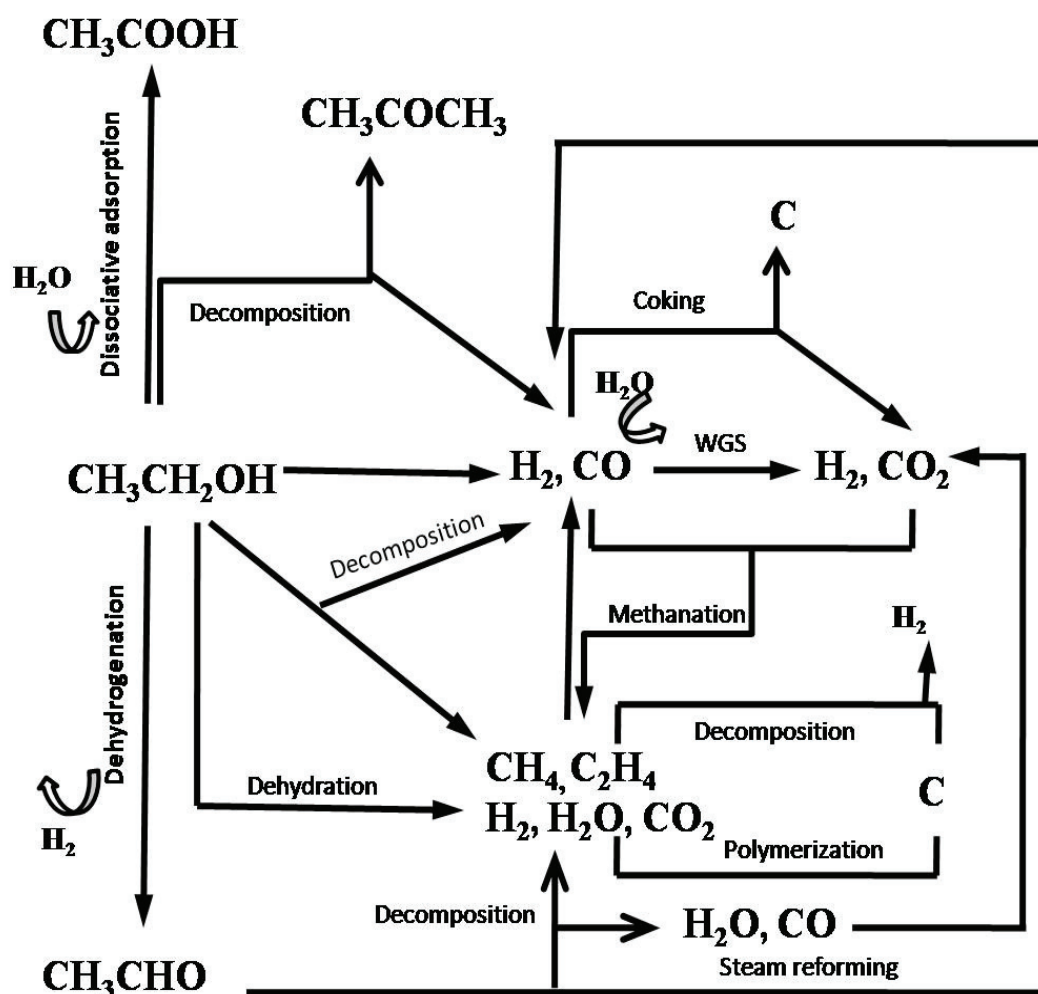
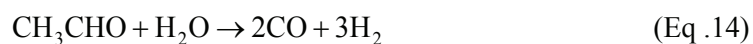
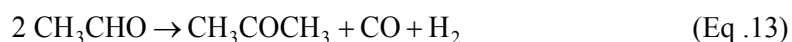


Figure I-5 Possible reaction pathways upon steam reforming of ethanol [20].

The main reaction paths involved upon steam reforming of ethanol are discussed below:

(1) Dehydrogenation of ethanol to acetaldehyde (Eq. 11), followed by decomposition (Eq. 12), aldolization (Eq.13) or steam reforming (Eq. 14) of acetaldehyde:



(2) Dehydration of ethanol to ethylene (Eq. 15), followed by the polymerization of ethylene (Eq. 16):

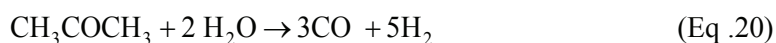
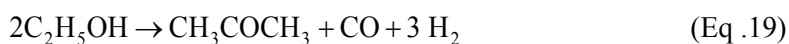


Both Eq.7 (dehydrogenation to acetaldehyde) and Eq.11 (dehydration to ethylene) depend on the nature of the support. Acidic supports would promote ethanol dehydration producing ethylene, a well-known coke precursor, whereas basic supports would favor the dehydrogenation of ethanol producing acetaldehyde and secondary products like acetone, crotonaldehyde, ethyl acetate, acetates, butanes...

(3) Decomposition of ethanol to CH_4 (Eq. 17), followed by steam reforming of CH_4 (Eq. 18):



(4) Decomposition of ethanol to acetone (Eq. 19), followed by steam reforming (Eq. 20):



(5) Water gas shift:



(6) Coke deposition from CH_4 or CO decomposition.



A reaction pathway for the steam reforming of ethanol over Rh and Rh-Pt supported catalysts is illustrated on Figure I-6 as proposed by Sheng et al. [57]. The mechanism over Rh catalysts was proposed to be different compared to the other metal catalysts. On Pt, Pd and Ni, ethanol is first dissociated to ethoxy and further oxidized to acetaldehyde, whereas on Rh, the ethoxy would undergo dehydrogenation to form an oxometallacycle (a)-OCH₂CH₂-(a) intermediate, where (a) is an adsorption site. The presence of Rh would subsequently favor the C-C bond breaking to produce CO and CH_x; while the presence of Pt as a second metal would enhance the H₂ production through CH₄ reforming.

Figure I-6 Proposed reaction pathways for steam reforming of ethanol over Rh supported catalysts [57].

Figure I-7 Reaction pathways upon steam reforming of ethanol over Rh supported catalysts [30].

Frusteri et al. [30] proposed another mechanism over the Rh catalysts. As can be seen on Figure I-7, ethanol is first dehydrogenated to acetaldehyde, which subsequently decomposes to CH₄ and CO. The formation of H₂ and CO₂ is then governed by the CH₄ steam reforming and WGS reactions. The dehydration of ethanol would produce ethylene. Coke deposition could occur through the polymerization of ethylene and/or the disproportionation of CO (Boudouard reaction).

I.3.3. TPD and infrared investigations

A detailed analysis of the reactants, intermediates and final products was also performed using transient methods, like temperature programmed desorption (TPD), temperature programmed surface reaction (TPSR), combined with *operando* spectroscopy (DRIFT etc.) or mass spectrometer.

Yee et al. [58] studied the reactions of ethanol over a Pt/CeO₂ catalyst using TPD and *in situ* infrared (FTIR). In the TPD experiments, acetaldehyde, resulting from ethanol dehydrogenation, was desorbed at 400-700 K. Desorption of CO and CH₄ occurred at 665-695 K, which might come from the decomposition of acetaldehyde. Benzene also desorbed at 610-690 K, which suggested the reaction between surface-bound crotonaldehyde and acetaldehyde species.

The FTIR studies after ethanol adsorption revealed the rapid formation of ethoxy species at room temperature. Heating up to 473 K, acetaldehyde species formed, as confirmed by the previous TPD. When the temperature increased up to 523 K, ethoxy and acetaldehyde species vanished, while carbonate and crotonaldehyde species appeared. The former was due to the oxidation of acetaldehyde, and the latter was formed from the aldolization of acetaldehyde.

Cai et al. [48] studied the ethanol activation via FTIR and the reaction between the adsorbed ethanol and water species via TPSR over an Ir/CeO₂ catalyst. It was found that the ethoxy and acetate species were easily formed at room temperature. Increasing the temperature to 473-573 K, the ethoxy species decomposed into metal carbonyl, leading to CO, or converted to acetate and carbonate species. When the temperature was further increased, the ethoxy species disappeared completely and most acetates converted to carbonate (over ceria) and CH_x (over Ir) species. TPSR studies further demonstrated that acetaldehyde and acetone were the main products below 450 K, which were formed by dehydrogenation of the ethoxy species and condensation of acetaldehyde, respectively. At 626 K, desorption of H₂ and CO₂ occurred, and traces of CH₄ and CO were formed, indicating the decomposition of the acetate and carbonate species at this temperature.

Llorca et al. [59] studied the steam reforming of ethanol over a Co/ZnO catalyst via *in situ* DRIFT-mass spectrometry. Ethoxy and acetaldehyde species were formed at room temperature. The ethoxy species could be stable up to 573 K over the Co/ZnO catalyst. The IR data, after quenching at 298 K after reaction at 673 K, revealed that not only ethoxy species, but also acetates were present at the catalyst surface, indicating that acetaldehyde could be oxidized during the reaction. When the temperature was increased to 473 and 673 K, the concentration of the ethoxy and acetate species decreased. In the meantime, H₂, CO₂, CH₄, acetaldehyde and acetone were detected by mass spectrometry. It was proposed that these products derived from surface acetates. This work confirmed the transformation of the ethoxy species to acetaldehyde and acetate species upon reaction.

To sum up, it appears that most authors agree on key steps of the reaction pathway, like the ethoxy formation and the transformation of ethoxy species; but the entire scheme remains a matter of debate, depending on the nature of the catalysts and the reaction conditions.

I.3.4. Kinetic studies

In contrast to the large number of studies on the reaction mechanism, kinetic analyses and modeling of the steam reforming of ethanol reaction remain relatively scarce. Vaidya et al. [60] reported a kinetic study in the steam reforming of ethanol over a Ru/Al₂O₃ catalyst in the temperature range of 873-973 K. The decomposition of adsorbed ethanol to intermediates was considered as the rate-determining step. The activation energy was calculated to be 96 kJ·mol⁻¹ and the apparent reaction order with respect to ethanol was 1.

The most relevant study was reported in reference [61], in which a kinetic model was developed to describe the steam reforming of crude ethanol over a 15% Ni/Al₂O₃ catalyst. The experiments were carried out in a packed bed tubular reactor in the temperature range of 593-793 K. Four models were proposed based on an Eley-Rideal-type mechanism, and the dissociation of adsorbed ethanol was treated as the rate determining step. The final rate equation was:

$$-r_A = \frac{2.08 \times 10^3 \exp\left(-\frac{4430}{RT}\right) N_A}{(1 + 3.83 \times 10^7 N_A)^2} \quad (\text{Eq. 24})$$

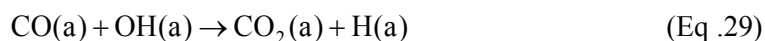
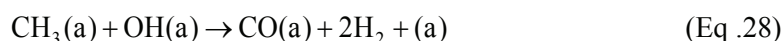
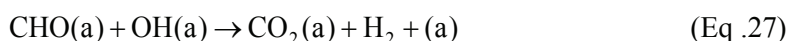
Where N_A is the flow rate of A feedstock (kmol/s). The average absolute derivation between the experimental and predicted rates was only 6%.

Mathure et al. [62] studied the kinetics of the steam reforming of ethanol using a commercial nickel-based catalyst. The effects of temperature (673-873 K), steam/ethanol molar ratio (3:1-18:1) and contact time ($W/F_{\text{EtOH}} = 46.2-555.25$ g min/mol) were investigated. The rate equation was proposed in the form of a power-law:

$$r_{\text{EtOH}} = 439 \exp\left(-\frac{2.3 \times 10^4}{RT}\right) P_{\text{EtOH}}^{0.711} * P_{\text{H}_2\text{O}}^{2.71} \quad (\text{Eq. 25})$$

The latest kinetic study of the steam reforming of ethanol reaction was proposed by Graschinsky et al. [63] over a RhMgAl₂O₄/Al₂O₃ catalyst. The analysis suggested that two active sites of the same type were involved in the rate-determining step. The possible rate-determining step and the corresponding rate expressions were suggested. By fitting the

experimental data, the reaction scheme was assumed to include ethanol decomposition and reforming, WGS and methane steam reforming, in which the following surface reactions were proposed as rate-determining steps:



Since the development of a kinetic model is required for any further engineering study, it must be stated that much efforts should be dedicated to the kinetic modelling, despite the difficulty for the reaction to be run in a proper chemical regime, with a minimum impact of heat and mass transfer limitations. Finally, it should be mentioned that to our knowledge, no search of relationships between the kinetic parameters and the intrinsic descriptors of the different catalysts has been attempted till now, which might lead to quantitative structure-activity relationships, useful for predicting the catalytic behaviour of new or improved formulas.

I.4. Catalyst deactivation investigations

Though there are few advanced studies in the literature, the catalyst deactivation under steam reforming of ethanol conditions is generally assigned to catalyst sintering and/or to carbon deposition. Several reactions may contribute to carbon formation [64, 78]:

- The Boudouard reaction:



- The reverse carbon gasification reaction:



- The methane decomposition:



- The condensation/polymerisation reactions from ethylene and other reaction intermediates:



The deposition of carbon depends on the nature of the active metal, the support and the reaction conditions. Filamentous carbon is readily produced on Ni and Co [65, 66], while encapsulation would occur in the case of noble metals, such as Rh and Pt [67, 68]. The acidic and basic properties of the support also strongly influence the product distribution and the catalyst stability. Al_2O_3 promotes the dehydration of ethanol to ethylene, while MgO was proposed to be highly active for ethanol dehydrogenation to acetaldehyde [24, 69]. Ceria and ceria-based oxides were suggested to improve the catalyst stability because of the high oxygen storage capacity (OSC) [70]. The reaction conditions also determine the reaction pathways that lead to carbon formation. Low temperature favours the formation of carbon through the Boudouard and reverse carbon gasification reactions, while high temperature leads to methane decomposition [71].

As for catalyst sintering, few studies were devoted to this ageing aspect under SR conditions. In general, the sintering of the metal particles at high temperature is assumed to proceed via a migration-coalescence process (Oswald ripening) possibly favoured by the loss of interaction between the particles and the surface support in the presence of steam, as proposed by Cai et al for the oxy-steam reforming of ethanol over Ir/CeO₂ materials [72] and the sintering of Rh over the Rh/Al₂O₃ catalyst for steam reforming of ethanol [73]. The sintering of the oxide supports was still less studied and will be presented in details later in the present study.

Note also that the combined analysis of various forms of deactivation was scarcely proposed, as it was in the paper from Araque et al [74]. Here, the ageing of $\text{Ce}_2\text{Zr}_{1.5}\text{Co}_{0.47}\text{Rh}_{0.07}\text{O}_{8-\delta}$ oxide was shown to be related to i) the accumulation of carbonates species leading to the blocking of active sites, ii) the formation of carbonaceous deposits and iii) the structural change of the catalyst under the reaction conditions, which gradually loses its redox capacity.

I.4.1. Deactivation studies over Ni and Co catalysts

The carbon formation over Ni and Co catalysts upon steam reforming of ethanol was widely investigated [75-80]. Alberton et al. [75] studied the formation of carbon and its influence on the steam reforming of ethanol reaction over a Ni/Al₂O₃ catalyst. Filamentous carbon was observed over the Ni/ α -Al₂O₃ at 723 K, while encapsulating carbon was formed above 773 K. Generally, the formation of encapsulating carbon caused a much faster deactivation than the filamentous carbon. The additives also had a certain influence on the type of carbon produced. For example, the addition of Ag induced a rapid deactivation of the Ni-Ag/MgAl₂O₄ catalyst due to the enhanced formation of gum carbon, whereas the addition of K delayed the carbon formation and the deactivation [76] due to the modified electronic structure of the catalyst. Similarly, the coke deposition could be suppressed when Cu was added to the Ni/SiO₂ catalyst, thus enhancing the stability of the catalyst [77].

Not only the addition of a second metal to the Ni catalysts, but also the modification of the support could decrease the coke formation and enhance the stability. Coleman et al. [81] studied a series of 10 wt% Ni/Mg-Al mixed oxide supported catalysts in the steam reforming of ethanol. The H₂ yield as a function of time on stream for pure and mixed oxides supported Ni catalysts at 773 and 923 K demonstrated that much higher hydrogen production was obtained over the Mg-Al mixed oxides supports than MgO and Al₂O₃ supports. The improved performances of the mixed oxides-supported catalysts were related to the formation of MgAl₂O₄, which kept nickel in its active form and exhibited moderate acidic and basic site strength and density compared to pure oxides supported catalyst, reducing the by-products formation.

Despite their high activity in the steam reforming of ethanol and the selectivity of hydrogen, Co-based catalysts were also prone to deactivation. Coke deposition over Co/CeO₂ was

studied as a function of temperature [78]. Co particles were found to be encapsulated by coke between 623 and 723 K. When the temperature was increased to 773 or 823 K, carbon filaments were observed but the catalyst could remain stable for 8 h. It is indicated that the filament carbon had a limited influence on catalyst deactivation at high temperatures. Above 873 K, carbon was not detected by TEM analysis. Lima et al. [80] studied the catalyst deactivation upon steam reforming of ethanol, POX and OSR over a Co/CeO₂ catalyst using temperature-programmed oxidation (TPO) and HRTEM. The TPO profiles exhibited two peaks in the range of 721-730 K and 753-760 K, which indicated the presence of amorphous carbon and filamentous carbon over the used Co/CeO₂ catalysts. The HRETEM images further confirmed the presence of amorphous and filamentous carbon deposited on the surface. Based on the DRIFT experiments over a Co/CeO₂ catalyst under steam reforming conditions, a deactivation mechanism was proposed, in which the decomposition of acetaldehyde, acetyl and acetate species produced hydrogen, CO and CH_x species. The catalyst would be deactivated when the rate of decomposition is higher than the rate of desorption of CH_x. Such species could indeed block the Co-support interface or further dehydrogenate to H and C, leading to catalyst deactivation.

The possible modification of the Co catalysts was also investigated. Kazama et al. [82] studied the promotion effect of Fe addition onto Co catalysts supported on Al₂O₃ in the steam reforming of ethanol. At 823 K and high W/F conditions, the amount of carbon deposited over the Fe/Co/Al₂O₃ catalyst was much lower compared to the Co/Al₂O₃ catalyst. Furthermore, the amount of carbon over the Fe/Co/Al₂O₃ catalyst did not increase above W/F = 1.3 g·h·mol⁻¹. A synergetic effect between the two metals (Fe and Co) was observed and the formation of methane and coke was reduced.

I.4.2. Deactivation studies over noble metal catalysts

The deactivation of noble metal based catalysts under steam reforming of ethanol conditions has also been studied, considering oxide supports with different acidic, basic and redox properties [73, 83,84]. In general, the deactivation rate was related to the formation of carbonaceous deposits and/or the sintering of the active phase and of the support.

S. Cavallaro et al. [73] showed that a Rh/Al₂O₃ catalyst was deactivated during steam reforming of ethanol by coke deposition, even at a high steam/ethanol ratio of 8.4. HRTEM revealed that the coke was mainly “encapsulating” carbon, an egg-shell like morphology covering and encapsulating the Rh particles. The coke deposition was attributed to the thermal decomposition of ethanol and the acidic nature of the Al₂O₃ support. The addition of oxygen in a proper ratio was found to significantly reduce the coke deposition, improving the stability of the catalyst.

T. Montini et al. [83] modified the acido-basicity of Al₂O₃ by addition of Ce_xZr_{1-x}O₂. The modified Rh/Ce_xZr_{1-x}O₂-Al₂O₃ catalyst was very active and stable in the steam reforming of ethanol at 873 K under diluted conditions and water/ethanol ratio of 5. However, TPO of the used sample revealed the evolution of CO₂ at 823 K, indicating the presence of carbonaceous deposits. The amount of deposits on the used Rh/Ce_xZr_{1-x}O₂-Al₂O₃ (0.49-0.71 mg C/g_{cat}) catalyst was much lower compared to the used Rh/Al₂O₃ catalyst (1.49 mg C/g_{cat}). The resistance towards coke deposition increased as the Ce_xZr_{1-x}O₂ content increased.

Lima et al. [68] studied the catalytic performances and the deactivation profiles of CeZrO₂ and Pt/CeZrO₂ catalysts in the ethanol decomposition and steam reforming of ethanol reactions at 773 K. Surprisingly, the former exhibited good stability, while the latter displayed rapid deactivation at all feed compositions. Based on DRIFT, TPO and TPD studies, it was found that acetate intermediates became dominant as a function of time on stream due to the degradation of the Pt-oxide interface. After 30 h on stream, HRTEM images revealed the presence of carbonaceous deposits, as 5-20 nm chain-like aggregates. The coke deposit would block the sites between the oxide and the Pt particles, which preventing the desorption of the acetate species and leading to catalyst deactivation.

Platon et al. [84] attributed the deactivation of a Rh/Ce_{0.8}Zr_{0.2}O₂ catalyst to the significant build-up of reaction intermediates on the surface of the catalyst. The formation of by-products like acetone and ethylene would be responsible for a more severe deactivation compared to acetic acid and acetaldehyde. Erdohelyi et al. [51] reported that the accumulation of acetate-like species over the support hindered the formation of ethoxy species and decreased the metal-support interaction. Guil et al. [85] considered that the deactivation was attributed to the blockage of the active sites by acetaldehyde.

To summarize, despite many studies on the catalyst deactivation phenomena, it can be stated that no general deactivation mechanism has been established, but a number of trends depending on the catalyst nature and the operating conditions. As for coke deposition, the type of coke and the location of the coke at the catalyst surface still need further works to be able to predict catalysts ageing and further regeneration for given catalytic systems and operating conditions. We have noted also an obvious lack of advanced studies on sintering and/or surface restructuring of both the metallic phase and of the support, which might lead as well to deep changes in the catalytic behaviour of the studied systems.

I.5. Objectives of the present thesis

From the above literature analysis and considering the main targets for a future industrial application, the following questions have to be addressed:

(I) Activity: the challenge in the steam reforming of ethanol reaction is to develop a highly active catalyst, to ensure full conversion of ethanol with a minimum production of undesired by-products at the lowest possible temperature.

(II) Stability: the developed catalysts also need to be stable at industrial level. This requires to understand and control the two main ageing factors : (a) the coke formation on the surface of the catalyst, and (b) the sintering of the supports and/or the active phase.

(III) Selectivity: hydrogen selectivity has to be maximized, within the thermodynamic constraints, by playing on the general reaction scheme including key steps like WGS and methane steam reforming. The challenge is to minimize the production of CO and CH₄.

(IV) Mechanism and kinetics: an advanced knowledge of the mechanistic pathways supporting a kinetic modeling, which may be specific of the catalyst and the operating conditions, is required for any further improvement of the catalytic performances and engineering design.

The main objectives of this work are directly derived from the above statements, such as to identify a well performing catalyst and to investigate carefully the causes of catalyst deactivation, in order to find new ways to limit it for long term operations. In previous studies carried out in the two French and Chinese laboratories involved in this joint program, an Ir/CeO₂ catalyst was developed for the steam and oxy-steam reforming of ethanol[48,86-90].

It was found that with this catalyst, ethanol could be fully converted at 723 K at a space velocity of 6000 mL/(gh), without apparent deactivation for at least 60 h[90]. However, deactivation phenomena were observed at higher space velocity (eg., 75000 mL/(gh) in [48]). In this work, we have considered this catalyst formula as a reference i) to follow up its fundamental investigation, by focusing on kinetic and deactivation analysis, and ii) to carry out catalyst modification to improve its performances, like ceria doping and shaping. Other works on different systems like Ni based catalysts are reported in annex.

This work was structured as follows, including this first introduction/state-of-the-art analysis:

- (i) Chapter II: Experimental: catalysts preparation and characterization techniques
- (ii) Chapter III: Kinetic studies of steam reforming of ethanol over an Ir/CeO₂ catalyst
- (iii) Chapter IV: Ageing analysis of a model Ir/CeO₂ catalyst in steam reforming of ethanol
- (iv) Chapter V: Enhancing catalyst performance by PrO_x-doping in an Ir/Ce_{0.9}Pr_{0.1}O₂ system
- (v) Chapter VI: Influence of CeO₂ shape/structure on Ir/CeO₂ catalyst for hydrogen production from steam reforming of ethanol
- (vi) Chapter VII: General conclusions and perspectives
- (vii) Chapter VIII in annex: Hydrogen production from steam reforming of ethanol over Ni and Ni-Cu catalysts

References

- [1] EIA/AER. Annual Energy Review 2007. Energy Information Administrations, US Department of Energy, Washington, DC. DOE/EIA-0384 (2007), June 2008
- [2] G. J. Stiegel, M. Ramezan, *Inter. J. Coal Geol.* 65 (2006) 173-190.
- [3] K. Liu, C. S. Song, V. Subramani, Hydrogen and syngas production and purification, John Wiley, 2010
- [4] E. C. Wanat, K. Venkataramen, L. D. Schmidt, *Appl. Catal. A: Gen.* 276 (2004) 155-162.
- [5] A. N. Fatsikostas, D. I. Kondarides, X. E. Verykios, *Catal. Today* 75 (2003) 145-155.
- [6] J. R. Salge, G. A. Deluga, L. D. Schmidt, *J. Catal.* 235 (2005) 69-78.
- [7] S. Cavallaro, *Energy Fuels* 14 (2000) 1195-1199.
- [8] S. M. de Lima, A. M. D. Silva, L. O. O. Costa, U. M. Graham, G. Jacobs, B. H. Davis, L. V. Mattos, F. B. Noronha, *J. Catal.* 268 (2009) 268-281.
- [9] D. J. Wilhelm, D. R. Simbeck, A. D. Karp, R. L. Dickenson, *Fuel Process. Technol.* 71 (2001) 139-148.
- [10] R. M. Navarro, M. A. Pena, J. L. G. Fierro, *Chem. Rev.* 107 (2007) 3952-3991.
- [11] J. D. Holladay, J. Hu, D. L. King, Y. Wang, *Catal. Today* 139 (2009) 244-260.
- [12] J. Han, H. Kim, *Renew. Sust. Energy Rev.* 12 (2008) 397-416.
- [13] M. Asadullah, S. I. Ito, K. Kunimori, M. Yamada, K. Tomishige, *Environ. Sci. Technol.* 36 (2002) 4476-4481.
- [14] R. Zhang, R.C. Brown, A. Suby and K. Cummer, *Energy Convers. Manage.* 45 (2004) 995-1014.
- [15] P. Barbaro, C. Bianchini, Catalysis for sustainable Energy Production, 2009, WILEY-VCH Verlag GmbH & Co. KGaA, Weinheim
- [16] V. Goltsov, T. N. Veziroglu, L. F. Goltsova, *Int. J. Hydrogen Energy* 31 (2003) 153-159.
- [17] M. Ni, M. K. H. Leung, K. Sumathy, D. Y. C. Leung, *Int. J. Hydrogen Energy* 31 (2006) 1401-1412.
- [18] Y. Sun, J. Y. Cheng, *Bioresource Technol.* 83 (2002) 1-11.
- [19] B. S. Dien, M. A. Cotta, T. W. Jeffries, *Appl. Microbiol. Biotechnol.* 63 (2003) 258-266.
- [20] A. Haryanto, S. Fernando, N. Murali, S. Adhikari, *Energy & Fuels* 19 (2005) 2098-2106.
- [21] F. Marino, M. Boveri, G. Baronetti, M. Laborde, *Int. J. Hydrogen Energy* 29 (2004) 67-71.
- [22] H. V. Fajardo, L. Fernando, D. Probst, *Catal. Today* 306 (2006) 134-141.
- [23] T. Nishiguchi, T. Matsumoto, H. Kanai, K. Utani, Y. Matsumura, W. Shen, S. Imamura, *Appl. Catal. A: Gen.* 279 (2005) 273-277.
- [24] J. Llorca, P. R. de la Piscina, J. Sales, N. Homs, *Chem. Commun.* (2001) 641-642.

- [25] J. Llorca, N. Homs, J. Sales, P. R. de la Piscina, *J. Catal.* 209 (2002) 306-317.
- [26] C. B. Wang, C. C. Lee, J. L. Bi, J. Y. Siang, J. Y. Liu, C. T. Yeh, *Catal. Today* 146 (2009) 76-81.
- [27] J. Y. Liu, C. C. Lee, C. H. Wang, C. T. Yeh, C. B. Wang, *Int. J. Hydrogen Energy* 35 (2010) 4069-4075.
- [28] J. Xu, X. Zhang, R. Zenobi, J. Yoshinobu, Z. Xu, J. T. Yales Jr., *Surf. Sci.* 256 (1991) 288-300.
- [29] J. Kugai, S. Velu, C. Song, *Catal. Lett.* 101 (2005) 255-264.
- [30] F. Frusteri, S. Feni, L. Spadaro, V. Chiodo, G. Bonura, S. Donado, S. Cavallaro, *Catal. Commun.* 5 (2004) 611-615.
- [31] A. N. Fatsikostas, D. I. Kondarides, X. E. Verykios, *Catal. Today* 75 (2002) 145-155.
- [32] J. Sun, X. P. Qiu, F. Wu, *Int. J. Hydrogen Energy* 30 (2005) 437-445.
- [33] J. Comas, F. Marino, M. Laborde, N. Amadeo, *Chem. Eng. J.* 98 (2004) 61-68.
- [34] Y. Yang, J. X. Ma, F. Wu, *Int. J. Hydrogen Energy* 31 (2006) 877-882.
- [35] F. Frusteri, S. Freni, V. Chiodo, L. Spadaro, O. Di Blasi, G. Bonura, S. Cavallaro, *Appl. Catal. A: Gen.* 270 (2004) 1-7.
- [36] G. Zhou, L. Barrio, S. Agnoli, S. D. Senanayake, J. Evans, A. Kubacka, M. Estrella, J. C. Hanson, A. M. Arias, M. F. Garcia, J. A. Rodriguez, *Angew. Chem. Int. Ed.* 49 (2010) 9680-9684.
- [37] A. J. Akande, R. O. Idem, A. K. Dalai, *Appl. Catal. A: Gen.* 287 (2005) 159-175.
- [38] V. Klouz, V. Fierro, P. Denton, H. Katz, J. P. Lisse, S. Bouvot-Mauduit, C. Mirodatos, *J. Power Sources*, 105 (2002) 26-34.
- [39] H. Song, U. S. Ozkan, *J. Catal.* 261 (2009) 66-74.
- [40] H. Song, B. Mirkelamoglu, U. S. Ozkan, *Appl. Catal. A: Gen.* 382 (2010) 58-64.
- [41] A. Kaddouri, C. Mazzocchia, *Catal. Commun.* 5 (2004) 339-345.
- [42] S. D. Jones, L. M. Neal, H. E. Hagelin-Weaver, *Appl. Catal. B: Environ.* 84 (2008) 631-642.
- [43] S. Cavallaro, S. Freni, *Int. J. Hydrogen Energy* 21 (2006) 465-469.
- [44] B. Lorenzut, T. Montini, L. de Rogatis, P. Canton, A. Benedetti, P. Fornasiero, *Appl. Catal. B: Environ.* 101 (2011) 397-408.
- [45] D. K. Liguras, D. I. Kondarides, X. E. Verykios, *Appl. Catal. B: Environ.* 43 (2003) 345-354.
- [46] F. Aupretre, C. Descorme, D. Duprez, *Catal. Commun.* 3 (2002) 263-267.
- [47] F. Aupretre, C. Descorme, D. Duprez, D. Casanave, D. Uzio, *J. Catal.* 233 (2005) 464-477.

- [48] W. Cai, F. Wang, E. Zhan, A. C. Van Veen, C. Mirodatos, W. Shen, *J. Catal.* 257 (2008) 96-107.
- [49] T. Yamazaki, N. Kikuchi, M. Katoh, T. Hirose, H. Saito, T. Yoshikawa, M. Wada, *Appl. Catal. B: Environ.* 99 (2010) 81-88.
- [50] F. Frusteri, S. Freni, L. Spadaro, V. Chiodo, G. Bonura, S. Donato, *Catal. Commun.* 5 (2004) 611-615.
- [51] A. Erdohelyi, J. Rasko, T. Kecskes, M. Toth, M. Domok, K. Baan, *Catal. Today* 116 (2006) 367-372.
- [52] A. C. W. Koh, L. Chen, W. K. Leong, T. P. Ang, B. F. G. Johnson, T. Khimyak, J. Lin, *Int. J. Hydrogen Energy* 34 (2009) 5691-5703.
- [53] S. M. de Lima, A. M. Silva, I. O. da Cruz, G. Jacobs, B. H. Davis, L. V. Mattos, F. B. Noronha, *Catal. Today* 138 (2008) 162-168.
- [54] G. Rabenstein, V. Hacker, *J. Power Sources* 185 (2008) 1293-1304.
- [55] K. Vasudeva, N. Mitra, P. Umasankar, S. C. Dhingra, *Int. J. Hydrogen Energy* 21 (1996) 13-18.
- [56] I. Fishtik, A. Alexander, R. Datta, D. Geana, *Int. J. Hydrogen Energy* 25 (2000) 31-45.
- [57] P. Y. Sheng, A. Yee, G. A. Bowmaker, H. Idriss, *J. Catal.* 208 (2002) 393-403.
- [58] A. Yee, S. J. Morrison, H. Idriss, *J. Catal.* 191 (2000) 30-45.
- [59] J. Llorca, N. Homs, P. R. de la Piscina, *J. Catal.* 227 (2004) 556-560.
- [60] P. D. Vaidya, A. E. Rodrigues, *Ind. Eng. Chem. Res.* 45 (2006) 6614-6618.
- [61] A. Akande, A. Aboudheir, R. Idem, A. Dalai, *Int. J. Hydrogen Energy* 31 (2006) 1707-1715.
- [62] P. V. Mathure, S. Ganguly, A. V. Patwardhan, R. K. Saha, *Ind. Eng. Chem. Res.* 46 (2007) 8471-8479.
- [63] C. Graschinsky, M. Laborde, N. Amadeo, A. L. Valant, N. Bion, F. Epron, D. Duprez, *Ind. Eng. Chem. Res.* 49 (2010) 12383-12389.
- [64] P. Biswas, D. Kunzru, *Chem. Eng. J.* 136 (2008) 41-49.
- [65] J. M. Guil, N. Homs, J. Llorca, P. R. de la Piscina, *J. Phys. Chem. B* 109 (2005) 10813-10819.
- [66] F. Frusteri, S. Freni, V. Chiodo, S. Donato, G. Bonura, S. Cavallaro, *Int. J. Hydrogen Energy* 31 (2006) 2193-2199.
- [67] H. Roh, A. Platon, Y. Wang, D. L. King, *Catal. Lett.* 110 (2006) 1-6.
- [68] S. M. de Lima, A. M. Silva, U. M. Graham, G. Jacobs, B. H. Davis, L. V. Mattos, F. B. Noronha, *Appl. Catal. A: Gen.* 352 (2009) 95-113.
- [69] A. N. Fatiskostas, X. E. Verykios, *J. Catal.* 225 (2004) 439-452.

- [70] S. M. de Lima, I. O. da Cruz, G. Jacobs, B. H. Davis, L. V. Mattos, F. B. Noronha, *J. Catal.* 257 (2008) 356-368.
- [71] A. M. da Silva, L. O. O. da Costa, K. R. Souza, L. V. Mattos, F. B. Noronha, *Catal. Commun.* 11 (2010) 736-740.
- [72] W. Cai, F. Wang, C. Daniel, A. C. van Veen, Y. Schuurman, C. Descorme, H. Provendier, W. Shen, C. Mirodatos, *J. Catal.* 286 (2012) 137-152.
- [73] S. Cavallaro, V. Chiodo, S. Freni, N. Mondello, F. Frusteri, *Appl. Catal. A: Gen.* 249 (2003) 119-128.
- [74] M. Araque, J. C. Vargas, Y. Zimmermann, A.-C. Roger, *Int. J. Hydrogen Energy*, 36 (2011) 1491–1502.
- [75] A. L. Alberton, M. M. V. M. Souza, M. Schmal, *Catal. Today* 123 (2007) 257-264.
- [76] J. R. Hansen, C. H. Christensen, J. Sehested, S. Helveg, J. R. Rostrup-Nielsen, S. Dahl, *Green Chem.* 9 (2007) 1016-1021.
- [77] A. J. Vizcaino, A. Carrero, J. A. Calles, *Int. J. Hydrogen Energy* 32 (2007) 1450-1461.
- [78] H. Wang, Y. Liu, L. Wang, Y. N. Qin, *Chem. Eng. J.* 145 (2008) 25-31.
- [79] E. B. Pereira, N. Homs, S. Marti, J. L. G. Fierro, P. R. de la Piscina, *J. Catal.* 257 (2008) 206-214.
- [80] S. M. de Lima, A. M. da Silva, L. O. O. da Costa, U. M. Graham, G. Jacobs, B. H. Davis, L. V. Mattos, F. B. Noronha, *J. Catal.* 268 (2009) 268-281.
- [81] I. J. I. Coleman, W. Epling, R. R. Hudgins, E. Croist, *Appl. Catal. A: Gen.* 363 (2009) 52-63.
- [82] A. Kazama, Y. Sekine, K. Oyama, M. Matsukata, E. Kikuchi, *Appl. Catal. A: Gen.* 383 (2010) 96-101.
- [83] T. Montini, L. de Rogatis, V. Gombac, P. Fornasiero, M. Graziani, *Appl. Catal. B: Environ.* 71 (2007) 125-134.
- [84] A. Platon, H. Roh, D. L. King, Y. Wang, *Top Catal.* 46 (2007) 374-379.
- [85] J. M. Guil, N. Homs, J. Llorca, P. R. de Piscina, *J. Phys. Chem. B* 109 (2005) 417-426.
- [86] B. Zhang, X. Tang, Y. Li, Y. Xu, W. Shen, *Int. J. Hydrogen Energy* 32 (2007) 2367-2373.
- [87] B. Zhang, W. Cai, Y. Li, Y. Xu, W. Shen, *Int. J. Hydrogen Energy* 33 (2008) 4377-4386.
- [88] B. Zhang, X. Tang, Y. Li, W. Cai, Y. Xu, W. Shen, *Catal. Commun.* 7 (2006) 367-372.
- [89] W. Cai, F. Wang, C. Daniel, A. C. van Veen, Y. Schuurman, C. Descorme, H. Provendier, W. Shen, C. Mirodatos, *J. Catal.* 286 (2012) 137-152.
- [90] W. Cai, B. Zhang, Y. Li, Y. Xu, W. Shen, *Catal. Commun.* 8 (2007) 1588-1594.

Chapter II Experimental: catalysts preparation and characterization techniques

This chapter presents the methods for catalyst preparation, the main techniques of characterization and the experimental protocols.

II.1. Catalysts preparation

II.1.1. Preparation of the 2 wt.% Ir/CeO₂ catalyst

As indicated in Chapter I, this formula was selected on the basis of previous works demonstrating the efficiency of such a material [1]. It will serve as reference catalyst all over the present study.

The CeO₂ support was prepared by precipitation of ammonium cerium (IV) nitrate with urea in aqueous solution. 60 g of (NH₄)₂Ce(NO₃)₆ and 200 g of CO(NH₂)₂ were dissolved into 2000 mL of water and the mixture was gradually heated to 363 K under stirring and maintained at this temperature for 5 h. A light yellow powder was progressively formed. After filtration and thorough washing with hot water and ethanol, the obtained solid was dried at 373 K for 12 h, and calcined at 673 K for 5 h in air, to form the basic CeO₂ powder material further used as catalyst support.

The Ir/CeO₂ catalyst, with an Ir nominal loading of 2 wt.%, was prepared via the deposition-precipitation method. 5 g of CeO₂ powder was dispersed into 500 mL of aqueous solution containing 0.27 g of H₂IrCl₆·6H₂O at room temperature. The mixture was then heated to 348 K under stirring, and 100 mL of a 0.2 mol/L Na₂CO₃ aqueous solution were gradually added with a final pH value of 10. The slurry was further aged at 348 K for 3 h. After filtration and thorough washing with hot water and ethanol, the resulting solid was dried at 373 K overnight and calcined at 673 or 923 K for 5 h in air.

II.1.2. Preparation of the 2 wt.% Ir/Ce_{0.9}Pr_{0.1}O₂ catalyst

This catalyst was prepared in order to improve the stability of the reference system, on the basis of the literature analysis and prescreening not reported here.

A commercially available Ce_{0.9}Pr_{0.1}O₂ sample (Rhodia Electronics and Catalysis, La Rochelle) was calcined at 673 K for 5 h in air. The Ir/Ce_{0.9}Pr_{0.1}O₂ catalyst with an Ir nominal loading of 2 wt.% was prepared via deposition-precipitation, as described above. The final sample was dried at 373 K overnight and calcined in air at 673 K for 5 h.

II.1.3. Preparation of the 2 wt.% Ir/CeO₂-nanorods catalyst

This catalyst was prepared in order to test the effect of shaping/structuring on the reference system.

The CeO₂ nanorods were synthesized by the hydrothermal method [2]. 0.86 g of Ce(NO₃)₃·6H₂O and 16 g of NaOH were dissolved into 80 mL distilled water. The solution was then transferred to an autoclave (100 mL) and gradually heated to 373 K and kept at this temperature for 24 h. The obtained solid was washed with hot water and ethanol. Then it was dried at 373 K overnight and finally calcined in static air at 673 K for 5 h. The sample was denoted CeO₂-NR.

The Ir/CeO₂-NR catalyst with an Ir nominal loading of 2 wt.% was also prepared by deposition-precipitation as described above.

II.2. Catalytic measurements and set-ups

II.2.1. Catalytic performance

Steam reforming of ethanol was conducted in a continuous-flow fixed-bed quartz reactor (8 mm internal diameter) at atmospheric pressure (Figure II-1). 100 mg of catalyst (40–60 mesh) were loaded in between two layers of quartz wool plugs. Before the reaction, the catalyst was reduced under 10% H₂/He mixture (50 mL·min⁻¹) at 673 K for 1 h. The flow was then turned to pure He (30 mL·min⁻¹) and the temperature was set at 673-923 K. The ethanol/water solution (1/3 molar ratio) was fed via a micro-pump to the pipeline and the feed pipeline was heated to 443 K for the vaporization of ethanol and water before the mixture pass through the

reactor. The gas hourly space velocity (GHSV) was 18,000 mL/(gh) without dilution, in which the flow rate of ethanol was 7.5 mL/min. After the reforming reaction, the gas product was mixed with N₂ for GC analysis.

The effluent from the reactor was analyzed by on-line gas chromatography (GC, Agilent 6890). H₂, CO, and CO₂ were separated on a packed column (HaySep D) and analyzed by a thermal conductivity detector (TCD). Hydrocarbons and oxygenates were separated with a capillary column (INNOWAX) and analyzed with a flame ionization detector (FID).

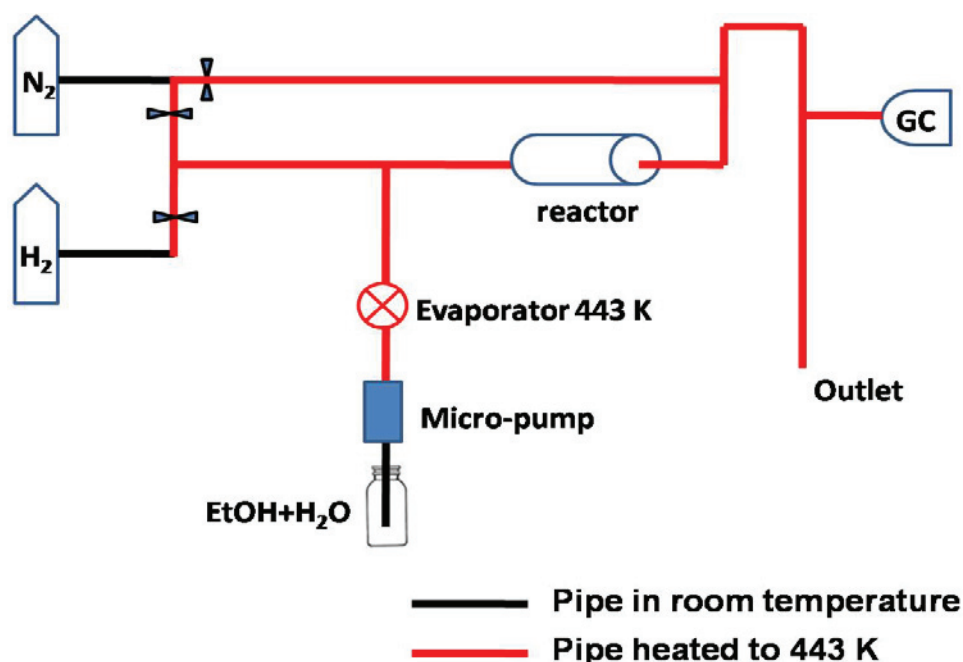


Figure II-1 Setup for the catalytic testing with a fixed-bed reactor (Lab at DICP).

II.2.2. Calculations

The ethanol conversion is calculated by the following equation:

$$X_{\text{EtOH}} (\%) = \frac{n_{\text{EtOH}}^{\text{in}} - n_{\text{EtOH}}^{\text{out}}}{n_{\text{EtOH}}^{\text{in}}} \times 100 \quad (\text{Eq II.1})$$

where $n_{\text{EtOH}}^{\text{in}}$ and $n_{\text{EtOH}}^{\text{out}}$ are the inlet and outlet molar flow of ethanol, respectively.

The outlet molar gas composition (products and unconverted ethanol) was calculated by excluding water, that is, a dry-based gas composition. It will be named "selectivity" for each of the reaction product, following the formula:

$$S_X(\%) = \frac{n_X^{\text{out}}}{\sum n_X^{\text{out}}} \times 100 \quad (\text{Eq II.2})$$

where n_X^{out} is the molar flow rate of X at the outlet of the reactor.

In all the experiments reported in this work, the C and H mass balance was kept within 95-105%.

II.2.3. Kinetic experiments

The kinetic experiments were carried out in the temperature range of 773-923 K and at a total pressure of 1 atm in a fixed-bed reactor (Figure II-2). The amount of catalyst was varied in the range 10-30 mg (80-100 mesh) and was diluted with 300 mg of inert SiC with the same size to avoid hot spots. The homogeneous mixture of the catalyst and SiC was placed in the center of the reactor (6 mm internal diameter, 180 mm length). The desired ethanol-to-water molar ratio was fed to the reactor using a high performance liquid chromatography (HPLC) pump. Nitrogen was used as a carrier gas. Water and ethanol were vaporized at 443 K, mixed with the nitrogen and introduced into the reactor. The evaporator and the reactor were placed in a hot box heated at 443 K before the reaction was performed. The ethanol and water flow rate was varied from 20 to 175 mL/min, and the nitrogen flow rate was varied in the range 30 to 190 mL/min.

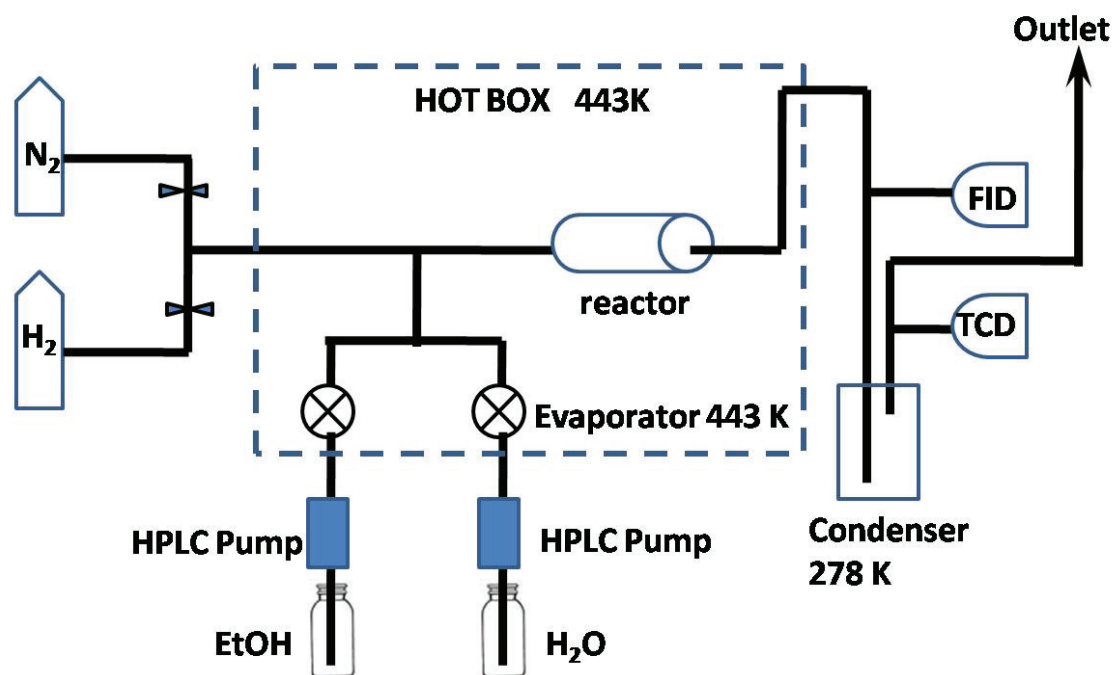


Figure II-2 Setup for the kinetic study in a fixed-bed reactor (Lab at IRCELYON).

The products were first analyzed on-line with a FID Varian gas chromatography apparatus to determine the amount of organic compounds (acetaldehyde, acetone and ethanol). Then the products passed through a condenser at 278 K to collect water and organic components. The uncondensed gases (H_2 , CO , CO_2 and CH_4) were then analyzed with a gas chromatograph equipped with a TCD. Data were collected and recorded every 20 min.

The contact time (t_c) is defined as the ratio between the mass of catalyst and the molar flow of the inlet ethanol:

$$t_c = \frac{W_{\text{cat}}}{F_{\text{EtOH}_{\text{in}}}} \quad (\text{Eq II.3})$$

From the curves of the ethanol conversion as a function of contact time, for different ethanol molar fractions, the reaction rates were calculated for each initial composition as follows [3]:

$$-r_{\text{EtOH}} = \frac{dX_{\text{EtOH}}}{d(W_{\text{cat}} / F_{\text{EtOH}_{\text{in}}})} \quad (\text{Eq II.4})$$

where X_{EtOH} is the conversion of ethanol, $F_{\text{EtOH}_{\text{in}}}$ is the flow rate of ethanol in the feed in mol/s, W_{cat} is the mass of catalyst in g, and $-r_{\text{EtOH}}$ is the reaction rate of ethanol in mol/(g s).

In order to solve the equation, the experimental data were fitted to an exponential function:

$$X_{\text{EtOH}} = 1 - e^{-k \cdot (W_{\text{cat}} / F_{\text{EtOH}})} \quad (\text{Eq II.5})$$

or a linear equation:

$$-\ln(1 - X_{\text{EtOH}}) = k \cdot (W_{\text{cat}} / F_{\text{EtOH}}) \quad (\text{Eq II.6})$$

II.3. Catalyst characterizations

II.3.1. Chemical analysis (ICP)

The actual loading of Ir was analyzed with inductively coupled plasma optic emission spectrometry (ICP-OES) using a PLASMA-SPEC-II instrument (Horiba JOBIN YVON). An appropriate amount of sample was dissolved into aqua regia, and the resulting mixture was diluted with nitric acid to meet the detection range of the instrument. The obtained solution was then vaporized in the plasma of the monochromatic spectrophotometer and the emitted wavelengths, which were characteristics of the elements, were quantitatively analyzed.

II.3.2. Specific surface area (BET)

The specific surface areas were measured before and after the catalytic tests using BET method. Before the measurement, the sample was first degassed at 573 K for 3 h under vacuum. Then nitrogen adsorption-desorption isotherms were recorded at 77 K using an ASAP2020 instrument (Micromeritics). The specific surface area was calculated based on the multipoint Brunauer-Emmett-Teller (BET) analysis of the nitrogen adsorption isotherm.

For the BET measurement of the reduced catalysts, the fresh samples were reduced under a 10%H₂/He mixture at 673 K for 3 h. After the temperature was decreased to room temperature, the reduced catalysts were then transferred without contact with air to the vacuum setup for outgassing before BET measurements.

II.3.3. X-ray diffraction (XRD)

X-ray Power diffraction (XRD) patterns were recorded using a D/MAX-RB diffractometer (Rigaku) with a Ni-filtered Cu K_α radiation operated at 40 kV and 100 mA. The mean crystallite size of the sample was calculated from the strongest diffraction peak according to the Scherrer equation [4].

II.3.4. X-ray photoelectron spectroscopy (XPS)

X-ray photoelectron spectra were recorded on a VG Escalab spectrometer using Al K α (1486.6 eV) source. The X-ray source was operated at an accelerating voltage of 10 kV and a power of 150 W. For *in-situ* measurement, the samples were initially reduced with H₂ at 673 K for 30 min in the pretreatment chamber. The charging effect was corrected by referencing the binding energy of C_{1s} at 284.6 eV, and the spectra were curve-fitted by a Gaussian-Lorentzian procedure after subtracting the background.

II.3.5. Raman spectra

Raman spectra of the samples were obtained on a HR Raman spectrometer (Horiba-Jobin Yvon). The 514.53 nm exciting line of a 2018 RM Ar⁺ laser (Spectra Physics) was focused using a $\times 100$ long working distance objective with a power of 0.95 mW.

II.3.6. Temperature-programmed reduction (TPR)

Hydrogen temperature programmed reduction (TPR) of the catalysts was performed with an Auto Chem II chemisorption analyzer by using a thermal conductive detector (TCD). 100 mg sample were loaded and pretreated with Ar (50 mL/min) at 573 K for 1 h. After cooling down to 233 K, a 10%H₂/Ar (50 mL/min) mixture was introduced and the temperature was raised to 1073 K at a rate of 10 K/min. Hydrogen consumption versus time or temperature was monitored with a TCD.

II.3.7. Oxygen storage capacity (OSC)

Oxygen storage capacity (OSC) of the samples was measured after the above H₂-TPR process. The samples were firstly cooled down to 673 K under Ar flow (50 mL/min) and kept at 673 K for 1 h. Then O₂ was periodically injected to the reduced sample until it was saturated (judged from the constant peak area in the final runs). The consumption of oxygen was calculated according to the difference in areas between the peaks at saturation and the peaks before saturation.

II.3.8. Hydrogen chemisorption

Hydrogen chemisorption was performed using the dynamic pulse method with the same equipment at low temperature to avoid spillover phenomenon [5-6]. 100 mg of a given sample were reduced with a 10% H_2 /Ar mixture (50 mL/min) at 673 K for 1 h. After that the sample was purged with Ar (50 mL/min), and cooled down to 183 K using a CycroCooler II apparatus to inject liquid nitrogen. Then hydrogen was pulsed until saturation. Subsequently, the sample was flushed for 10 min with Ar to remove the physically adsorbed hydrogen molecules and hydrogen was pulsed again until saturation. The amount of chemisorbed hydrogen was then derived, the mean size and dispersion of Ir particles were calculated accordingly. The ratio of Ir/H = 1 was considered for calculation of Ir dispersion

$$D_{Ir}(\%) = \frac{2n_{H_2} * M_{Ir}}{m_{cat} * \omega_{Ir}} \times 100 \quad (\text{Eq II.7})$$

where n_{H_2} (mol) is the amount of adsorbed H_2 , M_{Ir} (g/mol) is molar weight of Ir, m_{cat} (g) is the mass of samples used for hydrogen chemisorption and ω_{Ir} (%) is the weight fraction of the catalyst determined by ICP.

The Ir size was calculated based on [7]:

$$d_{Ir} = \frac{6M_{Ir}}{N_A \cdot \rho_{Ir} \cdot \sigma_{Ir} \cdot D_{Ir}} \quad (\text{Eq II.8})$$

where d_{Ir} (nm) is the size of Ir, N_A is the Avogadro constant ($6.02 \times 10^{23} \text{ mol}^{-1}$), ρ_{Ir} is the density of Ir (22.5 g/cm^3), and σ_{Ir} is the occupied area of a Ir atom ($\sim 0.01 \text{ nm}^2$).

II.3.9. Temperature-programmed desorption of oxygen (O₂-TPD)

Temperature programmed desorption of oxygen (O₂-TPD) was conducted with a fixed-bed reactor connected to a mass spectrometer (Omistar, Blazer). 100 mg of a given sample were treated at 573 K for 1 h with a 10% O_2 /Ar mixture (50 mL/min) and then cooled down to room temperature. After being purged with Ar (45 mL/min) for 30 min, the samples were then heated to 1073 K at a ramp of 10 K/min, and the desorption of oxygen ($m/e=32$) was monitored with the mass spectrometer.

II.3.10. Temperature-programmed oxidation (TPO) on aged catalysts

Temperature programmed oxidation (TPO) experiments were conducted on the aged catalysts after a given period on SR stream, by using the same mass spectrometer (Omistar, Blazer). The used catalysts were loaded and heated up to 573 K at a rate of 10 K/min under Ar flow. After being cooled down to room temperature, the catalysts were heated to 1073 K at a ramp of 5 K/min under the flow of a 5%O₂/Ar mixture (50 mL/min). The effluent resulting from the combustion of the carbon deposits was analyzed by the on-line mass spectrometer. CO (m/e=28), CO₂ (m/e=44) and O₂ (m/e=32) were monitored as a function of time and temperature.

II.3.11. Transmission electron microscopy (TEM)

The catalysts were characterized using High Resolution Transmission Electron Microscopy (HRTEM), in order to determine their homogeneity, the dispersion and the mean size of the ceria and metal particles. The measurements were carried out on a Philips Tecnai G²20 microscope operating at 300 kV. Samples were prepared by suspending the catalyst in ethanol and stirring in an ultrasonic bath for de-agglomeration of the particles. Several droplets of the suspended catalyst were deposited to a copper mesh grid with lacy carbon film and the ethanol evaporated rapidly.

References

- [1] W. Cai, F. Wang, E. Zhan, A. C. Van Veen, C. Mirodatos, W. Shen, *J. Catal.* 257 (2008) 96-107.
- [2] N. Ta, M. Zhang, J. Li, H. Li, Y. Li, W. Shen, *Catal. Today* 148 (2009) 179-183.
- [3] C. Graschisky, M. Laborde, N. Amadeo, A. Le Valant, N. Bion, F. Epron, D. Duprez, *Ind. Eng. Chem. Res.* 49 (2010) 12383-12389.
- [4] B. D. Cullity, *Elements of X-Ray Diffraction*, 2nd ed., Addison-Wesley, Menlo Park, CA, 1978, p102.
- [5] A. Birot, F. Epron, C. Descorme, D. Duprez, *Appl. Catal. B: Environ.* 79 (2008) 17-25.
- [6] Y. Madier, PhD thesis of University of Poitiers (1999)
- [7] H. Chen, H. Yu, F. Peng, H. Wang, J. Yang, M. Pan, *J. Catal.* 269 (2010) 281-290.

Chapter III Kinetic studies of steam reforming of ethanol over an Ir/CeO₂ catalyst

III.1. Introduction

Steam reforming of ethanol is a strong endothermic and complex reaction. Though aiming at producing essentially syngas (carbon monoxide, carbon dioxide and hydrogen), other major products like ethylene, acetaldehyde, and acetone are formed as well, depending on the operating conditions. Thus, ethylene and acetaldehyde are produced at low temperature due to dehydration and dehydrogenation of ethanol, respectively. Acetone can be produced by condensation of acetaldehyde. The product distribution is therefore highly depending on the catalytic system, which will bring the system more or less close to the thermodynamic equilibrium. This large distribution of products reflects or derives from a large number of potential pathways occurring on different active phases of the selected catalysts (generally bi-functional). This complexity makes the mechanism of steam reforming of ethanol reaction remains a matter of discussion so far. Kinetic models are therefore relative scarce. Akande et al. [1] have studied the kinetic behaviour of steam reforming of crude bio-ethanol over a co-precipitated Ni/Al₂O₃ catalyst in the temperature range of 593-793 K. Three basic steps based on an Eley-Rideal mechanism were applied in the derivation of the mechanistic rate equation. By fitting values of kinetic constants, they found that the dissociative adsorption of ethanol on the active sites was the rate determining step. However, the model didn't explain the formation of intermediates species such as acetaldehyde, acetic acid and diethyl-ether and carbon. Vaidya et al. [2] studied the reaction kinetics over a commercial 1% Ru/Al₂O₃ catalyst in the temperature range of 873-973 K at atmosphere pressure. They found the reaction order of one with respect to ethanol and the activation energy was 96 kJ/mol.

This chapter will present a preliminary kinetic study carried out on the model Ir/CeO₂ catalyst, based on our knowledge of the reaction mechanism gained throughout this PhD thesis. A systematic study of the main kinetic variables (temperature, molar ratio and partial

pressure) has been performed and attempts to fit these data with a simple power law rate expression.

III.2. Preliminary kinetic investigation of steam reforming of ethanol

III.2.1. Gas phase mass transfer resistance

In order to study the kinetics of solid-catalyzed gas phase reactions, the reaction rates must be measured when the intrinsic chemical reaction rate controls the overall reaction rate, i.e., in the absence of heat and mass transfer limitations. This was done by keeping the contact time constant, the molar ratio of steam to ethanol, the particle size of catalyst and the temperature and by changing the flow rate of reactants as well as the mass of the catalyst to measure the ethanol conversion. As seen in Figure III-1, the ethanol conversion stays around 15% within the investigated flow rate range, demonstrating the absence of gas phase mass transfer resistance.

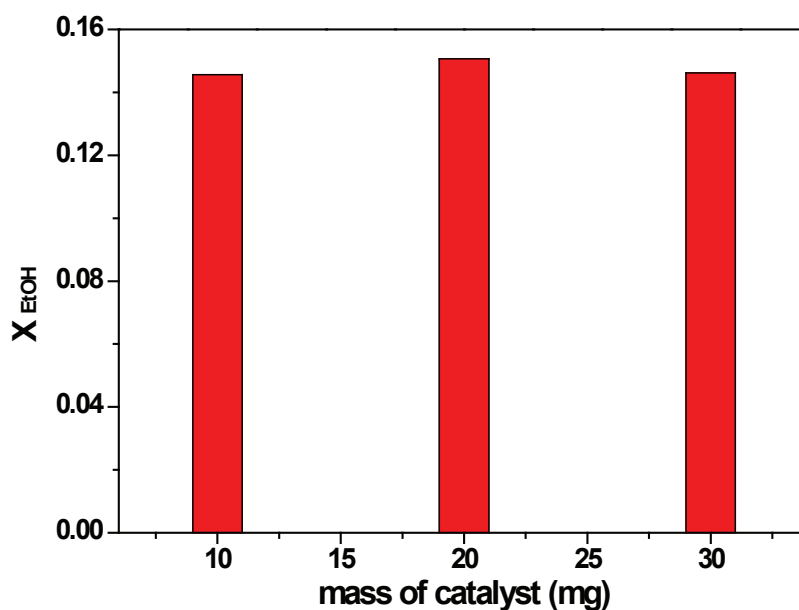


Figure III-1 gas phase mass transfer resistance of the Ir/CeO₂ catalyst.

Reaction conditions: Mass of catalyst: 10-30 mg, SiC: 300 mg, Particle size: 80–100 mesh, T: 773 K, Molar ratio: H₂O:EtOH:N₂ = 3:1:6, GHSV=300000 mL/(gh).

III.2.2. Intra-particle mass transfer resistance

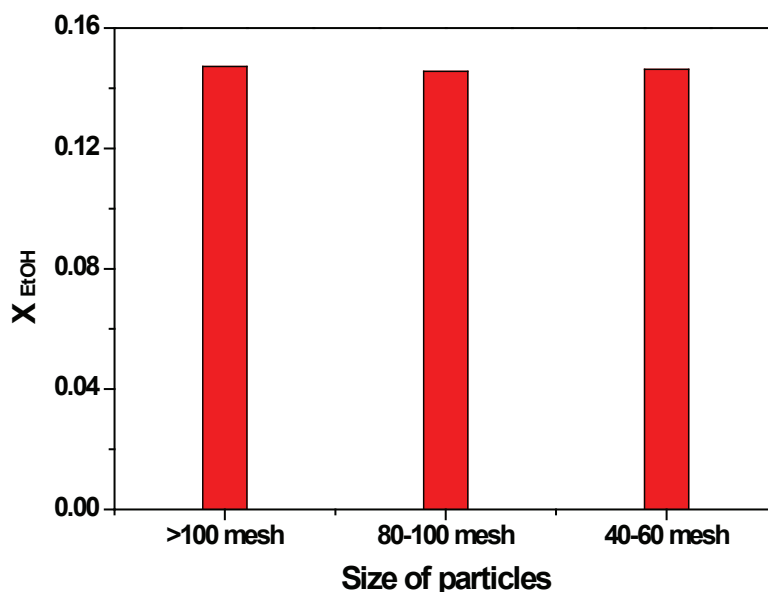


Figure III-2 Intra-particle mass transfer resistance of the Ir/CeO₂ catalyst.

Reaction conditions: Mass of catalyst: 10 mg, SiC: 300 mg, T: 773 K, Molar ratio: H₂O:EtOH:N₂ = 3:1:6, Total flow rate: 50 mL/min, GHSV=300000 mL/(gh).

The intra-particle mass-transfer resistance should also be avoided for intrinsic kinetic measurements. To check its possible occurrence, the particle size is varied between 40 to 100 mesh at a given temperature, molar ratio of water to ethanol and contact time. As seen in Figure II-2, the identical ethanol conversion at various particle sizes revealed that there was no intra-particle mass-transfer resistance under the selected operating conditions.

In addition, in order to eliminate the axial dispersion, the $D_{tube}/D_{particle} > 10$ and $L_{bed}/D_{particle} > 50$ criteria were also satisfied [3].

As similar conversions of ethanol were obtained for particle size diameter ranging from 40 to 100 meshes, the catalyst with particle size in the range of 80-100 mesh (180-150 μ m) was selected for all the kinetic experiments.

III.2.3. Temperature gradient of the catalyst bed

A direct access to intrinsic kinetics also requires the absence of axial temperature gradients (flow direction), thus ensuring isothermal conditions. Figure III-3 presents the temperature gradient profiles along the catalyst bed under different temperatures. The rather flat

temperature profiles indicated that isothermal conditions were reached under the investigated conditions.

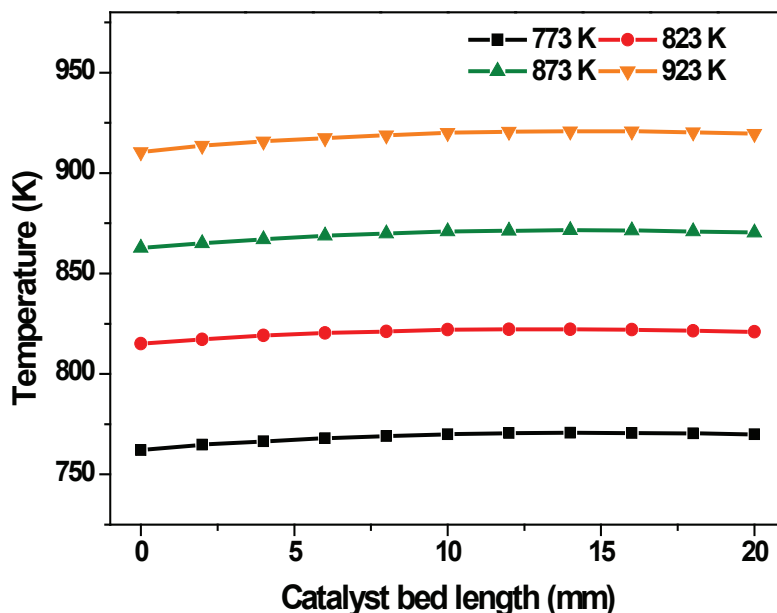


Figure III-3 Temperature gradient profiles of catalyst bed length.

Reaction conditions: Mass of catalyst: 10 mg, SiC: 300 mg, Molar ratio: H₂O:EtOH:N₂ = 3:1:6, Total flow rate: 50 mL/min, GHSV=300000 mL/(gh).

III.2.4. Time on stream study

Though the various deactivation processes will be thoroughly analyzed in a dedicated chapter, a very preliminary effect of deactivation on the reaction rates measured at 773 K was checked as reported in Figure III-4. The conversion of ethanol was firstly decreased from 20% to 15% after 2.5 h, and then kept stable enough to measure reliable reaction rates. The decreased conversion of ethanol in the initial 2 h on stream will be assigned to a structuring effect of the fresh catalyst, involving essentially a decrease of BET surface due to a loss of porosity and the coverage of various reacting intermediates and hydroxyl groups. Hence the kinetic data were collected after 2.5 h on stream, after reaching a pseudo steady state, compatible with a kinetic study disconnected from ageing phenomena.

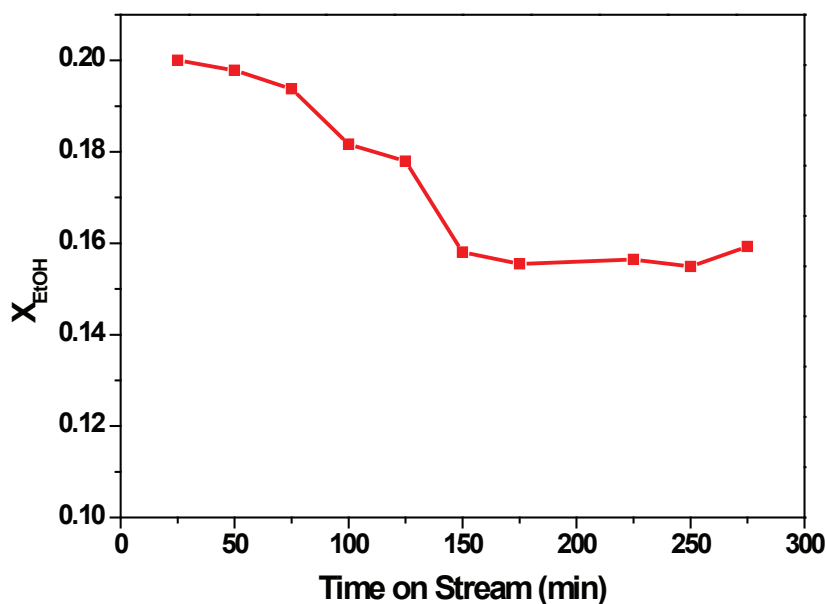


Figure III-4 Time on stream study of the Ir/CeO₂ catalyst.

Reaction conditions: Mass of catalyst: 10 mg, SiC: 300 mg, Molar ratio: H₂O:EtOH:N₂ = 3:1:6, Total flow rate: 50 mL/min, W_{cat}/F_{EtOH} = 577 g/(mol/s), T=773 K.

III.3. Influence of reaction conditions on the kinetics

III.3.1. Effects of temperature and space velocity

Figure III-5 shows the conversion of ethanol and the main gas products yield as a function of temperature at a given W/F_{EtOH} of 577 s.g/mol. The conversion of ethanol was about 3% at 773 K, and it was progressively increased to 11% at 923 K. CO₂ and H₂ were the main products over the whole temperature range, with only minor CO and CH₄ below 873 K. CO and CH₄ increase significantly at higher temperature while CO₂ goes through a maximum. Note also that only traces of CH₃CHO were detected at low temperature, probably due to the uncertainty for measuring this by-product at low conversion. A slightly higher amount is detected at higher temperature.

These results indicate that the main reactions to consider over this range of temperature are decomposition of ethanol, steam reforming of methane and the WGS/RWGS reactions:





The dehydrogenation of ethanol to acetaldehyde further decomposed into CO and methane could be considered as well as side reactions:



At 923 K, the RWGS reaction is favored, explaining the decreased production of CO₂ at the benefits of CO:

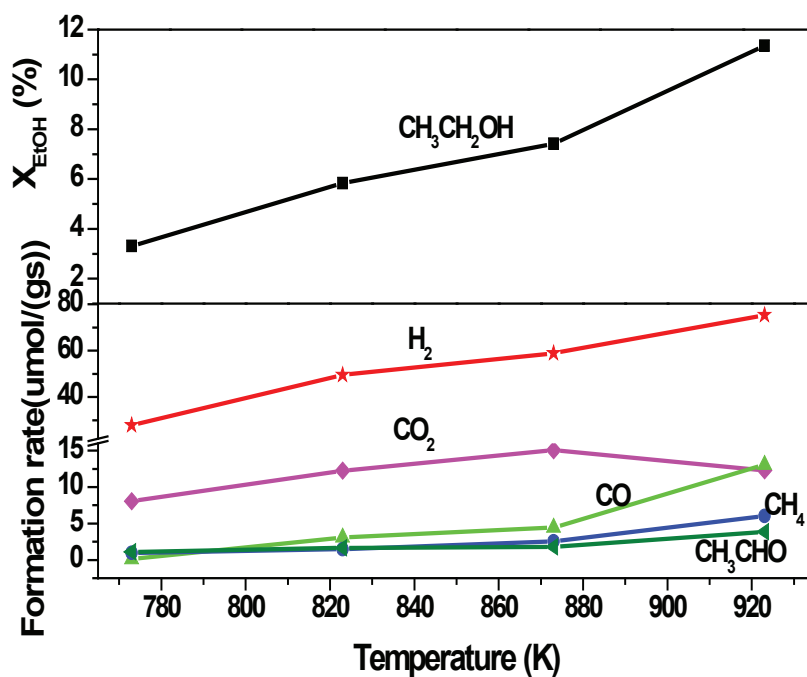


Figure III-5 Temperature performance on steam reforming of ethanol.

Reaction conditions: Mass of catalyst: 10 mg, SiC: 300 mg, Molar ratio: H₂O:EtOH:N₂ = 3:1:6, W/F_{EtOH} = 2884 g/(mol/s).

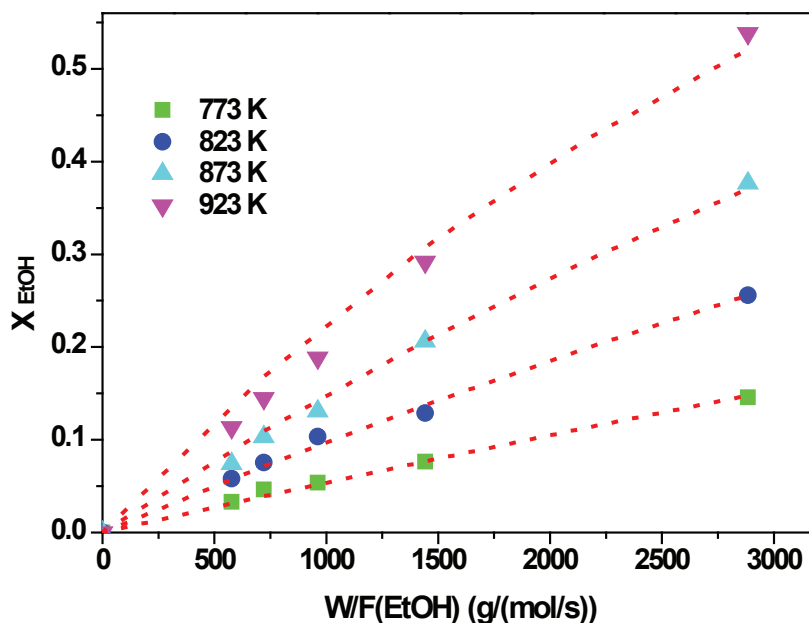


Figure III-6 Effects of W/F_{EtOH} on steam reforming of ethanol at different temperatures.

Reaction conditions: Mass of catalyst: 10 mg, SiC: 300 mg, Molar ratio: H₂O:EtOH:N₂ = 3:1:6.

Figure III-6 shows the conversion of ethanol as a function of contact time W/F_{EtOH} within 773-923 K. At 773 K, the conversion of ethanol was increased from 3.3% to 15% with an increasing contact time from 577 to 2885 g/(mol/s); In the meantime, the conversion of ethanol was increased from 3.3% to 11% when the temperature was increased from 773 to 923 K at a constant contact time of 577 g/(mol/s). This result was indeed expected for an activated reaction in a kinetic regime.

The initial rates of ethanol were calculated from integral data by numerical differentiation of the X_{EtOH} versus W/F_{EtOH} curves, extrapolated at zero contact time [4]:

$$-r_{\text{EtOH},0} = \frac{dX_{\text{EtOH}}}{d\left(\frac{W_{\text{cat}}}{F_{\text{EtOH}}}\right)} \Bigg|_{\substack{W_{\text{cat}} \rightarrow 0, X_{\text{EtOH}} \rightarrow 0}} \quad (\text{EqIII.15})$$

From the Arrhenius plot (Figure III-7), the activation energy of steam reforming of ethanol over the Ir/CeO₂ catalyst was calculated to be 58 kJ/mol.

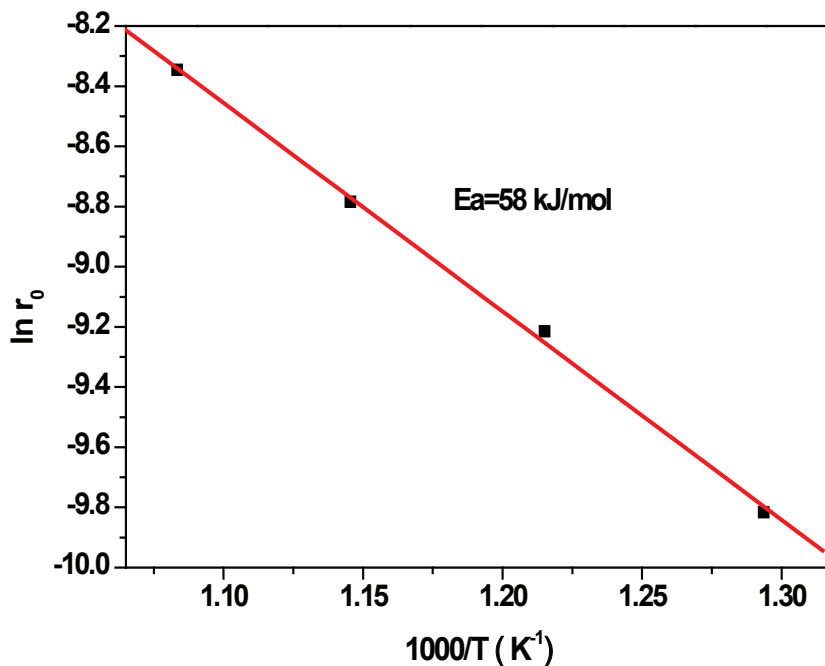


Figure III-7 Arrhenius plot of steam reforming of ethanol over the Ir/CeO₂ catalyst.

III.3.2. Effect of water/ethanol (S/E) molar ratio

The effect of water/ethanol molar ratio (S/E) on the conversion of ethanol at different contact time and the product yield in steam reforming of ethanol at 823 K is shown in Figure III-8. The result brings evidence that the conversion of ethanol was increased upon increasing S/E at constant contact time, and was also progressively increased upon increasing contact time at constant S/E. The above trends reveal that the addition of water could promote the conversion of ethanol in the water/ethanol molar ratio range of 1 to 6. The product yield of steam reforming of ethanol at a contact time of 577 g/(mol/s) indicated that the production of H₂ and CO₂ was increased upon increasing the water/ethanol molar ratio. The higher production of H₂ and CO₂, and the much lower production of CH₄ and CO indicated that the methane steam reforming (EqIII.2) and the water gas shift reaction (EqIII.3) were much favored by the addition of water, indeed as expected from the thermodynamics.

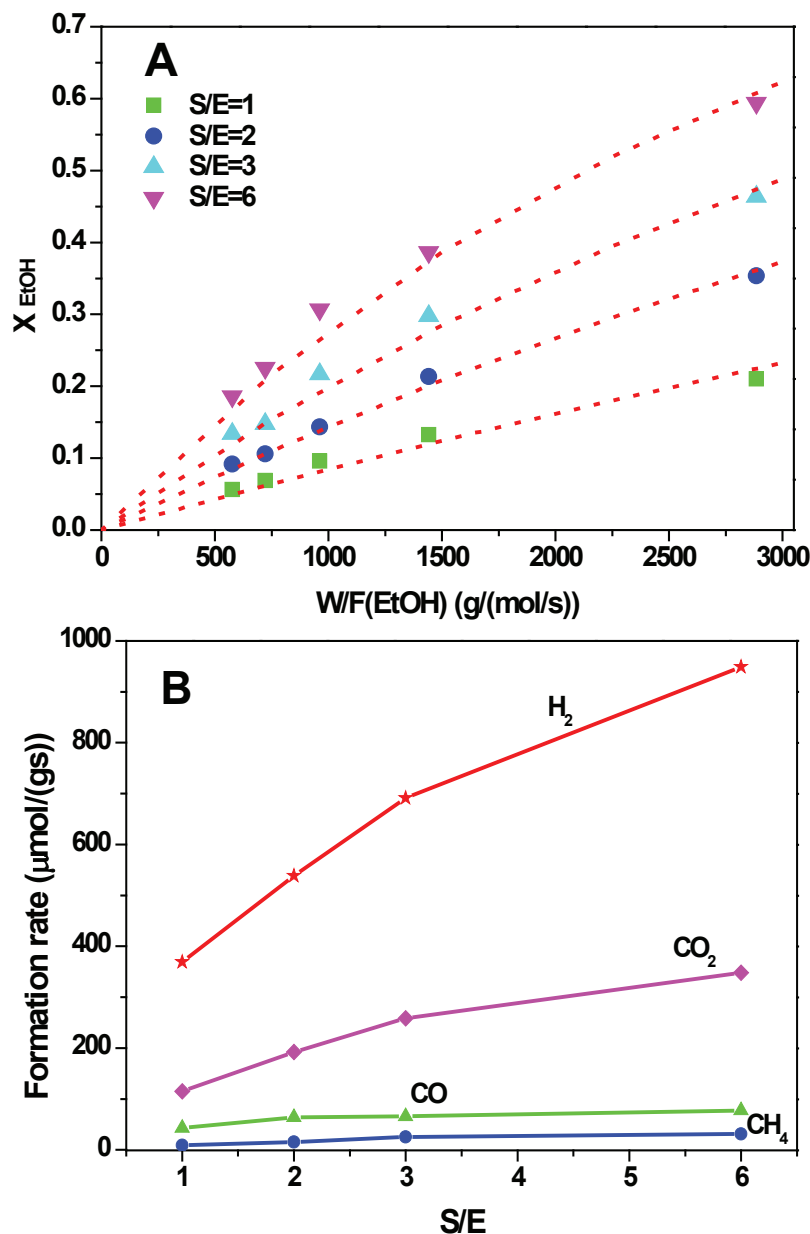


Figure III-8 Effect of W/F_{EtOH} on the conversion of ethanol at different S/E at 823 K (A) and the gas yield versus S/E molar ratio at 823 K and $W_{cat}/F_{EtOH} = 577$ g/(mol/s) (B).

Reaction conditions: (A): Mass of catalyst: 10 mg, SiC: 300 mg, Molar ratio: $H_2O:EtOH = (1\sim6):1$, Ethanol flow rate: 5~25 mL/min, Total flow rate: 200 mL/min, $T=823$ K.

III.3.3. Effect of the partial pressure of the products

The effect of the main gaseous products (CO , CO_2 , H_2 and CH_4) addition in the inlet was also studied. The experimental results are illustrated in Figure III-9. The results indicated that the conversion of ethanol was significantly inhibited by the addition of these main gas products in the inlet feed. According to the mechanistic approach reported elsewhere, it might be speculated that i) the CO_2 addition increases the carbonate concentration on the ceria,

inhibiting the ethoxy and acetate migration from ceria to Ir particles, ii) the CO addition increases the carbonylate concentration at the Ir particles inhibiting the decomposition of acetate and methyl fragments into CO and iii) the CH₄ addition favors its steam reforming at the expenses of the fragments coming from the ethanol decomposition.

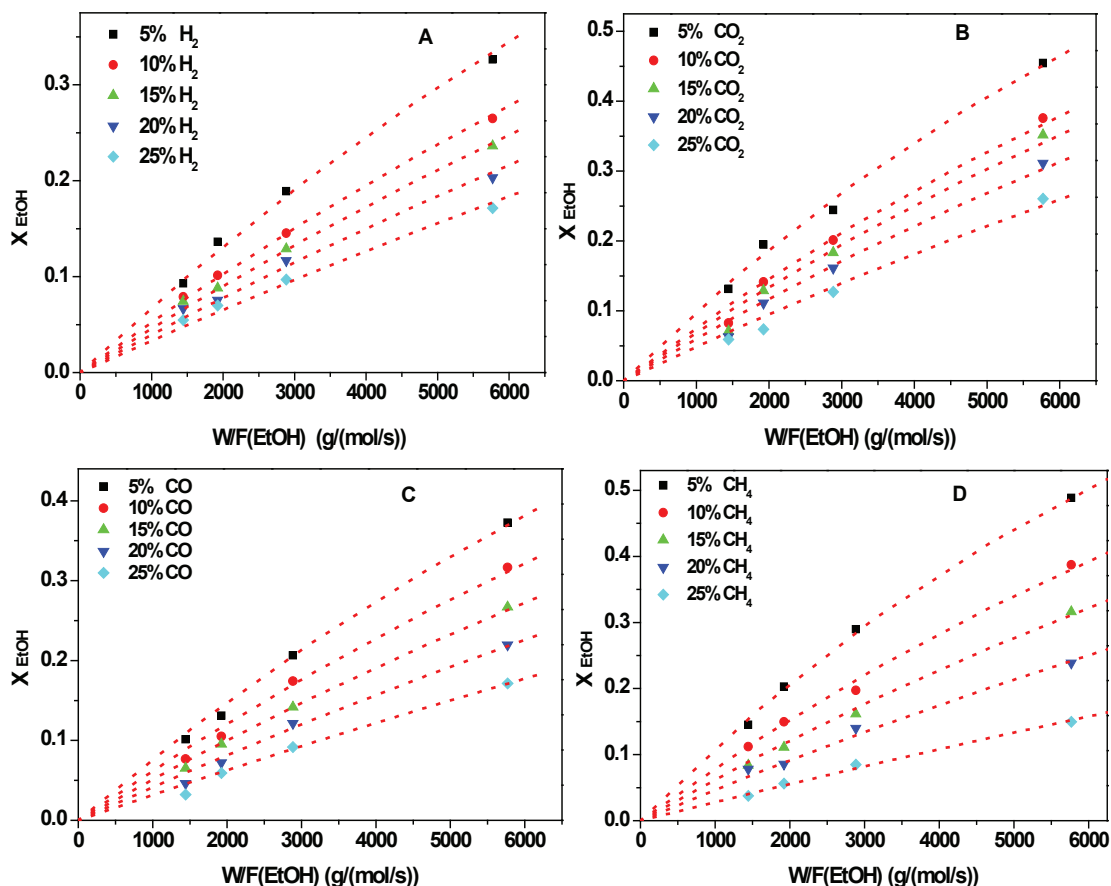


Figure III-9 Effects of (A) H₂, (B) CO₂, (C) CO and (D) CH₄ partial pressure on the conversion of ethanol at different W/F(EtOH) at 823 K.

The influence of the products partial pressure on the kinetic behaviour of ethanol steam reforming has only very scarcely been reported. Laosiripojana et al. [5] studied the steam reforming of ethanol (S/E=3) with co-fed hydrogen over Ni supported high surface area ceria catalyst, the production of CH₄, C₂H₄ and C₂H₆ was decreased with increasing the ratio of H₂/C₂H₅OH molar ratio to 3.0 at 1123 K. However, the effect of hydrogen on the conversion of ethanol was not reported due to the complete ethanol conversion at high temperature. Jacobs et al. [6] investigated the steam reforming of ethanol over Pt/CeO₂ with co-fed

hydrogen. They found that decreasing of hydrogen partial pressure did not change the conversion of ethanol at 673 K, but the sensitivity of CO₂/CO_x was increased.

As seen above, in the current case, the increase of hydrogen partial pressure, like the one of CO₂, CO and CH₄ resulted in a decrease of ethanol conversion, which might be associated with the general trend of kinetic data governed by thermodynamics as already mentioned above.

III.4. Kinetic modelling

As reported in the literature analysis, the rate of ethanol can be correctly expressed by a general power law equation as:

$$-r_{\text{C}_2\text{H}_5\text{OH}} = [k_0 \exp(-\frac{E_a}{RT})]^* (P_{\text{C}_2\text{H}_5\text{OH}})^a (P_{\text{H}_2\text{O}})^b (P_{\text{H}_2})^c (P_{\text{CO}_2})^d (P_{\text{CO}})^e (P_{\text{CH}_4})^f \quad (\text{EqIII.16})$$

where, parameters of a to f are the apparent reaction orders of the responding gas, k_0 is the pre-exponential factor, and E_a is the apparent activation energy of the reaction.

The estimated kinetic parameters derived from this simple formalism (reaction orders, pre-exponential factor and activation energy) based on the above presented kinetic data were listed in Table III-1 and compared to kinetic parameters reported in the literatures.

Therdthianwong et al. [7] performed steam reforming of ethanol (S/E=7.5) reaction at 673 K over a Ni/Al₂O₃ catalyst, and reported reactions orders of 2.52 and 7 for ethanol and water, respectively. Ciambelli et al.[8] studied the preliminary kinetic study of Pt/CeO₂ catalyst for steam reforming of ethanol in 573-723 K, they got apparent reaction orders are 0.5 and 0 for ethanol and water, respectively, and an apparent activation energy was 18 kJ/mol. In our case, the activation energy of steam reforming of ethanol over the Ir/CeO₂ catalyst was estimated to 58 kJ/mol, which is very close to that of the Pd/CeO₂ catalyst (40 kJ/mol) [9] and the Pt-Ni/Al₂O₃ catalyst (59 kJ/mol) [10]. The huge discrepancies of the reported activation energy might be explained for the different catalysts, as well as the different reaction conditions.

Table III-1 Estimated kinetic parameters of ethanol reforming rate over the Ir/CeO₂ catalyst

Catalysts	Temp (K)	k ₀	E _a (kJ/mol)	a	b	c	d	e	f	Ref.
Ir/CeO ₂	773-923	0.028 mol g ⁻¹ s ⁻¹ (kPa) ^{0.9}	57.6	0.6	0.5	-0.9	-0.4	-0.4	-0.3	This work
Ni/Al ₂ O ₃	523-623	2.32 x 10 ⁻³ m ³ kg _{cat} ⁻¹ s ⁻¹	17	1	--	--	--	--	--	[15]
0.2Pt-15Ni/Al ₂ O ₃	673-723	0.013 mol g _{cat} ⁻¹ s ⁻¹ kPa ^{-0.107}	39.3	1.25	-0.215	--	--	--	--	[17]
0.3Pt-15Ni/Al ₂ O ₃	673-823	9.23 mol g _{cat} ⁻¹ h ⁻¹ atm ^{-0.92}	59.3	1.01	-0.09	--	--	--	--	[14]
Ni/MgO/Al ₂ O ₃	673-873	439 mol g _{cat} ⁻¹ min ⁻¹ atm ^{-3.42}	23	0.71	2.71	--	--	--	--	[16]
Ru/Al ₂ O ₃	873-973	--	96	1	--	--	--	--	--	[2]
Pd/CeO ₂	< 450	4.70 x 10 ⁵ mL g ⁻¹ s ⁻¹	40	1	--	--	--	--	--	[13]
CeO ₂	< 450	3.81 x 10 ⁹ mL g ⁻¹ s ⁻¹	75.4	1	--	--	--	--	--	[13]
Pt/CeO ₂	573-723		18	0.5	0	--	--	--	--	[12]
Ni/Al ₂ O ₃	673	77.8 mol g _{cat} ⁻¹ s ⁻¹ atm ^{-9.52}	--	2.52	7	--	--	--	--	[11]

--: Not available

Sun et al. [11] have reported a first order with respect to ethanol over Ni based catalyst. The same result was also obtained by P. D. Vaidya et al. [2] over a Ru/Al₂O₃ catalyst, but they didn't give the apparent order of water. Therdthianwong reported firstly that the orders for ethanol and water were 2.52 and 7, respectively. Mature [12] reported an order for water was 2.71, which in line with the positive effect of water on the conversion of ethanol. Orucu [13] reported that the orders of ethanol and water over a 0.2Pt-15Ni/Al₂O₃ catalyst were 1.25 and -0.215, respectively, while the results over 0.3Pt-15Ni/Al₂O₃ from Baltacioglu [14] were 1.01 and -0.09, respectively. They considered that the negative order of water indicated the competitive adsorption between water and ethanol over the catalyst. In the present study, the

orders of ethanol and water were estimated to be 0.6 and 0.5, respectively. These partial orders might indicate that the ethanol and water adsorption steps are not determining, but participate to accelerate the overall rate of conversion, probably by ensuring a dominant ceria surface occupancy by intermediates arising from these two adsorption steps, i.e., ethoxy and hydroxyls active intermediates, as suggested from our mechanistic study.

Figure III-10 compares the conversion of ethanol predicted by the estimated parameters and the measured conversion of ethanol obtained from various kinetic experiments related to changes in S/E molar ratio, contact time, H₂ and CO₂ addition. It can be seen that the estimated and measured values presented similar trends for ethanol conversion, which indicates that the above kinetic formalism could reasonably describe the experimental conversion of ethanol. Further and more advanced kinetic modeling is in progress to improve this fit between experiments and prediction.

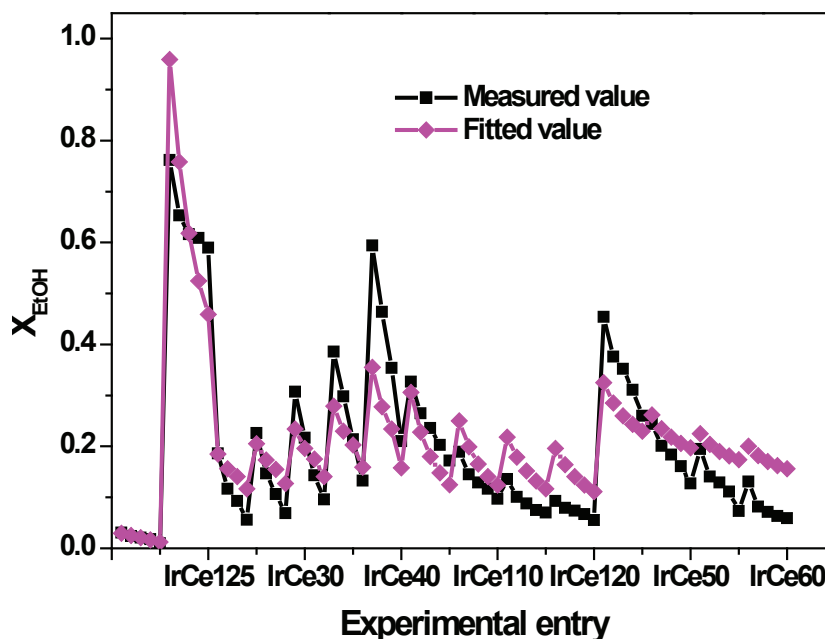


Figure III-10 Fitting and measured curves of conversion of ethanol.

III.5. Summary

A preliminary kinetic study of steam reforming of ethanol was carried out over the Ir/CeO₂ catalyst in a fixed-bed catalytic reactor in 773-923 K at atmospheric pressure. The results

indicated that the operating conditions (temperature, molar ratio of water to ethanol and partial pressure of products) had a significant influence on the ethanol conversion. The apparent activation energy was measured to be ca 58 kJ/mol, in line with the literature data for other types of catalysts. A power law rate equation was found to correctly describe the main kinetic trends, from which the reaction orders of ethanol and water were derived as 0.6 and 0.5, respectively. The addition of the main reaction products in the feed resulted in a significant inhibition of the ethanol conversion and tentative mechanistic effects were proposed to account for these kinetic trends. Indeed, much more work is required to progress significantly towards more robust models in view of being used for any further process development.

References

- [1] A. Akande, A. Aboudheir, R. Idem, A. K. Dalai, *Int. J. Hydrogen Energy* 31 (2006) 1707-1715.
- [2] P. D. Vaidya, A. E. Rodrigues, *Ind. Eng. Chem. Res.* 45 (2006) 6614-6618.
- [3] G. F. Froment, K. B. Bischoff, *Chemical Reactor Analysis and Design*, John Wiley, 1979.
- [4] C. Graschisky, M. Laborde, N. Amadeo, A. Le Valant, N. Bion, F. Epron, D. Duprez, *Ind. Eng. Chem. Res.* 49 (2010) 12383-12389.
- [5] N. Laosiripojana, S. Assabumrungrat, S. Charojrochkul, *Appl. Catal. A: Gen.* 327 (2007) 180-188.
- [6] G. Jacobs, R. A. Keogh, B. H. Davis, *J. Catal.* 245 (2007) 326-337.
- [7] A. Therdthianwong, T. Sakulkoakiet, S. Therdthianwong. *Sci. Asia* 27 (2001) 193-198.
- [8] P. Ciambelli, V. Palma, A. Ruggiero, *Appl. Catal. B: Environ.* 96 (2010) 190-197.
- [9] A. Yee, S. J. Morrison, H. Idriss, *J. Catal.* 186 (1999) 279-295.
- [10] F. S. Baltacioglu, A. E. Aksoylu, Z. I. Onsan, *Catal. Today* 138 (2008) 183-186.
- [11] J. Sun, X. P. Qiu, F. Wu, W. T. Zhu, *Int. J. Hydrogen Energy* 30 (2005) 437-445.
- [12] P. V. Mathure, S. Ganguly, A. V. Patwardhan, R. K. Saha, *Ind. Eng. Chem. Res.* 46 (2007) 8471-8477.
- [13] E. Orucu, F. Gokaliler, A. E. Aksoylu, Z. I. Onsan, *Catal. Lett.* 120 (2008) 198-203.

Chapter IV Ageing analysis of a model Ir/CeO₂ catalyst in steam reforming of ethanol

Although hydrogen production by steam reforming and oxidative steam reforming of ethanol has been studied extensively, the general occurrence of catalyst deactivation requires an in depth study for catalysts design that able to meet industrial stability requirements.

For most cases in catalytic reforming, the deactivation comes from the loss of active surface, either due to "toxic carbon" deposition or due to the loss of oxide or metal surface arising from the catalyst sintering or restructuring.

Concerning the carbon deposits under the reforming conditions, two main categories have to be considered.

i) By essence a catalytic reaction like the ethanol reforming involves that the active surface (metal and support) is more or less covered with reacting intermediates which are precursors of the reaction products. As such, the ethoxy species and the acetates are accumulating on the ceria surface as shown in previous works on oxy-reforming [1], the CH_x and carbonyls adsorbed on the Ir particles have to be considered as part of the carbonaceous deposits on the reacting catalysts. In general, the build-up of these active carbonaceous deposits occurs rapidly, which corresponds to the period necessary for the catalysts to reach a steady-state or pseudo steady-state catalytic regime.

ii) Less or non active carbon deposits can also accumulate with time on stream, possibly hindering the reaction to proceed and leading to deactivation [2]. The origin of these "toxic" deposits has to be found in the various secondary routes occurring under reforming conditions. Thus, depending on the type of acidic or basic sites of the oxide supports, ethylene, acetaldehyde and/or acetone can be formed through dehydration, dehydrogenation, and condensation/decarbonylation of ethanol, respectively. These products may then oligomerize to carbonaceous species depending on contact time and reaction temperature [3]. For example, the formation of ethylene was shown to provoke a severe carbon deposition on Co/Al₂O₃ catalyst in steam reforming of ethanol [4]. Similarly, acetaldehyde was formed

on a Co/ZnO catalyst and it was further polymerized to carbonaceous species, severely blocking the active sites [5]. Other types of carbon deposition can also occur on the metal phase, such as filament or encapsulating graphite via various C1 condensation and/or carbide formation processes. The nature and dispersion of the metal particles was found to strongly influence these processes. For example, two types of carbon deposits were observed on an aged Ni/Al₂O₃ catalyst, being located on the active metal and the support surfaces, respectively [6]. The deposition of graphite or polyaromatics resulted in severe deactivations of Rh catalysts [7-9]. Similarly, Ir/La₂O₃ catalyst was found to be highly active for oxidative steam reforming of ethanol, but the insufficient reforming of reaction intermediates, mainly acetaldehyde, resulted in coke deposition [10].

Generally, the accumulating rate of these deactivating carbon deposits is related to the rate of the reforming reaction itself, i.e. it is faster initially on the fresh and active catalyst and slower on a deactivated system. Other more complex kinetics of carbon deposits can be considered as well [11].

Concerning the second major deactivation process by loss of active surface, both metal particles and support grains sintering were observed under reforming conditions. Thus, in our previous work on Ir/ceria catalysts in steam reforming or oxidative steam reforming of ethanol [1, 12], it was observed that under the severe reforming condition, the initially well-dispersed metal and ceria particles tended to sinter at different levels, resulting in (i) an increase of the crystallinity and a decrease of the structural defect concentration of the ceria support, and (ii) a loss of metal dispersion, involving a major decrease in the metal-support interactions after long-term runs.

In the present work, a model Ir/CeO₂ catalyst was used for analyzing the ageing process to a deeper extent. The deactivation rates were analyzed on the basis of the observed changes in texture/structure of the catalysts and in the amount and type of carbonaceous deposits accumulating during short or long-term runs.

IV.1. Physical and chemical properties of the model Ir/CeO₂ catalyst

Most of the ageing experiments were carried out on a model Ir/CeO₂ catalyst calcined at 923 K, which was higher than the ageing reaction temperature (773 and 923 K), in order to keep the structure of the catalyst as stable as possible.

IV.1.1. BET specific surface area characterization

The BET specific surface area of the model Ir/CeO₂ catalyst calcined at 923 K was 77 m²/g. This value is significantly smaller than the same type catalyst calcined at 673 K (153 m²/g, [1]), which can be assigned straightforwardly to the sintering of the ceria support, already shown to occur for high temperature calcinations [12]. The actual Ir loadings of the model catalyst was 1.88 wt.%, closing to the nominal value of 2 wt.%.

IV.1.2. XRD characterization

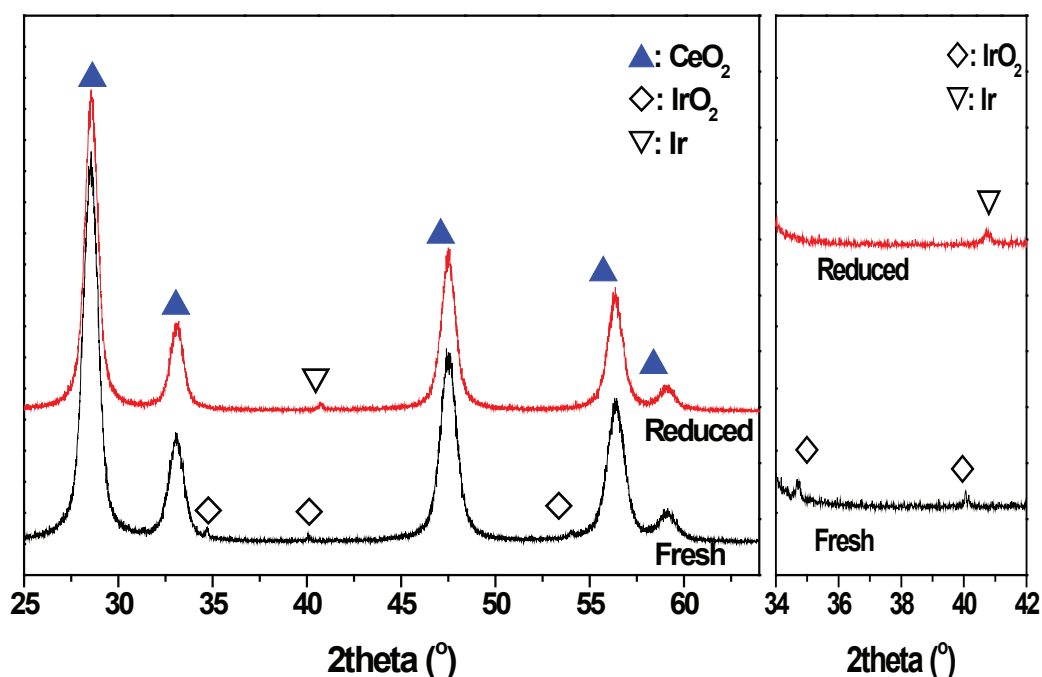


Figure IV-1 XRD patterns of the fresh and the reduced catalysts.

Figure IV-1 shows the XRD patterns of the fresh and the reduced catalyst. The diffraction lines of ceria with fluorite structure were clearly observed in both cases. The mean crystallite sizes of ceria were about 8 nm in both cases, calculated from the highest diffraction peak

according to the Scherrer equation. However, the diffraction line intensities in the reduced sample weakened considerably and the diffraction positions shifted towards lower 2θ values because of the defects that were generated by the reduction of the surface of ceria [1]. In addition, the appearance diffraction peaks of iridium oxide indicated that large crystalline domains of iridium oxide were formed in the Ir/CeO₂ sample. This can be attributed to the high calcination temperature, which led to the aggregation of iridium oxide particles. After reduction, the minor diffraction lines characteristic of Ir species were also detected in the reduced sample.

IV.1.3. HRTEM characterization

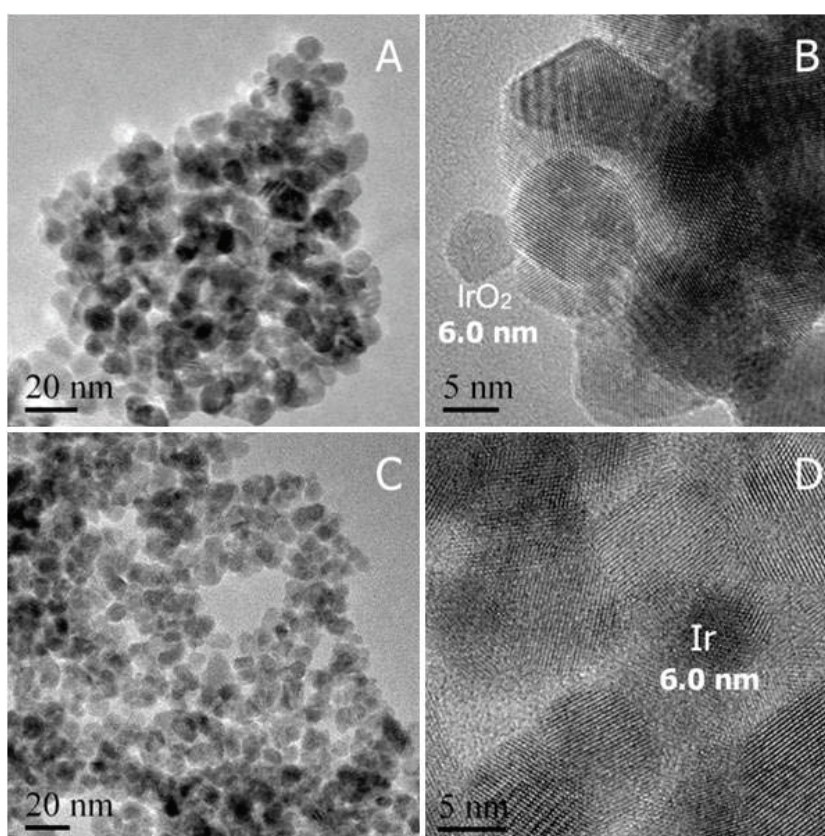


Figure IV-2 HRTEM images of the fresh (A-B) and the reduced (C-D) catalysts.

Figure IV-2 shows the TEM images of the fresh and the reduced catalysts. For the fresh sample (Figure IV-2 A&B), the size of the spherical ceria grains was in the range of 5-10 nm, in good agreement with the XRD measurements, which tends to indicate that the ceria grains were almost single crystals. The IrO₂ particles, with a size of about 5-7 nm, were found to be

well-dispersed and in tight contact with the ceria grains. After hydrogen reduction (Figure IV-2 C&D), the Ir particles (ca. 6 nm in size) were still homogeneously distributed and in tight contact with the ceria grains (ca. 5-10 nm, with well-defined edges). From these results, it was calculated (assuming cubic Ir particles) that the metallic surface in the reduced catalyst only accounts for 1.2% of the total BET surface developed by the sample, the rest being essentially Ce₂O₃ or CeO₂, depending on the redox conditions. This percentage, which may change slightly upon catalyst sintering, will be used further on to discuss the bi-functional mechanism of steam reforming of ethanol.

IV.1.4. H₂-TPR characterization

Figure IV-3 shows the H₂-TPR profile of the fresh catalyst, displaying three distinct reduction peaks. In good line with our previous studies [1, 12] and comments in the previous section, the reduction peak at about 463 K (ca. 355 μmol g_{cat}⁻¹) is assigned to both the reduction of IrO₂ species to metallic Ir (corresponding to an hydrogen consumption ca. 200 μmol g_{cat}⁻¹) and the partial reduction of the ceria surface (from Ce⁴⁺ to Ce³⁺), most likely around the Ir particles, where hydrogen can easily spill over from the reduced Ir particles to the ceria surface [13]. Note that the reduction of one monolayer of ceria would necessitate around 1600 μmol g_{cat}⁻¹ of hydrogen, considering the initial BET surface and a mean surface oxygen density of ca 21 μmol m⁻². From this value, it can be inferred that the peak at 553 K (ca. 251 μmol g_{cat}⁻¹) would correspond to the reduction of a part of the ceria surface located far from the Ir particles (where the spillover effect is less marked) and the broad peak at much higher temperature (maximum at 1023 K, around 139 μmol g_{cat}⁻¹) would correspond to a partial reduction of the ceria bulk. By integrating the whole amount of hydrogen consumed (about 745 μmol g_{cat}⁻¹) and accounting for the amount of hydrogen necessary for the Ir oxide reduction (200 μmol g⁻¹), the final stoichiometric state of the reduced ceria sample was estimated to be ca. CeO_{1.91}. This corresponds quite well to the quantitative evaluation of the ceria reducibility deduced from OSC measurements, as reported on similar samples in [12]. It was shown that only one to two monolayer of the oxide were reduced, i.e. less than 20% of the maximum possible reduction of CeO₂ to Ce₂O₃.

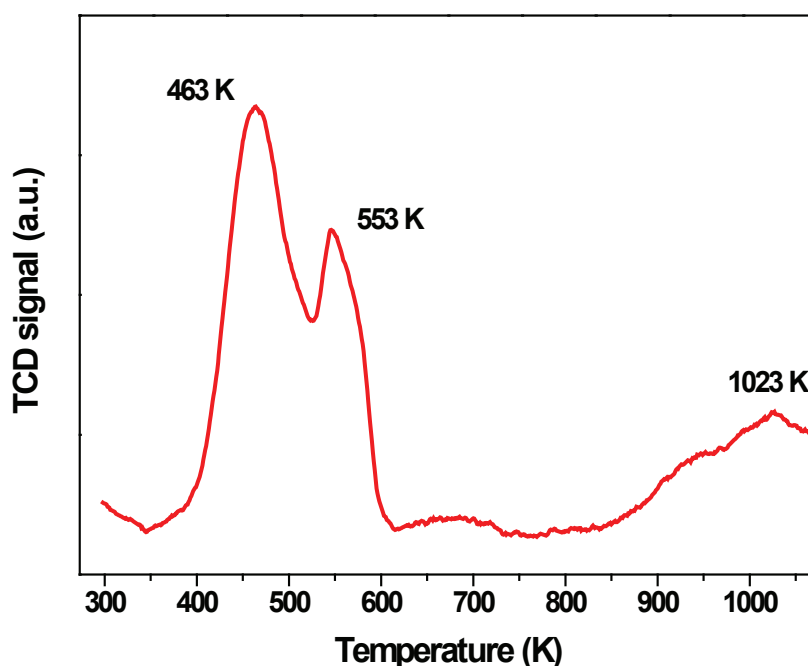


Figure IV-3 TPR profiles of fresh Ir/CeO₂ sample.

IV.2. Ageing analysis under steam reforming of ethanol conditions

In order to study the ageing phenomena on the model Ir/CeO₂ catalyst occurring under steam reforming conditions, we first checked the influence of the reaction temperature on the catalytic performances, by raising the temperature with the same catalyst sample, i.e., not accounting for the ageing of the catalyst all along this experiment.

Then, long-term stability (40-60 h on stream) was tested over the temperature range 773-923 K, i.e. under conditions where the reaction mechanism changes deeply from mainly ethanol dehydrogenation to mainly reforming into syngas (including WGS/RWGS equilibrium). Here, for each ageing experiment, a fresh catalyst (calcined at 923 K) was reduced in situ and contacted with the same ethanol/steam feedstock.

Several types of ageing experiments were carried out, either to focus on the primary ageing period, or to follow long term ageing processes, as it will be shown below.

In order to understand the causes of the catalytic deactivation, a series of analyses (BET, XRD, and TPO) were performed at key steps of the ageing processes, as it will be presented later.

IV.2.1. Catalytic performance and ageing tests

IV.2.1.1. Influence of the reaction temperature on catalytic performances

Figure IV-4 illustrates the temperature-dependence of the ethanol conversion and the dry product selectivity in steam reforming of ethanol over the Ir/CeO₂ catalyst. The conversion of ethanol increased progressively with increasing temperature. However, since these changes in catalytic performances with temperature also included temperature sensitive ageing phenomena (changes in texture and structure and/or carbon deposition) as it will be discussed later, no calculation of the apparent activation energy was attempted. Concerning the outlet product distribution at 673 K, the main constituent was indeed the unconverted ethanol (ca. 90%) while mainly acetaldehyde was produced (ca. 6% together with around 4% of hydrogen), indicating that only the primary dehydrogenation of ethanol occurred at that temperature. At 773 K, in addition to the predominant production of acetaldehyde, the production of CO₂, CO and H₂ was also observed, in agreement with the expected thermodynamic equilibrium calculated for the steam reforming of ethanol (H₂:CO:CO₂ = 19:9:2), as represented in Figure IV-5. Noteworthy, as already stated in this manuscript, this product distribution is essentially governed by the WGS/RWGS equilibrium. Furthermore, the quasi absence of methane is related to the weak methanation activity of Ir. By further increasing the temperature to 873 K, the dry product selectivity of CO, CO₂ and CH₄ increased, still close to the thermodynamic equilibrium, while the selectivity of acetaldehyde decreased markedly. This demonstrates that the primary route towards acetaldehyde formation is replaced progressively by the secondary steam reforming of ethanol into syngas and methane, as expected from thermodynamics. At 973 K, the conversion of ethanol approached 100% and the outlet dry gas consisted of 58 vol.% H₂, 22 vol.% CO, 17 vol.% CO₂ and 3 vol.% CH₄, again matching quite closely with the thermodynamic equilibrium calculated for the steam reforming of ethanol conditions (Figure IV-5, already presented in Chapter I).

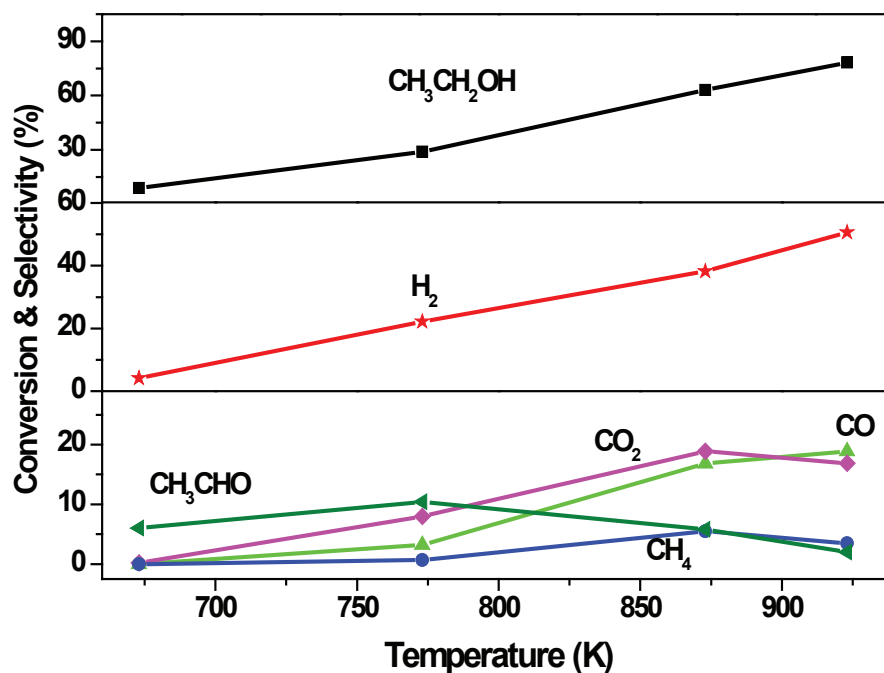


Figure IV-4 Ethanol conversion and product selectivity during steam reforming of ethanol over the Ir/CeO₂ catalyst. Reaction conditions: mass of catalyst: 25 mg, C₂H₅OH/H₂O = 1:3 (molar ratio), GHSV = 72,000 mL/(g·h).

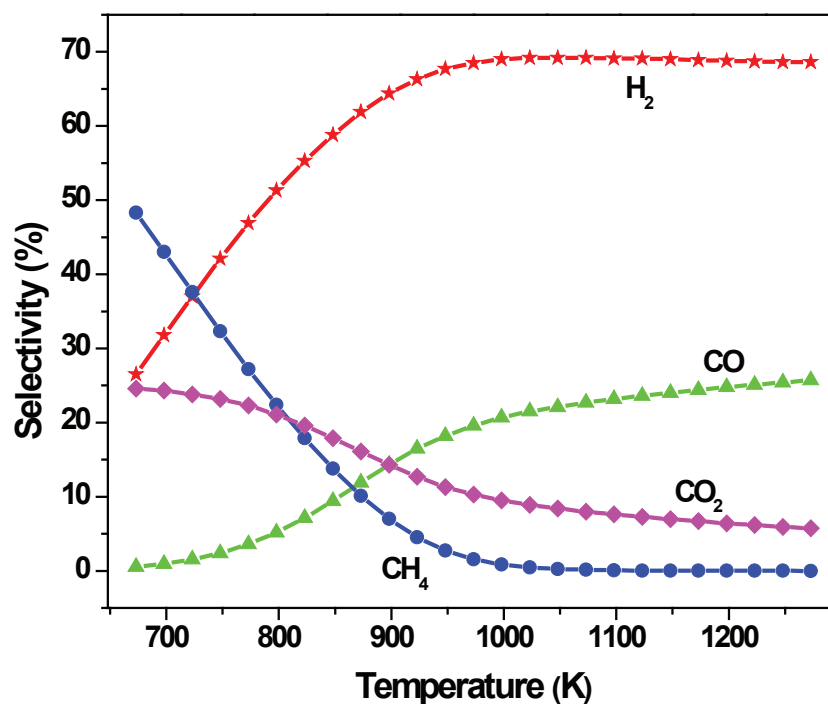


Figure IV-5 Thermodynamic equilibrium selectivity for the steam reforming of ethanol as a function of temperature (EtOH/H₂O=1/3, pressure: 1atm).

Therefore, in perfect agreement with the trends that already observed either in steam reforming or oxidative steam reforming of ethanol [1, 12, 14], one can see that the progressive

changes in selectivity with temperature reflect the changes in the mechanistic routes. At low temperature, the primary dehydrogenation of ethanol into acetaldehyde involves essentially the ceria surface as the active phase (via ethoxy and acetate intermediates), as demonstrated in [1, 12]. At medium temperature, this route is progressively replaced by the syngas chemistry involving the migration and decomposition of these C₂ adspecies at the Ir/ceria interface where they are cracked into C₁ adspecies (carbonyls and carbonates) to form the equilibrated CO/CO₂/H₂ mixture. At higher temperature, the metallic catalysis dominates and the methane, formed from the cracking of the acetates, can be converted by steam reforming into syngas. The question now arises how these changes in surface chemistry and catalytic performances are sensitive to the ageing phenomena occurring under these reaction conditions.

IV.2.1.2. Activity decay at various conditions

A first ageing experiment was carried out at rather low temperature (773 K) and low space velocity (GHSV = 72,000 mL/(g·h)) to focus on the initial deactivation. The same experiment carried out at higher temperature led to a complete initial conversion of ethanol, obscuring any ageing information.

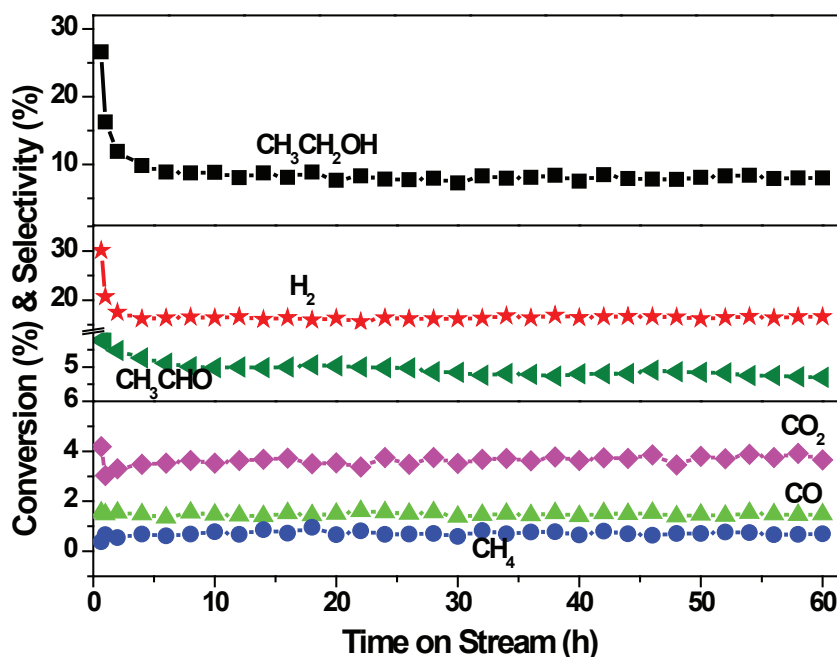


Figure IV-6 Steam reforming of ethanol over the Ir/CeO₂ catalyst at 773 K. Reaction conditions: mass of catalyst: 25 mg, C₂H₅OH/H₂O = 1:3 (molar ratio), GHSV = 72,000 mL/(g·h).

As can be seen in Figure IV-6, the conversion of ethanol was about 30% after 40 min on stream but it decreased to 10% after 5 h on stream, to practically level off at longer time on stream (TOS) (ca. 8% after 60 h on stream). During this fast initial deactivation process, the selectivity of hydrogen decreased from 30% to 16%, while the selectivity of acetaldehyde slightly decreased from 9% to 5%, while traces of ethylene were detected. The selectivity of CO₂, CO and CH₄ was only slightly fluctuating during this initial period, keeping the overall carbon balance equilibrated. The outlet gas composition was then leveling up over the whole test.

A second series of experiments was carried out at higher space velocity (GHSV = 360,000 mL/(g·h)) over the whole range of temperature (773-923 K), with only a partial conversion of ethanol over the testing period at any temperature. To avoid the unstable period already studied (Figure IV-6), the first activity measurements were taken after 2 h on stream, allowing to concentrate on the slow ageing processes only.

As can be seen on Figure IV-7A, the conversion of ethanol decreases to a larger extent at higher reaction temperatures. In order to check if a similar ageing process was governing this decay in activity, we normalized all the curves by dividing each data point by the initial conversion value, as depicted in Figure IV-7B. Even though all curves tend to follow similar trends (within experimental uncertainty), it seems that the deactivation rate is slower at 773 K than at the other temperatures, as it will be discussed later on. We will analyze in more detail the decay curves corresponding to the two extreme temperatures, i.e.; 773 and 923 K, on the basis of the catalyst changes in terms of morphology and structure during these long-term tests.

In the following of these preliminary ageing experiments, the used samples were characterized by XRD, HRTEM, TPO and TPD to analyze the catalyst structure, the particle size of iridium and ceria and the coke deposition over the aged catalyst.

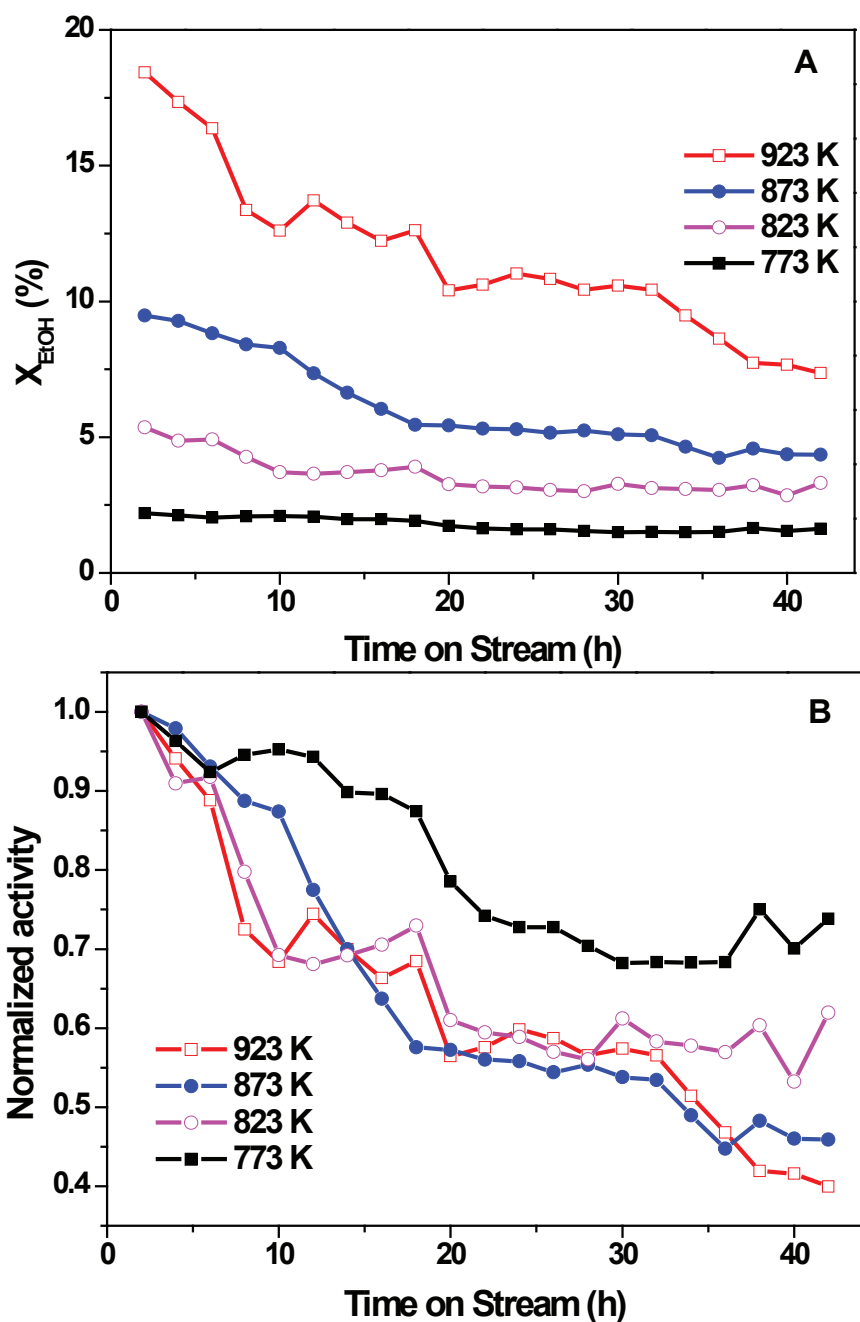


Figure IV-7 Steam reforming of ethanol over the Ir/CeO₂ catalyst at 773-923 K. Reaction conditions: mass of catalyst: 5 mg, C₂H₅OH/H₂O = 1:3 (molar ratio), GHSV = 360,000 mL/(g·h). A: raw data, B: normalized data.

IV.2.1.3. Changes in catalyst structure/texture/morphology with time on stream

Table IV-1 reports the characterization data obtained before testing (fresh and reduced sample), after 2 and 60 h on stream at 773 and 923 K. For convenience, we have also added various kinetic data which will be used later to discuss the ageing mechanisms.

Table IV-1: Changes in structure/morphology according to the reaction temperature and the time on stream. Reaction conditions: mass of catalyst: 5 mg, C₂H₅OH/H₂O = 1:3 (molar ratio), GHSV = 360,000 mL/(g·h).**Reaction temperature: 773 K**

	BET (m ² /g)	d _{CeO₂} nm	d _{Ir} nm	D _{Ir} (%)	X _{EtOH} (%)	r _{EtOH} (μmol/ (sg))	intrinsic rate (μmol/(m ² s))	D _d (%)	D _c (mg C/g)
Freshly reduced	77	8	6 ^a	16.7					
Reacted for 2 h	61	8 ^b	6.3 ^b	15.8	0.02	24.54	0.39 (1.9 ^d)		10 ^c
Reacted for 60 h	56	8 ^b	9.6 ^b	10.4	0.01	10.22	0.18 (1.7 ^d)	42.7	30 ^c

Reaction temperature: 923 K

	BET (m ² /g)	d _{CeO₂} nm	d _{Ir} nm	D _{Ir} (%)	X _{EtOH} (%)	r _{EtOH} (μmol/ (sg))	intrinsic rate (μmol/(m ² s))	D _d (%)	D _c (mg C/g)
Freshly reduced	77	8	6 ^a	16.7					
Reacted for 2 h	57	8 ^b	6.3 ^b	15.8	0.17	173.81	3.04 (18.2 ^d)		5.0 ^c
Reacted for 60 h	47	9 ^b	10.5 ^b	9.5	0.08	77.70	1.65 (17.4 ^d)	26.8	7.2 ^c

Note: d_{CeO₂}/d_{Ir}: the size of ceria and iridium; D_{Ir}: the dispersion of iridium; X_{EtOH}: the conversion of ethanol; r_{EtOH}: the reaction rate of ethanol; D_d: the deactivation degree; D_c: the amount of carbon deposition;

a: data obtained from the HRTEM images for the fresh catalyst

b: data obtained from the XRD patterns of the catalysts reacted

c: data obtained from the TPO patterns of the catalysts reacted

d: intrinsic rate divided by Ir dispersion and multiplied by 100

dispersion= 1/d_{Ir}, deactivation degree=(initial rate-final rate)/initial rate

Figure IV-8 shows the XRD patterns of the aged Ir/CeO₂ samples at different time intervals after the ageing test at 773 and 923 K. For the samples aged at 773 K, the typical diffraction lines of CeO₂ are detected for all samples, and the mean crystallite size keeps constant ca. 8 nm, similarly to that of the fresh sample (Table IV-1). This result indicates that the structure of the ceria crystallite remained rather stable at such relatively low temperature, as expected from its pretreatment under air at 923 K. The diffraction lines of iridium were slightly narrowed with the time on stream, indicating some sintering of iridium during the ageing process.

For the samples aged at 923 K, the sintering of iridium was even more important, from the decrease of the Full-Wide Half-Maximum (FWHM) of the diffraction peaks. In the meantime, the mean crystallite size of ceria grains was increased to 9 nm, demonstrating that ceria also sintered with time on stream (Table IV-1).

The BET values of the fresh catalyst and after different TOS (2 & 60 h) were compared in Table IV-1. At moderate temperature of 773 K, a significant loss of surface area was observed after the first two hours on stream with a decrease from 77 to 61 m² g⁻¹, while a moderate loss of surface was observed after 60 h on stream (56 m²/g). Close results were reported and analyzed by Pijolat et al. [15] showing that a fast loss of BET surface occurred as soon as a calcined ceria was contacted by steam at 943 K, followed by a much slower sintering process. A surface restructuring leading to the loss of microporosity was proposed for the fast initial loss of surface area. Other types of slower morphological restructuring under steam reforming of ethanol conditions underline the crucial role of the {100}/{110}- surface structures as compared to the more dense {111} faces [16].

Concerning the Ir particles, characteristic diffraction lines appeared after 2 h on stream and the intensity increased slightly with longer time on stream, indicative of a significant increase of the Ir mean particle size from 6.3 to 9.6 nm. This sintering process, which corresponds to a decrease of the Ir dispersion from ca. 15 to 10%, can be considered however as relatively limited, due to the initial high temperature treatment (923 K), leading to a relatively low initial Ir dispersion. As a matter of fact, much more marked sintering effects were observed when starting from initially well dispersed catalysts, as reported in our previous studies [1, 12].

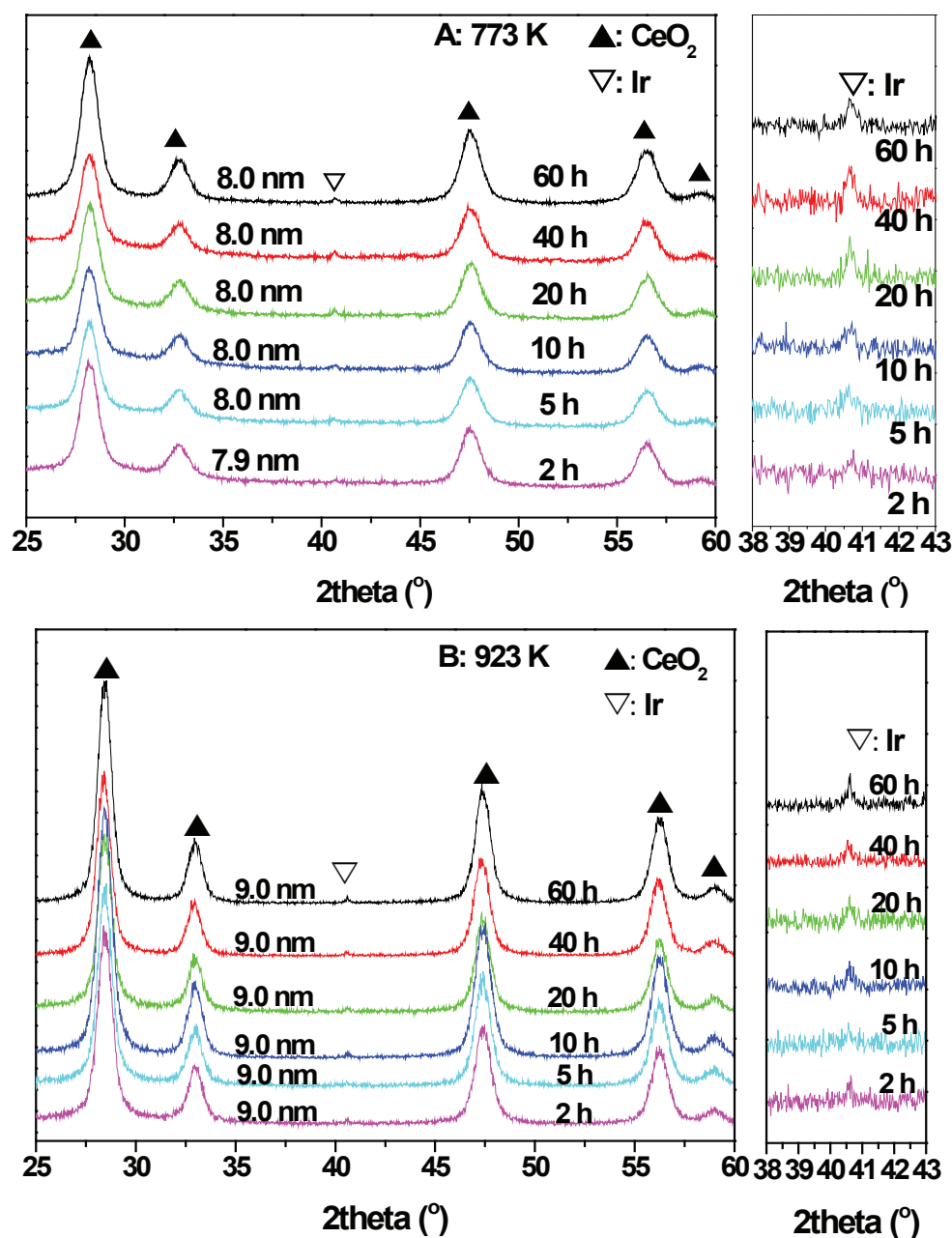


Figure IV-8 XRD patterns of the aged Ir/CeO₂ samples after different reaction intervals at (A) 773 K and (B) 923 K.

The HRTEM images of the used Ir/CeO₂ sample at different intervals are reported in Figure IV-9. After 2 h on-stream, the size of Ir particles was around 6 nm (Figure IV-9 A and B). In the meantime, amorphous carbon was observed on the catalyst surface, partially covering the metal particles. After 5 h, a thin layer of amorphous carbon deposit was clearly seen on the catalyst surface and some of the Ir particles (still around 6 nm) were fully covered by the

carbon species (Figure IV-9 C and D). After 20 h on-stream, the Ir particles enlarged to 9 nm and heavy carbon deposition occurred, covering the surfaces of both Ir particle and ceria support (Figure IV-9 E and F). After 60 h on-stream, the carbon deposits almost fully covered the catalyst surface and the size of Ir particles was around 9.0 nm (Figure IV-9 G and H). It was also observed by TEM in Figure IV-9 and on other pictures not reported here some changes in the ceria crystallite shape all along the ageing process, with a slow ceria restructuring from spherical crystallites (initial state) to polygonal cubes (after long period on stream).

A rationale of all these changes in catalyst structure/texture/morphology with time on stream at the relatively low temperature of 773 K can be formulated as follows:

- i) No major changes in the structure/texture of the ceria were noted by XRD and TEM after the initial 2h on stream period. Therefore, the fast initial decrease in the BET surface is deemed to come from a smoothing effect (i.e. loss of surface roughness and/or microporosity) induced by the presence of steam [15] and the build-up of a carbonaceous layer, as will be described later.
- ii) In turn, the slow and regular decrease of the BET surface (from 61 to 56 m²/g after 60 h on stream) would correspond to ceria restructuring, as observed by TEM, most likely as a consequence of steam present under the reacting conditions,
- iii) The Ir particle sintering is significant but to a moderate extent,
- iv) The significant accumulation of carbon deposits, progressively encapsulating ceria and Ir particles, is observed.

At higher temperature (923 K), slightly different changes in the structure/texture of the catalyst were observed, as reported in Table 1: the ceria mean grain size increased slightly from 8 to 9 nm, while the sintering of the Ir particles was a little more pronounced (dispersion decrease from 17 down to 10%). The BET surface area again strongly decreased during the first two hours on stream (from 77 to 57 m² g⁻¹), and decreased to 47 m²/g after 60 h on stream, i.e. a little more than at 773 K, as expected from the higher reaction temperature. From TEM images (not shown), the major difference compared to the long term run performed at 773 K was the absence of encapsulating carbon, since only traces of carbon could be observed on the sample used at 923 K.

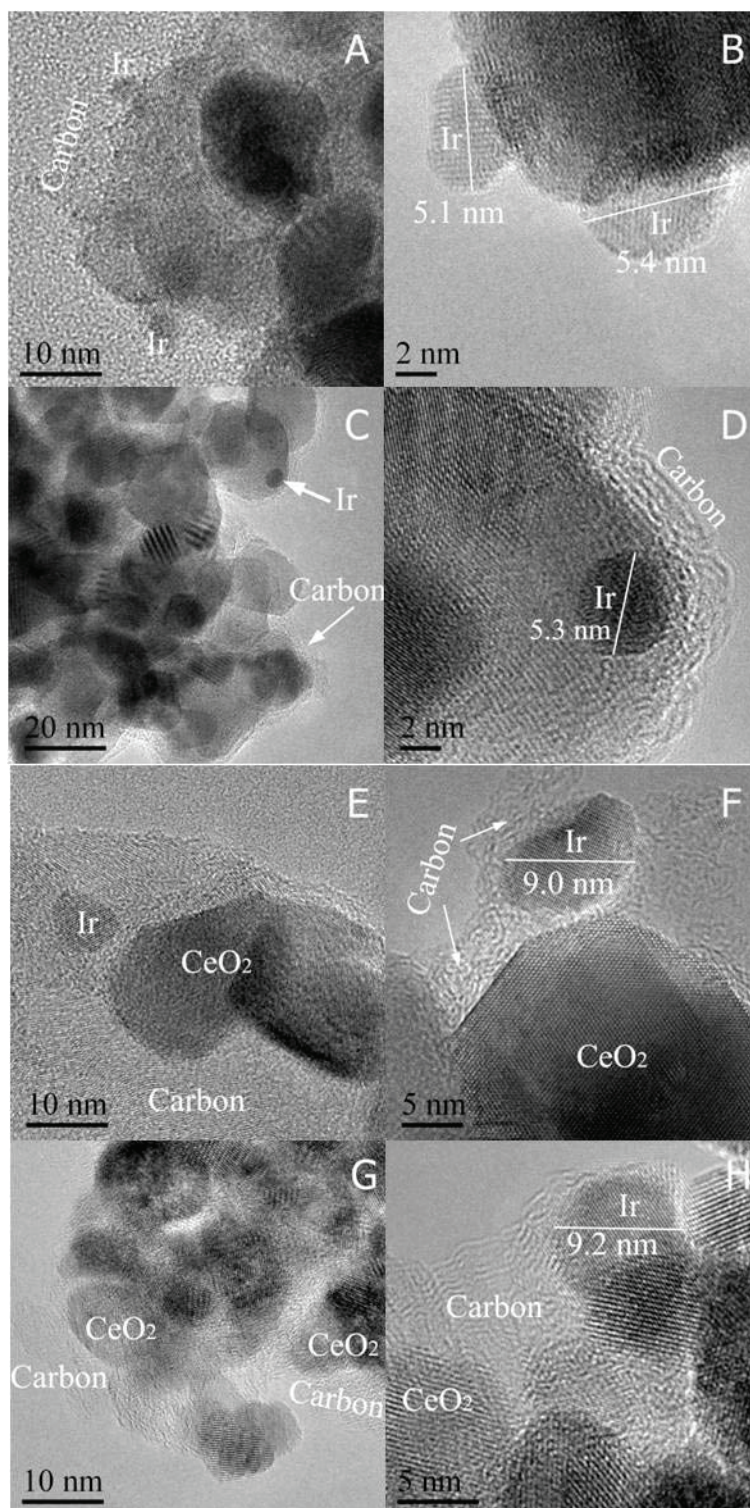


Figure IV-9 HRTEM images of the aged Ir/CeO₂ catalysts at 773 K: A-B, 2 h; C-D, 5 h; E-F, 20 h; G-H, 60 h.

In order to get more information on the carbon deposits, which derive directly from the catalytic performances, a TPO analysis was performed at various temperatures and times on stream.

IV.2.1.4. Analysis of carbon deposits by TPO

Figure IV-10 shows the TPO profiles of the used Ir/CeO₂ catalysts at 773 and 923 K and the corresponding amounts of CO₂ produced upon each TPO analysis. After the ageing test at 773 K (Figure IV-10 A&B), two domains of CO₂ release, corresponding to different types of carbon deposits, was clearly identified:

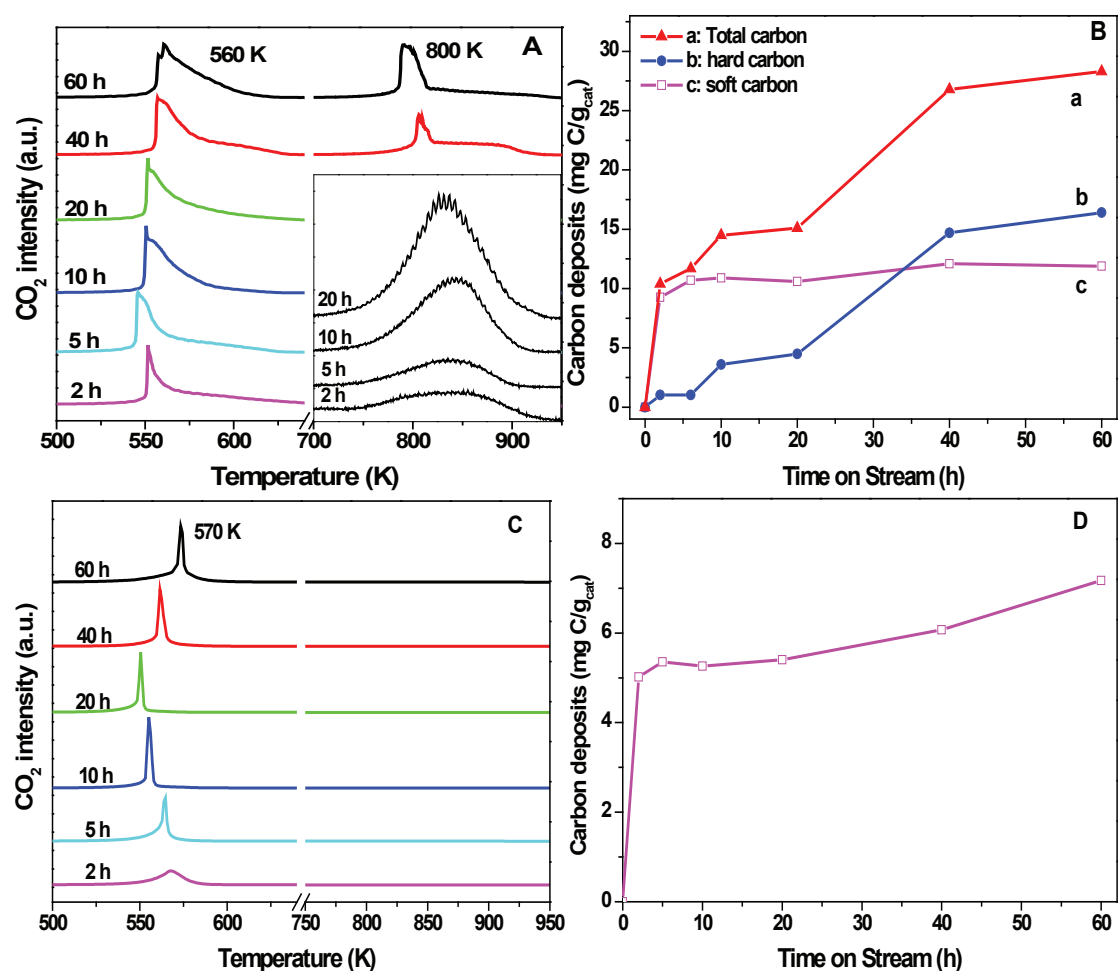


Figure IV-10 TPO files (A: 773 K, C: 923 K) and the carbon deposits (B: 773 K, D: 923 K) of the used Ir/CeO₂ catalysts at different time on stream.

i) The carbon deposits oxidized under TPO conditions at low temperature (named soft carbon, around 560 K) were formed within the first two hours on stream and then remained

practically stable over the whole testing period (Figure IV-10 B, curve c). From the shape of the CO₂ peak (one sharp maximum and a larger shoulder, see Figure IV-10 A), one could identify two types of carbonaceous ad-species with only a slight difference in reactivity. However, due to the lack of more precise data, no de-convolution was attempted. The carbon deposits oxidized at higher temperature (named hard carbon, around 800 K) were accumulating progressively with time on stream (Figure 10B, curve b). Several types of carbon deposits could be proposed but they were not quantified separately.

ii) After the ageing test at 923 K, only the low temperature carbon was detected by TPO (Figure IV-10 C&D). It formed very rapidly after the first two hours on stream, and increased only slightly with time on stream. Note in addition that this peak was narrower (without shoulder) than the soft carbon peak detected after the ageing test at 773 K and slightly shifted to higher temperature.

The amounts of carbon corresponding to these different adspecies are also reported in Table IV-1 at 773 and 923 K. Let us discuss now the nature and role of these carbon deposits on the ageing phenomena, in connection with the changes in morphology and structure reported before.

IV.2.2. Origin of the ageing phenomena

The striking coincidence between the initial fast deactivation (Figure IV-6), the loss of surface area and the formation of a quasi stable amount of carbon deposits which are highly reactive with oxygen under TPO conditions (soft carbon) leads us to propose that this initial period corresponds to a smoothing/restructuring of the surface after ceria re-oxidation by water and its coverage by a layer of reacting carbonaceous adspecies. The latter accumulate rapidly when the initially reduced ceria is oxidized by both the reacting water ($\text{Ce}_2\text{O}_3 + \text{H}_2\text{O} \rightarrow 2 \text{CeO}_2 + \text{H}_2$) [17] and possibly the reacting ethanol ($\text{Ce}_2\text{O}_3 + \text{CH}_3\text{CH}_2\text{OH} \rightarrow 2 \text{CeO}_2 + \text{CH}_2\text{CH}_2 + \text{H}_2$). The latter reaction would explain the observation of initial traces of ethylene. During this period of time, different reacting intermediates (ethoxy, acetates, carbonates, carbonyls) build up on the surface as shown elsewhere by operando spectroscopy [1, 18, 19, 20]. Indeed the exact nature of these intermediates strongly depends on various parameters, such as the nature of the catalyst and the operating conditions. Thus, Araque et al. [20] have

concluded that essentially carbonates were accumulating on a CeZrCoRh mixed oxide catalyst under steam reforming of ethanol conditions, leading to the blocking of active sites. For the present case, the formation of carbonates over the same Ir/CeO₂ was clearly identified by DRIFT in our reference [1] but together with acetate adspecies. Therefore, we consider that both acetates and carbonates are reacting intermediates of the steam reforming of ethanol (acetates decompose into carbonate and CH_x at metal/support interface) and we have lumped them into the category of "soft" carbonaceous overlayer built rapidly after the catalyst is contacted to the reacting feed.

To ascertain this assignment, we made a rough calculation of the amount of soft carbon deposited per surface oxygen atom of ceria (O_S) from the TPO measured specific carbon deposition and the density of surface oxygen. At 773 K and after 2 h on stream, about 10 mg C g_{cat}⁻¹ accumulated over the surface containing about 21 μmol O_S m⁻². Considering the final BET surface area of the catalyst (56 m² g⁻¹), the C/O_S ratio was calculated to be ca. 0.7. If one considers that most of the ceria adspecies at such low reaction temperature are C₂ (essentially acetate type) with some C₁ (carbonate type) adspecies, this ratio corresponds to a surface occupancy by the reacting intermediates (including "spectators") of ca. 1/3. This surface coverage is quite plausible if one assumes a similar coverage by hydroxyl groups as can be foreseen from elementary reaction stoichiometry, e.g. the oxidation of an ethoxy species into an acetate one (CH₃CH₂O_S + O_S → CH₃CHO_S + OH_S). It could be added that the shape of the soft carbon TPO peak with a small and sharp peak followed by a large shoulder (Figure IV-10 A) could arise from the difference between i) the adspecies on or in close vicinity of the metal particles where the oxygen dissociates and therefore easily oxidized and ii) the ones located far away from the metal particles, which requires oxygen spillover along the ceria surface, and therefore slightly higher temperature for being oxidized.

A slightly lower ratio (C/O_S = 0.4) is found at 923 K (BET surface area = 47 m² g⁻¹). This indicates a lower surface coverage by the reacting adspecies, which is quite expected at higher temperature. In addition, the higher temperature also changed the nature of the reacting intermediates (possibly more CH_x than C₂) which might explain the already mentioned change in the soft carbon TPO peak shape (Figure 10 C). The surface metallic sites were not

considered here, being in too low concentration as compared to the surface ceria sites (ca. 1%), and therefore only weakly affecting the above reasoning.

To summarize, the initial catalyst start-up period corresponds to both a ceria surface restructuring (loss of microporosity) while it is re-oxidized and the build-up of a reacting adspecies layer (C₂-C₁ adspecies and hydroxyl groups). The latter does not contribute to the long term ageing phenomena.

If one considers now the hard carbon deposits observed essentially at low reaction temperature (773 K), they obviously correspond to the carbon layers progressively encapsulating the catalyst particles (both Ir and ceria), revealed by TEM on Figure IV-9. They are most likely originate from the polymerization of acetaldehyde or ethylene intermediates into amorphous carbon layers, formed in measureable amounts at low testing temperature, as seen previously. Thus, Platon et al. [8] found that co-feeding of ethylene doubled the deactivation rate for steam reforming of ethanol over a Rh/Ce-Zr catalyst, which is close to our system. From the TEM and TPO analyses, these amorphous carbon layers are no longer formed at higher reaction temperature, likely due to the fact that the reacting C₂ intermediates are much more easily cracked into syngas at higher temperatures. Therefore, since these "hard" carbon deposits do not accumulate at high temperature, though the catalyst deactivates even faster, as shown on Figure IV-7B, these carbon deposits cannot be considered as the main factor responsible for the long-term ageing processes. Note however that this statement refers to the present operating conditions, at rather high space velocity and low conversion, therefore not favoring the hard carbon deposition. It might be foreseen that much more severe conditions favoring the accumulation of this type of encapsulating carbon would also lead to long term deactivation. It can be added that for the case of non noble based catalysts (like the cobalt based materials reported in [21, 22]), the favored production of filamentous carbon likely via carbide intermediates might explain serious deactivation at mild temperature, where these filaments are deemed to break the strong metal-support interaction required for allowing the bi-functional process of steam reforming of ethanol.

Let us consider now the structural changes in more details. If one accounts for the changes in BET surface area (between 2 and 60 h on stream), it comes that the intrinsic rates (in $\mu\text{mol m}^{-2} \text{s}^{-1}$) reported in Table 1 are about two times larger after 2 h than after 60 h on stream (0.39 vs.

0.18 at 773 K and 3.04 vs. 1.65 at 923 K). Therefore, the changes in the BET surface area (essentially due to ceria restructuring from spherical crystallites to polygonal cubes) cannot explain the changes in the intrinsic activity. If one considers also the changes in the Ir dispersion due to the metal particle sintering (just by dividing the intrinsic rates by the Ir dispersion), we obtain very close values after 2 and 60 h on stream (1.9 vs. 1.7 at 773 K and 18.2 vs. 17.4 at 923 K) as can be seen in Table IV-1. Therefore, these simple calculations demonstrate that the long term deactivation observed at any reaction temperature is essentially due to combined changes in both the ceria surface area and the Ir dispersion. This important result is in line with our previous study on the oxidative steam reforming, stating that the interface between the ceria surface and the Ir particles, which depends both on the BET area and the Ir dispersion, essentially monitors the bi-functional mechanism of reforming reaction over such type of catalysts [12].

Finally, since "pseudo intrinsic" conversion rates (related to the active sites at metal/ceria interface) were obtained after correction of all the deactivating factors, the corresponding intrinsic activation energy has been evaluated from the rate values at 773 and 923 K. It leads to a value of 91 kJ/mol. This value compares rather well with the apparent activation energy values reported in the literature[23] (from 80 to 400 kJ/mol).

IV.3. Summary

This study of the ageing of the model Ir/CeO₂ catalyst under steam reforming of ethanol conditions has demonstrated that the changes in catalytic activity and selectivity are due to various factors, depending on the time on stream and the operating conditions. A fast but moderate loss of activity is observed during the initial period on stream (about 2 hours) due to a fast ceria oxidation and restructuring, coinciding with an active phase build-up, formed of a quasi steady single layer of C₂ adspecies over the ceria surface. Upon longer testing periods (from 2 to 60 h), a slow and continuous sintering of the Ir particles and the ceria crystallites (monitored essentially by the reaction temperature) leads to an irreversible deactivation essentially due to the degradation of the metal/ceria interface, which controls the cracking of the C₂ adspecies on the ceria surface into C₁ precursors and syngas. At 773 K an encapsulating layer of amorphous carbon is building up due to the presence of graphite

precursors like acetaldehyde and possibly ethylene. This encapsulating carbon layer does not seem to be detrimental to the catalytic activity, at least up to 60 h testing. Diffusion limitation effects might be expected for longer times on stream corresponding to industrial applications.

From this ageing analysis, it might be inferred that any marked improvement in catalyst stability would require the stabilization of both the ceria surface area (like doping the ceria with lanthanide ions as will be shown in Chapter V and in [24, 25]) and the metal dispersion (by reinforcing the metal-support interaction as shown in [26, 27]), as will be shown in the next Chapter V. In contrast, the rather stable graphite like layer formed at 773 K might be suppressed by catalyst reoxidation from time to time to avoid potential diffusion limitations. This engineering perspective remains however out of the scope of the present work.

References

- [1] W Cai, F. Wang, C. Daniel, A. C. Veen, Y. Schuurman, C. Descorme, H. Provendier, W. Shen, C. Mirodatos. *J. Catal.* 286 (2012) 137-152.
- [2] A. M. Da Silva, L. O. O. Da Costa, K. R. Souza, L. V. Mattos, F. B. Noronha, *Catal. Commun.* 11 (2010) 736-740.
- [3] S. Freni, S. Cavallaro, N. Mondello, L. Spadaro, F. Frusteri, *Catal. Commun.* 24 (2003) 259-268.
- [4] L. P. R. Profeti, E. A. Ticianelli, E. M. Assaf, *J. Power Sources* 175 (2008) 482-489.
- [5] J. M. Guil, N. Homs, J. Llorca, P. R. De La Piscina, *J. Phys. Chem. B* 109 (2005) 10813-10819.
- [6] A. N. Fatsikostas, X. E. Verykios, *J. Catal.* 225 (2004) 439-452.
- [7] H. S. Roh, A. Platon, Y. Wang, D. L. King, *Catal. Lett.* 110 (2006) 1-6.
- [8] A. Platon, H. S. Roh, D. L. King, Y. Wang, *Top. Catal.* 46 (2007) 374 -379.
- [9] T. Montini, L. De Rogatis, V. Gombac, P. Fornasiero, M. Graziani, *Appl. Catal. B: Environ.* 71 (2007) 125-134.
- [10] H. Chen, H. Yu, F. Peng, H. Wang, J. Yang, M. Pan, *J. Catal.* 269 (2010) 281-290.
- [11] J. J. Birtill, *Ind. Eng. Chem. Res.* 46 (2007) 2392-2398.
- [12] W. Cai, F. Wang, C. Daniel, A. C. Van Veen, Y. Schuurman, C. Descorme, H. Provendier, W. Shen, C. Mirodatos, *J. Catal.* 286 (2012) 137-152.
- [13] W. C. Conner, J. L. Falconer, *Chem. Rev.* 95 (1995) 759-788.
- [14] G. Rabenstein, V. Hacker, *J. Power Sources* 185 (2008) 1293-1304.
- [15] M. Pijolat, M. Prin, M. Soustelle, P. Nortier, *J. Chim. Phys.* 91 (1994) 51-62.
- [16] W. I. Hsiao, Y. S. Lin, Y. C. Chen, C. S. Lee, *Chem. Phys. Lett.* 441 (2007) 294-299.
- [17] F. Sadi, D. Duprez, F. Gerard, A. Miloudi, *J. Catal.* 213 (2003) 226-231.
- [18] A. Yee, S. J. Morrison, H. Idriss, *J. Catal.* 186 (1999) 279-295.
- [19] J. Rasko, A. Hancz, A. Erdohelyi. *Appl. Catal. A: Gen.* 269 (2004) 13-25.
- [20] M. Araque, J. C. Vargas, Y. Zimmermann, A. C. Roger, *Int J. Hydrogen Energy* 36 (2011) 1491-1502.

- [21] H. Wang, Y. Liu, L. Wang, Y. N. Qin, *Chem. Eng. J.* 145 (2008) 25-31.
- [22] A. E. Galetti, M. F. Gomez, L. A. Arrua, A. J. Marchi, M. C. Abello, *Catal. Comm.* 9 (2008) 1201-1208.
- [23] C. Grashinsky, M. Laborde, N. Amadeo, A. Le Valant, N. Bion, F. Epron, D. Duprez, *Ind. Eng. Chem. Res.* 49 (2010) 12383–12389.
- [24] B. M. Reddy, L. Katta, G. Thrimurthulu, *Chem. Mater.* 22 (2010) 467-475.
- [25] F. Wang, W. Cai, H. Provendier, Y. Schuurman, C. Descorme, C. Mirodatos, W. Shen, *Int. J. Hydrogen Energy* 36 (2011) 13566-13574.
- [26] G. Zhou, L. Barrio, S. Agnoli, S. D. Senanayake, J. Evans, A. Kubacka, M. Estrella, J. C. Hanson, A. M. Arias, M. F. Garcia, J. A. Rodriguez, *Angew. Chem. Int. Ed.* 49 (2010) 9680-9684.
- [27] S. Bernal, J. J. Calvino, M. A. Cauqui, J. M. Gatica, C. Larese, J. A. P. Omil, J. M. Pintado, *Catal. Today* 50 (1999) 175-206.

Chapter V Enhancing catalyst performance by PrO_x-doping in an Ir/Ce_{0.9}Pr_{0.1}O₂ system

The previous studies reported in this manuscript were mainly focused on the kinetics and the deactivation mechanisms occurring in the steam reforming of ethanol reaction over Ir/CeO₂ catalysts. The key catalytic role of the ceria support in the bi-functional process and the large impact of its structure/texture on the ageing processes were demonstrated. In order to further improve the performance (activity, selectivity and stability) of our reference material, its catalyst formulation was modified by PrO_x doping, on the basis of the literature analysis and preliminary screening experiments not reported in this manuscript.

Ceria binary oxides in which cerium are partially substituted, generating a defective fluorite structure, are known to present significantly improved redox properties and thermal stability. For example, the redox properties of Ce-ZrO₂, Ce-La₂O₃ and Ce-TiO₂, compared to pure CeO₂, are widely enhanced as far as solid solutions are formed [1-3]. Similarly, PrO_x-doping also significantly promotes the OSC of ceria and facilitates the mobility of surface oxygen species [4]. Recently, the Rh/Ce_{0.8}Pr_{0.2}O₂ catalyst was found to display a much higher catalytic activity and stability than the Rh/Ce_{0.8}Zr_{0.2}O₂ catalyst in the steam reforming of ethanol reaction at 823 K [5], although the detailed role of the PrO_x-doping was not clear. Inferentially, the role of PrO_x in promoting the catalyst activity and stability was carefully analyzed in the present chapter, by examining the performances of PrO_x-doped ceria supported Ir nanoparticles in the steam reforming of ethanol reaction at high space velocity, i.e. under conditions allowing to discard any mass transfer effects. The redox properties, oxygen storage capacity and thermal stability of the PrO_x-doped ceria-supported catalyst were extensively investigated.

V.1. Physical and chemical properties of the oxide supports and of the catalysts

V.1.1. The oxide supports characterizations

The BET surface area of the Ce_{0.9}Pr_{0.1}O₂ oxide was 197 m²/g, a value slightly higher than that of CeO₂ (153 m²/g) after calcination at 673 K [6].

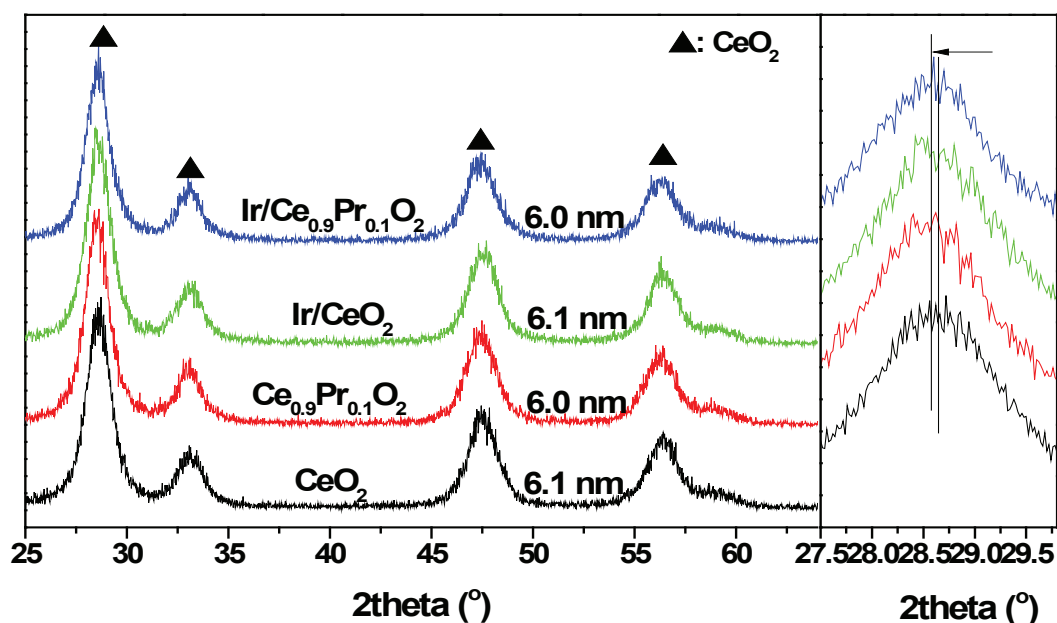


Figure V-1 XRD patterns of the oxides and the fresh Ir catalysts with the crystalline sizes of the oxides.

Figure V-1 shows the XRD patterns of the oxides. The characteristic diffraction lines of the CeO₂ fluorite structure (PDF#65-5923) were observed for both the pure CeO₂ and the doped Ce_{0.9}Pr_{0.1}O₂ oxide. The average crystallite size of the oxides was about 6 nm in both cases. However, the (111) diffraction line of the Ce_{0.9}Pr_{0.1}O₂ oxide shifted slightly towards lower angles as compared to the pure ceria. Accordingly, the lattice parameter increased from 0.5423 nm (CeO₂) to 0.5436 nm (Ce_{0.9}Pr_{0.1}O₂), indicating that Pr^{δ+} was incorporated into the ceria lattice [7]. Generally, doping of Mⁿ⁺ into the CeO₂ lattice may cause an expansion or shrinkage of the CeO₂ lattice, depending on the radius of the dopant. The ionic radii of Pr³⁺ and Pr⁴⁺ are 0.113 and 0.096 nm, respectively; while the ionic radius of Ce⁴⁺ is 0.097 nm.

Then, the substitution of Ce⁴⁺ by Pr³⁺ in the lattice structure should induce a slight expansion. This observation is in line with previous reports on PrO_x-doped ceria oxides [8].

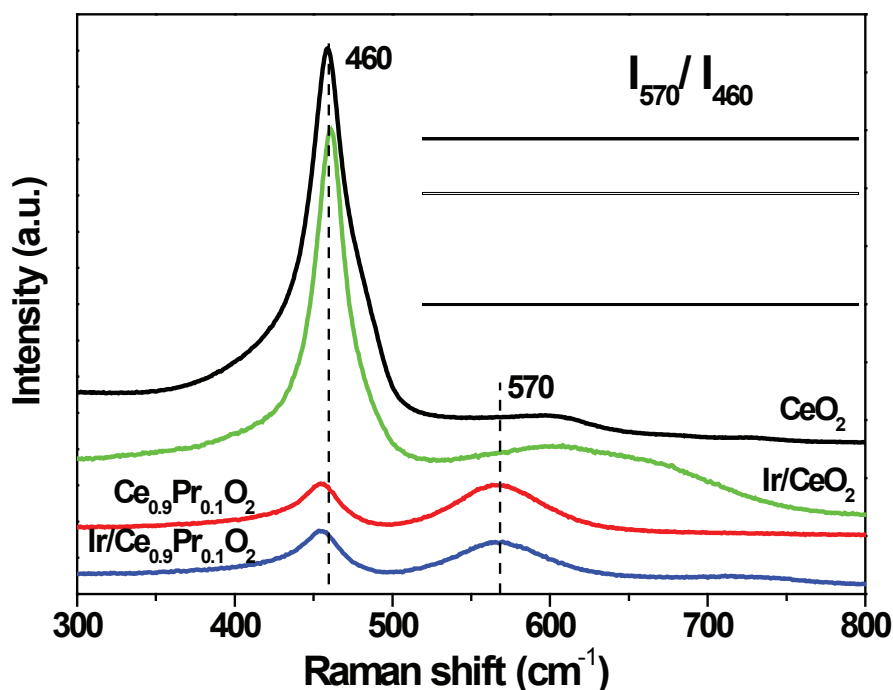


Figure V-2 Raman spectra of the oxides and the fresh Ir catalysts.

Figure V-2 shows the Raman spectra of the oxides. The band at 460 cm⁻¹ is ascribed to the active T_{2g} vibration mode of Ce-O bond in CeO₂ [9]. In the case of the mixed oxide, no Pr-O characteristic vibration was detected, but a small shift of the Ce-O bond was noticed, suggesting the effective incorporation of PrO_x into the fluorite structure [10]. It has been demonstrated that the insertion of PrO_x decreased the vibration frequency of Ce-O bond and broadened the Raman band because of the lattice extension [11]. Since the Ce_{0.9}Pr_{0.1}O₂ sample has a high UV-visible optical absorption at 514 nm [7], most of the excitation and scattered light is absorbed by the sample. As a result, the intensity of the Raman bands weakened considerably. Moreover, a new band at 570 cm⁻¹ appeared in the Ce_{0.9}Pr_{0.1}O₂ sample, which might be linked to the presence of lattice defects originating from the creation of oxygen vacancies [7, 10, 11]. Quantitatively, the I₅₇₀/I₄₆₀ ratio, which gives an indication on the relative amount of oxygen vacancies increased significantly in the Ce_{0.9}Pr_{0.1}O₂ mixed oxide, supporting the generation of large amounts of oxygen vacancies upon PrO_x doping. Note

however that a large band is also observed at 575 cm⁻¹ on pure Pr₂O₃ oxide, which does not allow us to conclude non ambiguously that only an effective and homogeneous insertion of Pr^{δ+} ions within the fluorite lattice has generated oxygen vacancies.

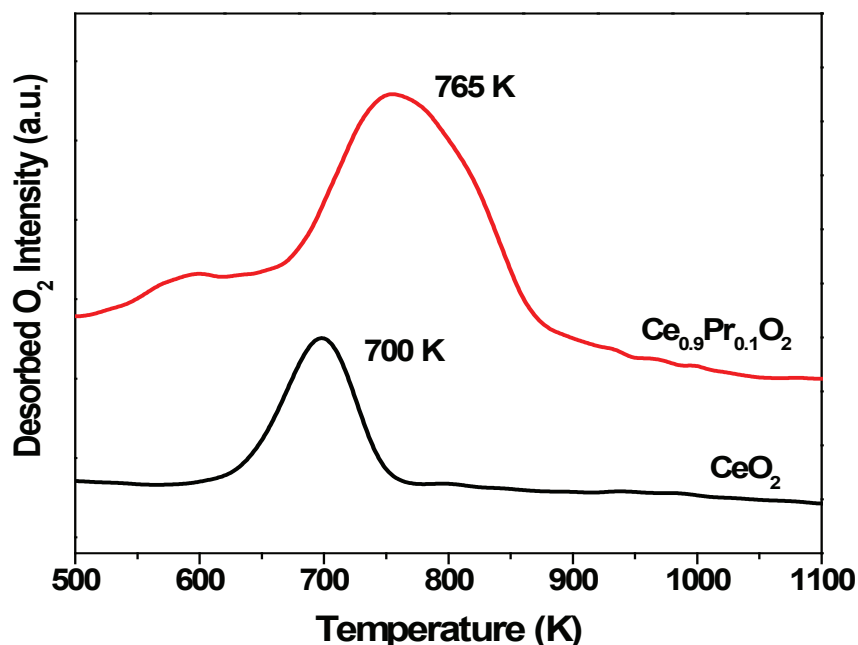


Figure V-3 O₂-TPD profiles of CeO₂ and Ce_{0.9}Pr_{0.1}O₂.

Figure V-3 presents the O₂-TPD profiles of the two oxides. Most of the molecular oxygen desorbed at about 700 K from pure CeO₂ and 765 K from Ce_{0.9}Pr_{0.1}O₂. The corresponding amounts were 44 and 170 μmol O₂/g, respectively. In line with literature analysis [12], this desorption can be ascribed to the weakly-bonded surface oxygen species. The relatively easier oxygen removal in the mixed oxide is intimately associated with the grain boundaries and defects created by the incorporation of PrO_x, favoring the diffusion of surface oxygen species. Table V-1 compares the oxygen storage capacities of the oxides. The OSC of Ce_{0.9}Pr_{0.1}O₂ is found much higher than that of CeO₂ [4]. Cerium is well known to undergo fast redox cycles between the Ce⁴⁺ and Ce³⁺ states as oxygen is stored and released [13]. In turn, after the incorporation of Pr³⁺ which is deemed to generate more oxygen vacancies, associated with the Pr⁴⁺/Pr³⁺ and Ce⁴⁺/Ce³⁺ redox sites [8], an enhanced oxygen storage capacity was revealed, tending to validate our reasoning on PrO_x doping effects.

V.1.2. The Ir catalysts characterizations

The ICP analysis revealed that the Ir loading of CeO₂ and Ce_{0.9}Pr_{0.1}O₂ was 1.86 and 1.87 wt.%, respectively. The specific BET surface area of CeO₂ and Ce_{0.9}Pr_{0.1}O₂ decreased only slightly from 170 to 153 m²/g and from 197 to 184 m²/g after the deposition of Ir, respectively (Table V-1). After hydrogen reduction at 673 K, the BET surface area further decreased to 148 and 170 m²/g, respectively, i.e., still without major change in the support texture. Thus, it can be concluded that the loading of iridium and the subsequent reduction did not affect significantly the textural properties of the oxides.

Table V-1 Texture properties of the oxides and the fresh Ir catalysts.

Sample	BET (m ² /g)	Ir (wt.%)	Ir dispersion (%)	Ir size (nm)	Support size (nm)	OSC (μmol O/g)
CeO ₂	170	--	--		6	1136
Ce _{0.9} Pr _{0.1} O ₂	197	--	--		6	1402
Ir/CeO ₂	153	1.86	65	1.5	6	1689
Ir/Ce _{0.9} Pr _{0.1} O ₂	184	1.87	70	1.4	6	2170

As seen in Table V-1, the Ir dispersion on the fresh Ir/CeO₂ and Ir/Ce_{0.9}Pr_{0.1}O₂ catalysts were 65% and 70% respectively, as estimated from hydrogen chemisorption. The corresponding particle size of Ir was 1.5 and 1.4 nm, respectively. Furthermore, no diffraction lines characteristic of Ir was observed on the XRD patterns shown in Figure V-1 since the particles were highly dispersed on the supports and too small to be detected. The I₅₇₀/I₄₆₀ ratios of the Ir catalysts were larger than the respective pure supports (Figure V-2), suggesting that the Ir species might favor the generation of oxygen vacancies, possibly by insertion of well dispersed Ir ions in the ceria or ceria doped matrix. Such a feature of highly dispersed noble metals insertion in the fluorite structure, generally in the defect zones (like the interface between polycrystalline domains) has been considered in the literature, e.g. for ceria based catalysts doped with lanthanides and dedicated to methane reforming [14]. This would lead to a reinforced metal/support interaction.

Figure V-4 shows the HRTEM images of the fresh catalysts. The size of the CeO₂ and Ce_{0.9}Pr_{0.1}O₂ particles ranged from 5 to 10 nm. The Ir particles were uniformly distributed on the oxides with average sizes of 1.2-1.6 nm. The Ir particles were relatively smaller on Ce_{0.9}Pr_{0.1}O₂ than on CeO₂, confirming a stronger interaction between the metal and the doped support. The loading of Ir led to an increase in the I₅₇₀/I₄₆₀ ratio in the Raman spectra (Figure V-2), strengthening the idea that part of the Ir phase, as ionic clusters, might reinforce or stabilize the concentration of oxygen vacancies.

Table V-1 also compares the OSC of the oxides and the fresh catalysts. Clearly, the loading of Ir significantly promotes the OSC, this effect being more significant for the doped Ir/Ce_{0.9}Pr_{0.1}O₂ catalyst than for the reference Ir/CeO₂ catalyst. This result is in good keeping with the above conclusion that the addition of noble metal to ceria, and even more for doped ceria, promotes the redox ability of the oxide via a reinforced concentration of ionic oxygen vacancies [15].

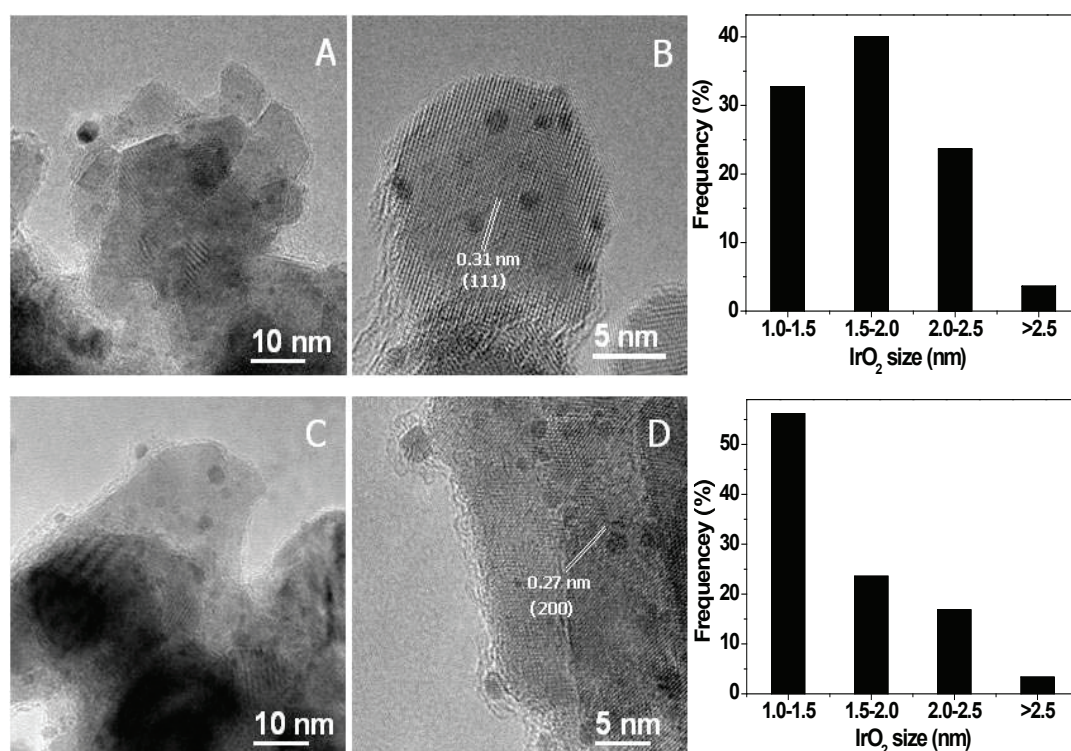


Figure V-4 TEM images of the fresh Ir/CeO₂ (A, B) and Ir/Ce_{0.9}Pr_{0.1}O₂ (C, D) catalysts and the related IrO₂ particles size distribution.

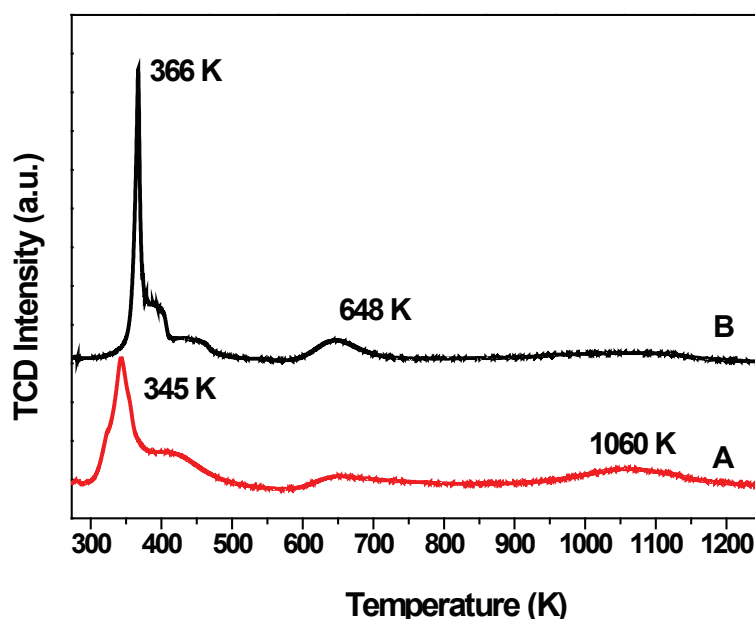


Figure V-5 H₂-TPR profiles of the fresh Ir/CeO₂ (A) and Ir/Ce_{0.9}Pr_{0.1}O₂ (B) catalysts.

Table V-2 Hydrogen consumption and reduction degree of the Ir catalysts from H₂-TPR experiments.

Samples	H ₂ consumption (μmol/g)	Reduction degree
Ir/CeO ₂	750 (345 K)	46%
	430 (600 K + 1060 K)	
Ir/Ce _{0.9} Pr _{0.1} O ₂	1180 (366 K)	68%
	988 (648 K + 1060 K)	

Figure V-5 shows the H₂-TPR profiles of the fresh catalysts. Three distinct reduction peaks were observed in both cases. The low-temperature reduction peak located at about 366 K was mainly assigned to the reduction of IrO₂ to metallic Ir, while the peak at about 648 K was related with the surface reduction of the oxides and the reduction at 1060 K was associated with oxygen removal from the bulk oxides. The amounts of hydrogen consumed by the low-temperature reduction were 750 and 1180 μmol/g for the Ir/CeO₂ and Ir/Ce_{0.9}Pr_{0.1}O₂ catalysts, respectively. These values are much higher than the stoichiometric amount required for reducing IrO₂ to metallic Ir (190 μmol/g), indicating that the reduction of the oxides also occurred at this stage, especially in the case of the Ir/Ce_{0.9}Pr_{0.1}O₂ catalyst. The surface of the oxides in close contact with the Ir particles was readily reduced through hydrogen spillover. The reduction led to the formation of Ir/CeO_{1.90} and Ir/Ce_{0.9}Pr_{0.1}O_{1.83}, respectively. The

subsequent hydrogen consumptions can be attributed to the further reduction of the oxides, resulting in the following final compositions: Ir/CeO_{1.77} and Ir/Ce_{0.9}Pr_{0.1}O_{1.66}. The hydrogen consumption and the reduction degree of Ir/CeO₂ and Ir/Ce_{0.9}Pr_{0.1}O₂ catalysts are displayed in Table V-2. The hydrogen consumption over the Ir/Ce_{0.9}Pr_{0.1}O₂ catalyst is relatively larger than on the Ir/CeO₂ catalyst, confirming that the Pr doping has promoted the redox properties of the catalyst. As mentioned above, the incorporation of Pr has induced the formation of significant amounts of lattice defects, and thus the mobility of the surface/bulk oxygen anionic species has been greatly improved [16].

Figure V-6A shows the XPS spectra of Ir_{4f} in the fresh and the reduced catalysts. The spectra of Ir_{4f} in the fresh samples show a doublet at 61.6 and 64.6 eV, characteristic of the IrO₂ species. After in situ hydrogen reduction at 673 K, characteristic bands of Ir⁰ appeared at 60.6 and 63.6 eV, suggesting that only metallic Ir was present. The Ce_{3d} spectra shown in Figure V-6B are composed of eight peaks corresponding to four pairs of spin-orbit doublets [17]. The surface proportion of Ce³⁺ was estimated according to the procedure proposed by Laachir et al. [18]. As shown in Table V-3, the proportion of Ce³⁺ after hydrogen treatment increased from 10.1 to 14.8% in the Ir/CeO₂ catalyst and from 9.5 to 20.3% in the Ir/Ce_{0.9}Pr_{0.1}O₂ catalyst. These variations in surface concentration of Ce³⁺ between the two samples and the decrease of the surface atomic percentage of Pr from 10.5 to 6.8 after reduction of the Ir/Ce_{0.9}Pr_{0.1}O₂ catalyst indicate that Pr has diffused from the surface to the bulk during the hydrogen treatment, possibly creating more oxygen vacancies due to valencies unbalance.

Figure V-6C shows the XPS spectra of Pr_{3d}. The bands at 952.6 and 932.6 eV are assigned to Pr⁴⁺ and those at 948.3 and 926.2 eV are attributed to Pr³⁺ [19]. The spectra consist of two sets of multiplets at 933 (3d_{5/2}) and 953 eV (3d_{3/2}), implying the co-existence of Pr³⁺ and Pr⁴⁺ [20]. However, the intensities of the Pr⁴⁺ and Pr³⁺ bands in the reduced sample are lower than those in the fresh one, because of their diffusion into the ceria lattice. The O_{1s} profiles show two peaks at 531 and 529 eV (Figure V-6D). The former corresponds to chemisorbed surface oxygen (O_H) [21] and the later to surface oxygen (O_L) [22]. The much higher O_H concentration in the mixed oxide catalyst confirms the large concentration of electrophilic surface oxygen species that generally act as active centres [23].

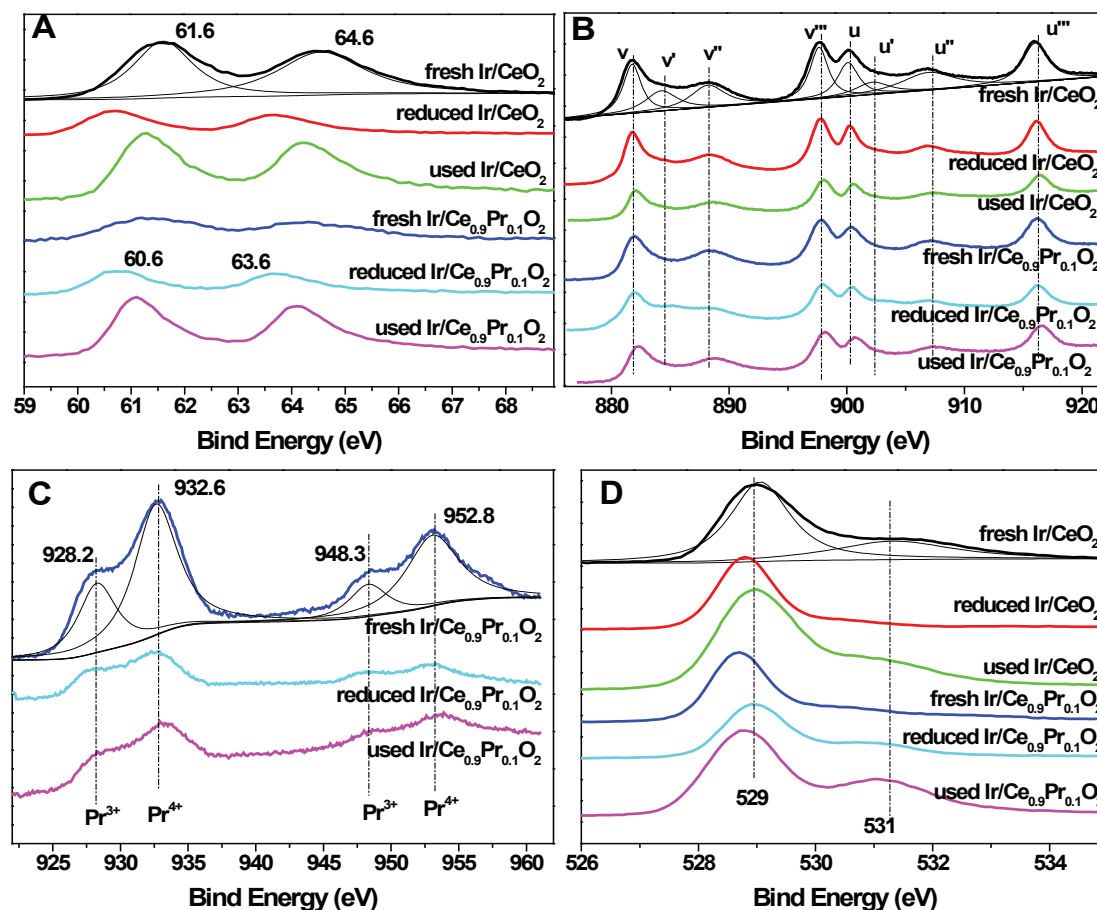
Figure V-6 XPS profiles of Ir_{4f} (A), Ce_{3d} (B), Pr_{3d} (C) and O_{1s} (D) of the Ir catalysts.

Table V-3 Surface atomic compositions from XPS measurements and OSCs of the Ir catalysts.

Samples	Surface composition (atom %)					O _H (%)	O _L (%)	Ce ³⁺ (%)	Pr ³⁺ (%)
	Pr	Ce	O	C	Ir				
Fresh Ir/CeO ₂	-	16.0	68.2	15.5	0.3	19.6	80.4	10.1	-
Reduced Ir/CeO ₂	-	40.3	51.1	8.2	0.4	18.1	81.9	14.8	-
Aged Ir/CeO ₂	-	11.3	31.0	57.2	0.5	26.5	73.5	13.3	-
Fresh Ir/Ce _{0.9} Pr _{0.1} O ₂	10.5	17.2	53.3	18.8	0.2	24.8	75.2	9.5	29.5
Reduced Ir/Ce _{0.9} Pr _{0.1} O ₂	6.8	35.5	54.8	2.5	0.4	22.3	77.7	20.3	40.5
Aged Ir/Ce _{0.9} Pr _{0.1} O ₂	3.1	11.0	36.4	48.9	0.6	32.5	67.5	12.2	43.3

V.2. Catalytic performances and stability of the Ir/CeO₂ and Ir/Ce_{0.9}Pr_{0.1}O₂ catalysts

V.2.1. Catalytic performances of the Ir/CeO₂ and Ir/Ce_{0.9}Pr_{0.1}O₂ catalysts

Figure V-7 illustrates the temperature-dependence of the ethanol conversion and the product selectivity upon steam reforming of ethanol over the Ir/CeO₂ and Ir/Ce_{0.9}Pr_{0.1}O₂ catalysts. Both the ethanol conversion and the selectivity into hydrogen progressively increased as the temperature increased. On the Ir/CeO₂ catalyst, acetaldehyde, acetone and methane appeared as the major carbon containing products below 773 K. A possible simplified reaction pattern would be to consider that ethanol is primarily dehydrogenated into acetaldehyde. Then, acetaldehyde or its precursor is further decomposed into methane and CO or condensed to acetone [24]. CO then reacts with H₂O to produce H₂ and CO₂ through the water-gas-shift (WGS) reaction. Indeed, a much more complex mechanism has to be considered, as it was described in Chapter-IV, involving a sequence of surface intermediates like ethoxy and acetate adspecies, migrating from the basic sites of the ceria towards the Ir/ceria interface to be cracked into CH_x, Ir carbonyls and possibly carbonates.

At 873 K, ethanol, acetaldehyde, and acetone were fully converted to H₂, CO₂, CO and CH₄. At higher temperature, the selectivity into CO increased rapidly while the selectivity into methane and carbon dioxide decreased. Thus, at 923 K, the outlet gas consisted of 69% H₂, 11% CO, 13% CO₂ and 7% CH₄. This clearly indicates, as already pointed out in the previous mechanistic part of the work, that the methane steam reforming and the reverse WGS reactions occur to a large extent at high temperature, as predicted by thermodynamics.

A similar reaction pattern was observed on the Ir/Ce_{0.9}Pr_{0.1}O₂ catalyst. However, the ethanol conversion readily approached 100% at ca. 773 K, whereas ethanol was totally converted only above 873K on the Ir/CeO₂ catalyst. The outlet gas contained 72% H₂, 12% CO, 12% CO₂ and 4% CH₄ at 923 K. Thus, at higher temperature, the syngas chemistry including the WGS tends to control the reaction selectivity.. The lower selectivity into methane and the higher hydrogen selectivity over the Ir/Ce_{0.9}Pr_{0.1}O₂ catalyst could imply an enhanced activity in methane steam reforming.

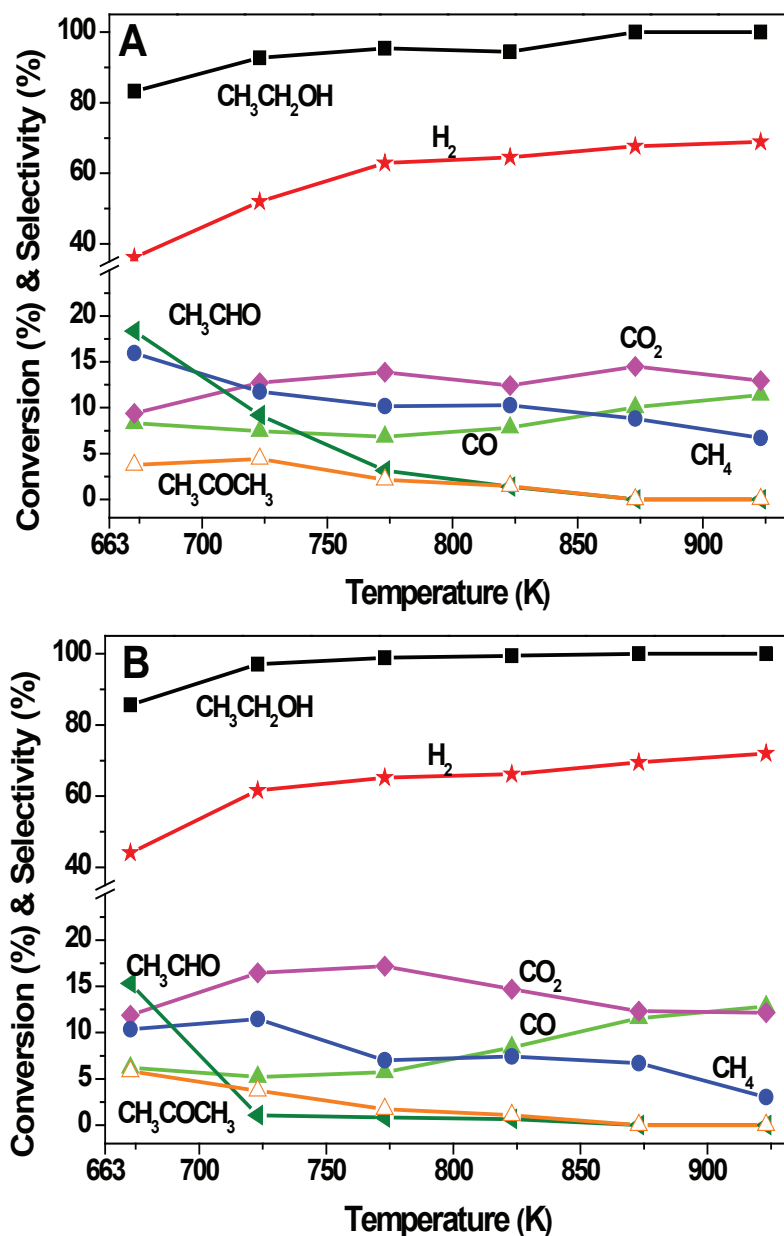


Figure V-7 Ethanol conversion and product selectivity upon steam reforming of ethanol over Ir/CeO₂ (A) and Ir/Ce_{0.9}Pr_{0.1}O₂ (B) as a function of temperature.

Reaction conditions: 100 mg catalyst, C₂H₅OH/H₂O = 1:3 (molar ratio), GHSV = 18,000 mL/(g·h), P = 0.1 MPa.

In order to identify the intrinsic activity of the catalyst, the turnover frequency (TOF, the number of ethanol molecule converted per surface Ir atom and per second), was calculated by maintaining the ethanol conversion in the range 3-9%. On the Ir/Ce_{0.9}Pr_{0.1}O₂ catalyst, the TOF values were 0.09 s⁻¹ at 523 K and 0.17 s⁻¹ at 573 K, whereas the corresponding values were 0.07 and 0.14 s⁻¹ on the Ir/CeO₂ catalyst. Considering the almost similar Ir particle size on

both samples (1.5 vs 1.4 nm), this slight but significant variation in the intrinsic activity might be associated with some specificities of the oxide support and of the metal/support interface.

As said before, the activation of ethanol is mainly related to the ceria surface where the primary dehydrogenation and dehydration occur. Here, the nature and density of surface defect is expected to play a major role and might explain the observed differences between the un-doped and the doped ceria systems. Then, after migration towards the Ir/ceria interface, also controlled by this surface structure, the C₂ adspecies are cracked into C₁ adspecies at the Ir/ceria interface and again, the structure of that interface is likely to depend also on the lattice vacancies concentration. In addition, the oxygen vacancies might facilitate the water activation on the ceria surface into OH adspecies.

Thus, comparing both catalysts, the higher concentration of surface defects of the Ir/Ce_{0.9}Pr_{0.1}O₂ catalyst combined with a tighter interface between the oxide and the metal phases is likely to explain the slightly higher intrinsic activity observed experimentally for the doped system.

V.2.2. Stability tests of the Ir/CeO₂ and Ir/Ce_{0.9}Pr_{0.1}O₂ catalysts

We have previously reported that the Ir/CeO₂ catalyst was highly active in the steam reforming of ethanol at 923 K under stoichiometric conditions and relative low space velocity (6,000 mL/(g·h)), though some deactivation was observed under conditions where the conversion was only partial, as analyzed in the previous Chapter-IV and reported in [25, 26]. Here we have further investigated the stability of the Ir/CeO₂ and Ir/Ce_{0.9}Pr_{0.1}O₂ catalysts at 923 K at higher space velocity (18,000 mL/(g·h)), when the ethanol and the reaction intermediates were only partially converted into H₂, CO, CO₂ and CH₄.

Figure V-8A shows the conversion of ethanol and the selectivity of the outlet gases upon steam reforming of ethanol over the Ir/CeO₂ reference catalyst for 300 h time on-stream. The conversion of ethanol decreased from 100% initially down-to 80% after 60 hours. At the same time, the concentration of H₂ decreased from 61% down-to 55%. Thereafter, the conversion of ethanol gradually decreased down-to 62% after 300 h on-stream while the distribution of the products remained unchanged.

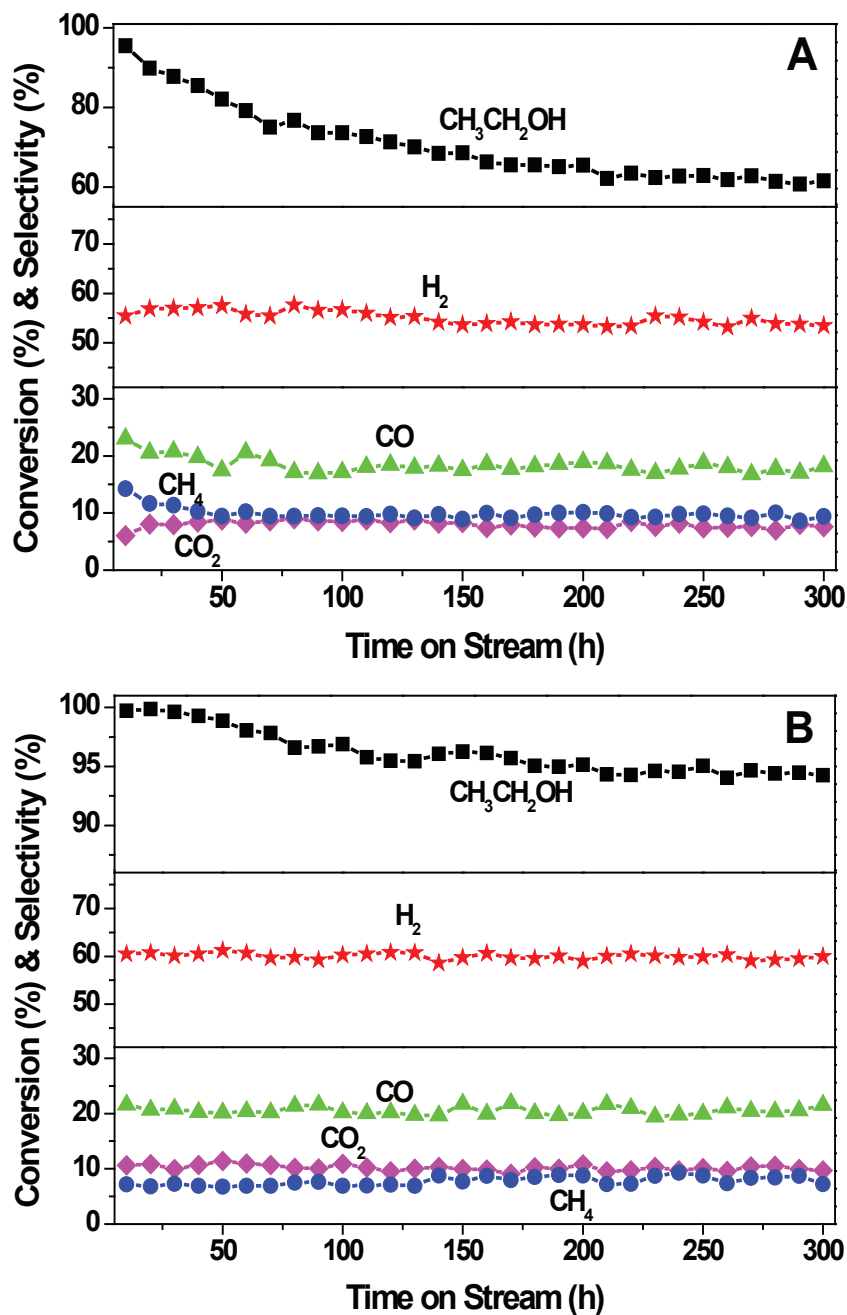


Figure V-8 Ethanol conversion and product selectivity upon steam reforming of ethanol over Ir/CeO₂ (A) and Ir/Ce_{0.9}Pr_{0.1}O₂ (B).

Reaction conditions: 100 mg catalyst, C₂H₅OH/H₂O = 1:3 (molar ratio), GHSV = 18,000 mL/(gh), T = 923 K, P = 0.1 MPa.

In contrast with the above results, the ethanol conversion on the Ir/Ce_{0.9}Pr_{0.1}O₂ catalyst only slightly decreased from 100% to 98% during the first 60 h time on-stream and was kept constant at 95% up to the end of the test (Figure V-8B). Meanwhile, the selectivity of H₂, CO, CO₂ and CH₄ in the outlet gas varied slightly during the whole process.

This question arises now to understand the origin of that improved stability for the PrO_x-doped system,

Our study of the deactivation process reported in the previous chapter stated that the deactivation was essentially due to a loss of active surface both for the ceria support and the Ir particles, and not to carbon deposition. We have therefore undertaken to characterize the aged catalysts after 300 h on stream to check again these important features.

V.3. Characterization of the aged Ir/CeO₂ and Ir/Ce_{0.9}Pr_{0.1}O₂ catalysts

V.3.1. OSC of the aged catalysts

Table V-3 compares the OSC of the used catalysts after 300 h time on-stream. The OSC of used samples were generally lower than those of the fresh ones, probably because of the sintering of the support under reaction conditions, as will be shown later. However, the OSC of the used Ir/Ce_{0.9}Pr_{0.1}O₂ was still higher than that of the used Ir/CeO₂, confirming the crucial role of the Pr doping.

V.3.2. XRD of the aged catalysts

Figure V-9 shows the XRD patterns of the used Ir/CeO₂ and Ir/Ce_{0.9}Pr_{0.1}O₂ catalysts. All the samples exhibit the characteristic diffraction lines of the fluorite structure. For the Ir/CeO₂ catalyst, the mean ceria crystallite size increased from 6.0 nm in the fresh sample to 12.0 and 13.8 nm in the used ones after 60 and 300 h on-stream, respectively. On the other hand, the crystallite size increased from 6.0 nm in the fresh Ir/Ce_{0.9}Pr_{0.1}O₂ catalyst to 10.0 nm after 60 h time on-stream and kept constant at this level for the remaining time. Moreover, a zoom on the (111) diffraction line evidenced that, the position of the highest diffraction line in the used Ir/Ce_{0.9}Pr_{0.1}O₂ catalyst has not changed between 60 h and 300 h on-stream, (the same shift towards lower 2theta values was observed between the diffraction lines of the used Ir/Ce_{0.9}Pr_{0.1}O₂ and those of the used Ir/CeO₂ catalyst), confirming the stable presence of the solid solution even operated for 300 h.

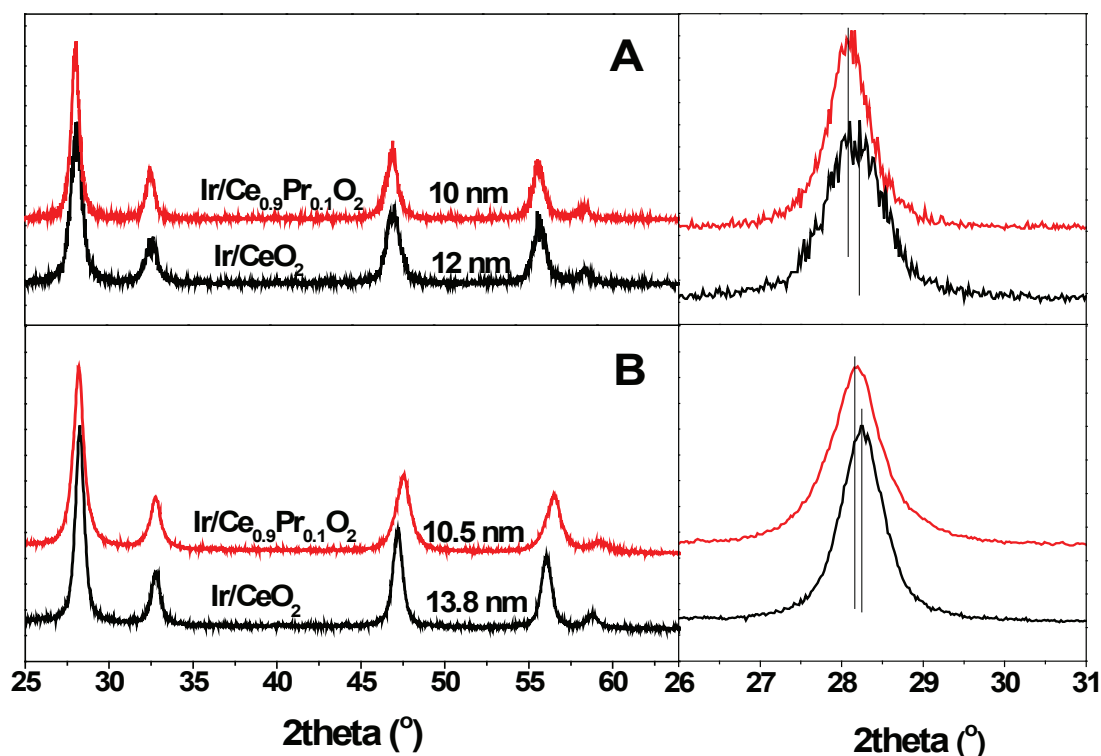


Figure V-9 XRD patterns of the used Ir/CeO₂ and Ir/Ce_{0.9}Pr_{0.1}O₂ catalysts after 60 (A) and 300 h (B) time on stream at 923 K, respectively.

V.3.3. Temperature-programmed oxidation (TPO)

Figure V-10 shows the TPO files of the used catalysts. For the catalysts tested for 60 h, the CO₂ desorption occurred at 553-603 K, which can be assigned to the oxidation of the reacting intermediates adspecies (mainly ethoxy, acetates and possibly carbonates) forming a quasi monolayer on the catalyst surface as shown in Chapter-IV and proposed in [25, 26]. The total amount of carbon deposited on the Ir/Ce_{0.9}Pr_{0.1}O₂ catalyst was 3.7 mg C/g_{cat}, slightly lower than that on the Ir/CeO₂ catalyst (5.6 mg C/g_{cat}). After 300 h on-stream, a significant production of CO₂ appeared at 940 K on the used Ir/CeO₂ catalyst, indicative of the presence of some hard coke, though it was shown in Chapter IV not to contribute essentially to the catalyst deactivation [25]. However, this type of hard coke was not detected on the used Ir/Ce_{0.9}Pr_{0.1}O₂ catalyst. The total amount of carbon deposited after 300 h was 11.8 and 4.5 mg C/g_{cat} for the Ir/CeO₂ and Ir/Ce_{0.9}Pr_{0.1}O₂ catalysts, respectively. Table V-4 compares the values of carbon deposits over the used catalysts and evaluate the surface concentration of carbon atom (in C atom per surface O atom). The amount of carbon atom deposited on the

Ir/CeO₂ catalyst was slightly higher than that on the Ir/Ce_{0.9}Pr_{0.1}O₂ catalyst after 60 h on stream, but this difference was much more marked after 300 h on-stream (about 2.6 times less carbon on the promoted system). Thus, the Ir/Ce_{0.9}Pr_{0.1}O₂ catalyst inhibits the deposition of long term hard carbon in a more efficient way than the un-promoted system. From the characterization analysis reported above, this trend is assigned to a favored water activation leading to better carbon gasification. The higher concentration of oxygen vacancy in the PrO_x-doped catalyst is likely to originate this effect.

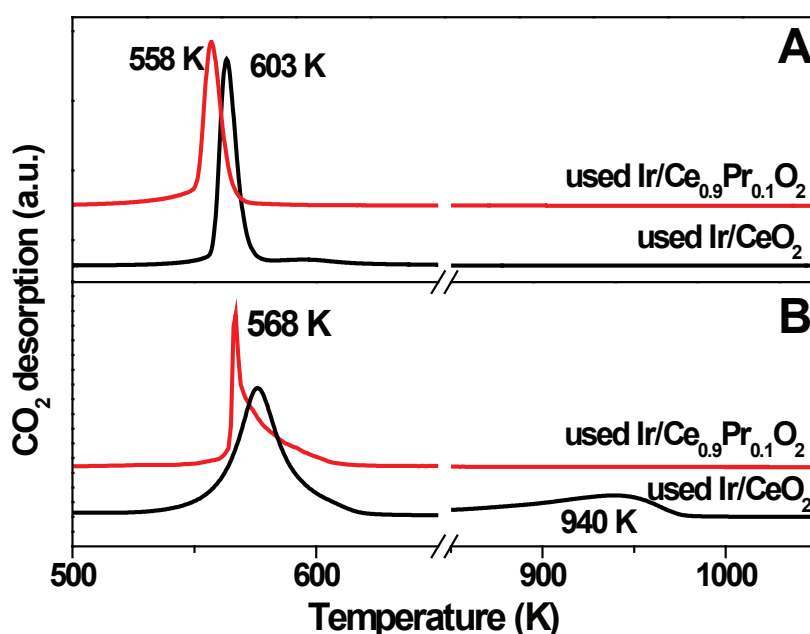


Figure V-10 TPO profiles of the used Ir/CeO₂ and Ir/Ce_{0.9}Pr_{0.1}O₂ catalysts after 60 (A) and 300 h (B) time on stream at 923 K.

Table V-4 Amounts of carbon deposits over the used catalysts.

Catalyst	Ir dispersion ^a	Amount of carbon deposits (mg C/g _{cat})		Surface coverage of carbon deposits (atom C/ surface atom O)	
		60 h	300 h	60 h	300 h
		Ir/CeO ₂	50%	5.6	11.8
Ir/Ce _{0.9} Pr _{0.1} O ₂	50%	3.7	4.5	6	7

a: The average size of Ir particle (d) was 2 nm, judged from the HRTEM images of the used catalysts (see Figure V-11), and the dispersion of Ir was calculated using the formula $D = 1/d \times 100\%$.

V.3.4. High Resolution Transmission Electron Microscopy (HRTEM)

The HRTEM images of the used catalysts showed that the Ir particles were still highly dispersed on the surface of the oxides (Figure V-11). For the used Ir/CeO₂ catalysts, encapsulating carbon (hard coke) was detected after 60 h on-stream and still more after 300 h, as already pointed out in the Chapter IV dedicated to catalyst ageing. The average Ir particle size was slightly increased, leading to a decrease of the Ir dispersion to 50%. It was also noted that some large Ir particles were detached from the support and covered by the deposited carbon. The average CeO₂ particle size increased to about 14 nm, and the surface area of CeO₂ was decreased to 60 m²/g after 300 h on stream. As already stated, these changes indicated the particle reconstruction under reaction conditions. The CeO₂ particles agglomerated and formed irregular polygonal crystallites [27], via an Ostwald ripening to form large polyhedra [28, 29]. This reconstruction of CeO₂ particles with respect to size and shape during the course of the reaction, combined to the Ir sintering, led to a weakened Ir-CeO₂ interaction, and therefore to the observed deactivation.

For the Ir/Ce_{0.9}Pr_{0.1}O₂ catalyst, the Ir and ceria phases also underwent sintering and reconstruction, but to a lesser extent. In addition, the spherical shape of the Ce_{0.9}Pr_{0.1}O₂ particles with rounded edges, and therefore a high surface concentration of defects were maintained even after 300 h on-stream, explaining the better performance of this doped system, as compared to the reference catalyst.

Table V-5 Texture properties of the aged Ir catalysts after 300 h on stream.

Sample	BET (m ² /g)	Ir (wt.%)	Ir dispersion (%)	Ir size (nm)	Support size (nm)	OSC (μmol O/g)
Ir/CeO ₂	60	1.86	50	1.5	14	1371
Ir/Ce _{0.9} Pr _{0.1} O ₂	70	1.87	50	1.4	11	1646

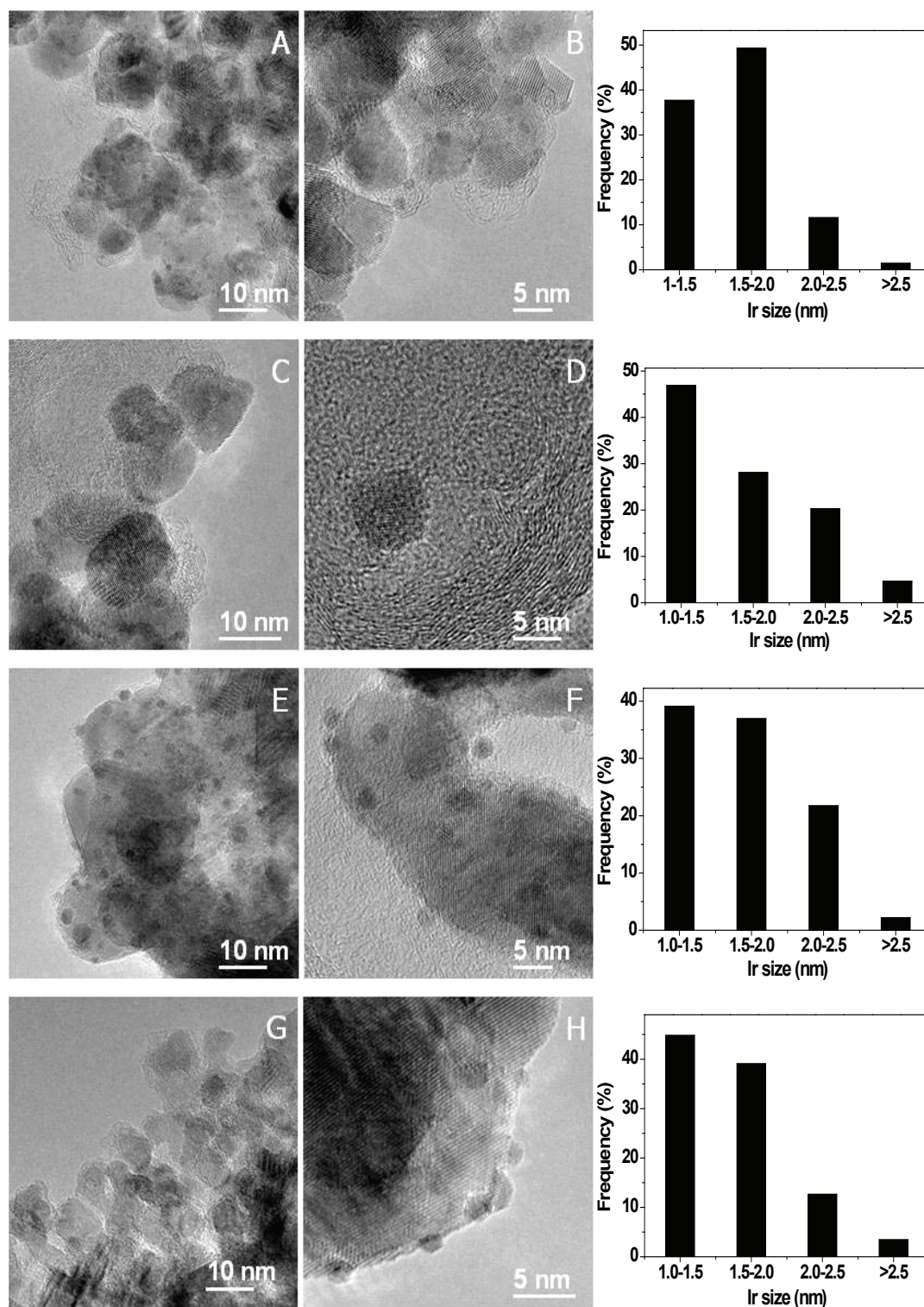


Figure V-11 HRTEM images of the used Ir/CeO₂ (A, B for 60 h, and C, D for 300 h) and Ir/Ce_{0.9}Pr_{0.1}O₂ (E, F for 60 h, and G, H for 300 h) catalysts and the size distributions of Ir species (the counted numbers of Ir species were more than 100).

V.4. Summary

As a conclusion, the following features can be drawn from these results:

- i) The observed deactivation for the two catalysts relates more to changes in the catalyst structure and texture (sintering of ceria grains and Ir particles) rather than to coke deposits, in line with the ageing analysis reported in Chapter IV.
- ii) The changes in texture/structure are much more limited for the PrO_x doped sample, confirming a stronger metal/support interaction able to limit the sintering phenomena. This leads to a much more stable catalytic system under long term SR conditions.
- iii) The main part of the deposited carbon corresponds to the surface occupancy by the reacting intermediates of the reaction, formed rapidly after contacting the catalyst with the reacting mixture, as shown in the previous Chapter-IV. The quasi absence of "hard coke" on the PrO_x doped sample while it accumulates on the non doped reference sample confirms the positive effect of doping on concentration of oxygen defects, which enhanced the ability in activating water for the carbon gasification.

This enhanced stability of the Ir/Ce_{0.9}Pr_{0.1}O₂ catalysts in the steam reforming of ethanol meets quite satisfactorily one of the main goals of the present work.

References

- [1] C. E. Hori, H. Permana, K. Y. Simon Ng, A. Brebber, K. More, K. M. Rahmoeller, D. Belton, *Appl. Catal. B: Environ.* 16 (1998) 105-117.
- [2] B. M. Reddy, L. Katta, G. Thrimurthulu, *Chem. Mater.* 22 (2010) 467-475.
- [3] A. K. Sinha, K. J. Suzuki, *J. Phys. Chem. B* 109 (2005) 1708-1714.
- [4] Z. Song, W. Liu, H. Nishiguchi, A. Takami, K. Nagaoka, Y. Takita, *Appl. Catal. A: Gen.* 329 (2007) 86-92.
- [5] A. M. Karim, Y. Su, J. Sun, C. Yang, J. J. Strohm, D. L. King, Y. Wang, *Appl. Catal. B: Environ.* 96 (2010) 441-448.
- [6] W. Cai, F. Wang, E. Zhan, A. C. Van Veen, C. Mirodatos, W. Shen, *J. Catal.* 257 (2008) 96-107.
- [7] M. F. Luo, Z. L. Yan, L. Y. Jin, M. He, *J. Phys. Chem. B* 110 (2006) 13068-13071.
- [8] B. M. Reddy, G. Thrimurthulu, L. Katta, *J. Phys. Chem. C* 113 (2009) 15882-15890.
- [9] S. Rossignol, F. Gerard, D. Mesnard, C. Kappenstein, D. Duprez, *J. Mater. Chem.* 13 (2003) 3017-3020.
- [10] S. Rossignol, C. Descorme, C. Kappenstein, D. Duprez, *J. Mater. Chem.* 11 (2001) 2587-2592.
- [11] J. R. McBride, K. Demirkol, B. D. Poindexter, W. H. Weber, *J. Appl. Phys.* 76 (1994) 2435-2441.
- [12] C. Bouly, K. Chandes, D. Maret, D. Bianchi, *Stud. Surf. Sci. Catal.* 96 (1995) 261-274
- [13] H. C. Yao, Y. F. Yao, *J. Catal.* 86 (1984) 254-265.
- [14] V. A. Sadykov, N. N. Sazonova, A. S. Bobin, V. S. Muzykantov, E. L. Gubanova, G. M. Alikina, A. I. Lukashevich, V. A. Rogov, E. N. Ermakova, E. M. Sadovskaya, N. V. Mezentseva, E. G. Zevak, S. A. Veniaminov, M. Muhler, C. Mirodatos, Y. Schuurman, A. C. van Veen, *Catal. Today* 169 (2011) 125-137.
- [15] A. Trovarelli, *Catal. Rev. Sci. Eng.* 38 (1996) 439-520.
- [16] H. Li, G. Lu, Y. Wang, Y. Guo, Y. Guo, *Catal. Commun.* 11 (2010) 946-950.

- [17] J. Y. Luo, M. Meng, X. Li, X. G. Li, Y. Q. Zha, T. D. Hu, Y. N. Xie, J. Zhang, *J. Catal.* 254 (2008) 310-324.
- [18] A. Laachir, V. Perrichon, A. Badri, J. Lamotte, E. Catherine, J. C. Lavalley, J. E. Fallah, L. Hilaire, F. Normand, E. Quéméré, G. N. Sauvion, O. Touret, *J. Chem. Soc., Faraday Trans.* 87 (1991) 1601-1609.
- [19] H. He, H. X. Dai, C. T. Au, *Catal. Today* 90 (2004) 245-254.
- [20] J. Mikulova, S. Rossignol, F. Gerard, D. Mesnard, C. Kappenstein, D. Duprez, *J. Solid State Chem.* 179 (2006) 2511-2520.
- [21] T. L. Barr, C. G. Fries, F. Cariati, J. C. Bart, N. Giordano, *J. Chem. Soc. Dalton Trans.* (1983) 1825-1829.
- [22] F. Larachi, J. Pierre, A. Adnot, A. Bernis, *Appl. Surf. Sci.* 195 (2002) 236-250.
- [23] S. Yang, W. Zhu, Z. Jiang, Z. Chen, J. Wang, *Appl. Surf. Sci.* 252 (2006) 8499-8505.
- [24] T. Nishiguchi, T. Matsumoto, H. Kanai, K. Utani, Y. Matsumura, W. Shen, S. Imamura, *Appl. Catal. A: Gen.* 279 (2005) 273-277.
- [25] F. Wang, W. Cai, T. Na, H. Provendier, Y. Schuurman, C. Descorme, C. Mirodatos, W. Shen, *Appl. Catal. B: Environ.* 125 (2012) 546-555.
- [26] W. Cai, F. Wang, E. Zhan, A. C. Van Veen, C. Mirodatos, W. Shen, *J. Catal.* 257 (2008) 96-107.
- [27] Z. L. Wang, X. Feng, *J. Phys. Chem. B* 107 (2003) 13563-13566.
- [28] R. L. Coble, *J. Appl. Phys.* 32 (1961) 787-792.
- [29] F. Huang, H. Zhang, J. F. Banfield, *Nano Lett.* 3 (2003) 373-378.

Chapter VI Influence of CeO₂ shape and structure on Ir/CeO₂ catalyst for hydrogen production from steam reforming of ethanol

After having investigated the impact of PrO_x doping on the catalyst performances and stability in Chapter V, we have undertaken to check the possible effect of catalyst shaping, since shaping represents the compulsory step after formulation to upscale new systems in view of testing them under realistic conditions and at a demonstration or pilot scale. In addition, it was reported that the properties of oxygen storage capacity (OSC), H₂-TPR redox behaviour and catalytic activity are highly dependent on the shape of CeO₂ [1-3].

The first level of catalyst shaping, at this stage of our study, is to explore the domain of nano-shaping, since many effects have been reported recently concerning the synthesis of ceria nanomaterials, like nanoparticles and shaped materials [4]. Ceria nanomaterials can be prepared through several approaches, such as nonisothermal precipitation, vapor-phase evaporation, and solution-based hydrothermal method of cerium precursors and spontaneous self-assembly of cerium oxide nanoparticles to nanorods [5-7]. Today, various morphology-controlled nanostructured ceria including nanorods, nanowires and nanotubes have been synthesized successfully [8, 9]. The question arises now if different shapes of CeO₂ would lead to different catalytic activities. As an example, the CO oxidation rate has been found on CeO₂ nanorods significantly higher than on CeO₂ nanoparticles, possibly due to the differences in exposed active planes [10]. In contrast, CO oxidation has been reported to be much easier on Au/CeO₂ nanoparticles than on Au/CeO₂ nanorods because of the smaller size of nanoparticles [11]. P. Gawade et al. [12] reported that a copper catalyst supported over CeO₂ nanoparticles showed significantly higher activity than supported on CeO₂ nanorods in water gas shift reaction (WGS), which was explained by the capacity of CeO₂ nanoparticles to stabilizing CuO in a much higher dispersion than the CeO₂ nanorods.

Main features of ceria nanocubes, nanoparticles and nanorods. Typical ceria nanoparticles are mainly composed of polyhedron which dominantly dense {111} planes with the size in range of 5-10 nm [1, 10, 13]. In contrast, rod-shaped CeO₂ systems, which can be defined as cylinders with a typical length higher than 50 nm, tend to expose preferentially less dense {110} and {100} planes [1, 3, 14]. Nanocubes can be defined as cubic, the size of which was normally more than 25 nm [1, 15, 16], tend to expose {100} planes. From theoretical calculations, it was found that the surface energy of the three low-index planes in the ceria fluorite structure follows the order {100} > {110} > {111} [17], which might suggest that the formation of anion vacancies is easier in {110} and {100} planes. This might be due to the higher surface energy in a crystal plane which would lead to the more unstable state, thus the easier oxygen extraction. In a consistent way, it was found that the oxygen storage capacity of ceria follows the order: nanocubes > nanorods > nanoparticles [1]. Finally and in good keeping with the above rankings, the {100} and {110} planes were found more active than the {111} planes [18, 19] for CO oxidation and water gas shift reaction in terms of CO conversion.

Thus it can be stated that most of the catalytic studies based on shaped ceria-based materials were focused till now on CO oxidation within the frame of gas exhaust cleaning [10, 11, 20, 21]. Only very scarce studies were devoted to the steam reforming of ethanol [22, 23]. Therefore, it was considered of high interest to analyze the impact of ceria shaping for steam reforming of ethanol on the basis of the mechanistic and kinetic features and the structure/texture sensitivity proposed in the previous chapters.

To that end, CeO₂ nanoparticles (CeO₂-NP) and nanorods (CeO₂-NR) were prepared by deposition and hydrothermal method, respectively. The supports were calcined at 973 K. The Ir phases were deposited on the CeO₂ nanoparticles (Ir/CeO₂-NP) and nanorods (Ir/CeO₂-NR) by precipitation, and the catalysts were calcined at 673 K [3,13]. Then, the catalytic activity and stability of the two catalysts under steam reforming of ethanol conditions were conducted in order to identify any relationship between activity and structure/texture related to the proper shape of the tested materials. In this chapter, the ethanol conversion was calculated according to the difference between the inlet and outlet flow rate, and the product selectivity

(namely the dry gas composition) was calculated based on the method mentioned in Chapter II.

VI.1. Physical and chemical properties of the fresh nanomaterials (supports) and the catalysts (after Ir loading)

XRD analysis. Figure VI-1 shows the XRD patterns of the fresh CeO₂ nanomaterials and the calcined Ir/CeO₂ catalysts. Typical diffraction peaks of CeO₂ with fluorite structure (PDF#65-5923) were observed for both the nanomaterials and catalysts. The average crystalline sizes of CeO₂-NP and CeO₂-NR nanomaterials were 21 and 11 nm, respectively. No significant diffraction peak of Ir species was observed, implying that the Ir species were highly dispersed on the surface of the CeO₂ supports and their sizes were too small to be detected.

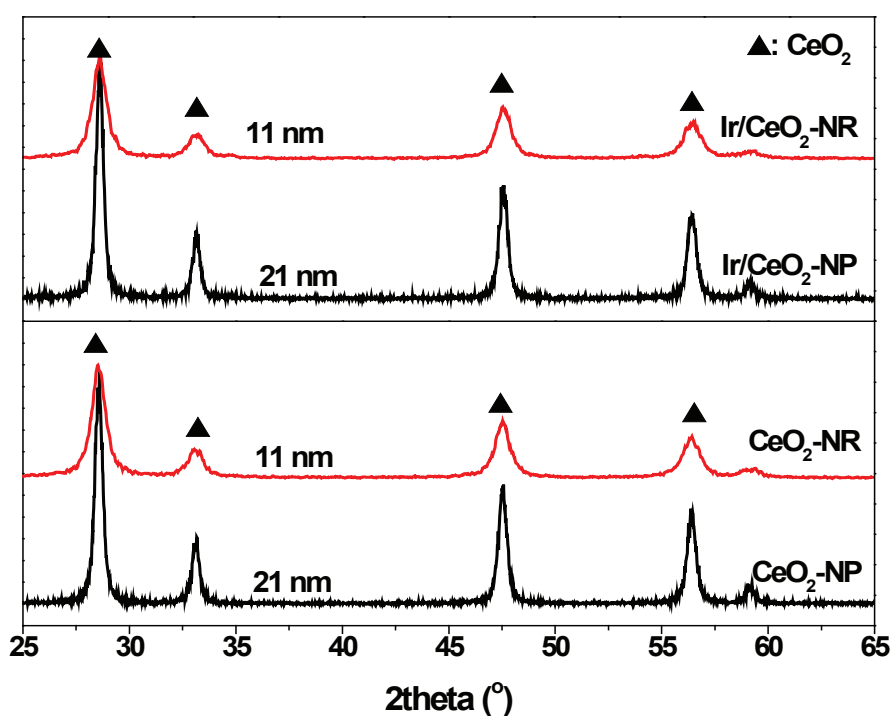


Figure VI-1 XRD patterns of CeO₂ nanomaterials and the Ir catalysts.

H₂ TPR analysis. Figure VI-2 compares the H₂-TPR profiles of the fresh CeO₂ nanomaterials and the calcined Ir/CeO₂ catalysts. Both CeO₂-NP and CeO₂-NR exhibited a low-temperature (LT) reduction peak centred about 770 K and a high-temperature (HT) reduction peak around 1000 K. In line with the previous H₂-TPR analyses, the LT reduction

peak was associated with the surface reduction CeO₂ and the HT reduction peak was related to the bulk reduction of CeO₂ [24]. The corresponding total amounts of H₂ consumption for the CeO₂-NR and CeO₂-NP samples were 883 and 800 μmol/g, corresponding to reduction states of CeO_{1.86}-NR and CeO_{1.85}-NP, respectively. Though these results indicate close reducibility within the measurements uncertainty, however a slightly higher reducibility of surface oxygen could be stated for the CeO₂-NP material.

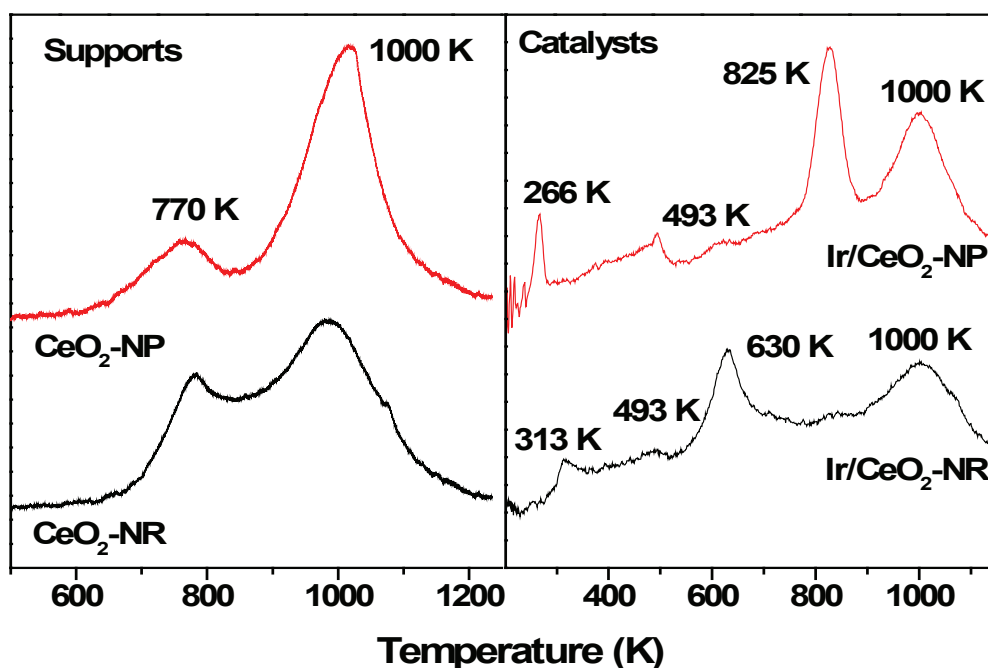


Figure VI-2 H₂-TPR profiles of the fresh CeO₂ nanomaterials and the calcined Ir/CeO₂ catalysts.

For the Ir/CeO₂ samples, three main domains of reduction were observed during the H₂ programmed temperature treatment.

i) For the Ir/CeO₂-NP sample, the first LT domain contains a sharp but small peak at 266 K, followed by a reduction zone till 493 K. The second mean T domain contains essentially a large peak at 825 K while the third HT domain displays a large and wide peak at 1000 K. On the basis of the amount of hydrogen consumed, the LT peaks were assigned to the reduction of IrO₂ to Ir, indicating a rather heterogeneous distribution of metal particles size and/or support interaction. In line with the previous H₂-TPR studies, the peaks at about 825 and 1000 K were assigned to surface and bulk ceria reduction, respectively. The total H₂ consumption by CeO₂-NP support was 982 μmol/g, resulting in a final composition of Ir/CeO_{1.82}-NP.

ii) For the Ir/CeO₂-NR sample, the same domains of reduction were observed, but with some marked changes for peak location. As for Ir/CeO₂-NR, IrO₂ was reduced between 313 and 493 K. In contrast, the surface reduction of CeO₂-NR occurred at 630 K, i.e at a much lower temperature than for the previous material, suggesting a stronger interaction between the Ir phase and the ceria surface. The bulk reduction was kept around 1000 K. The total hydrogen consumption by CeO₂-NR support was 937 μmol/g, giving a mean composition of Ir/CeO_{1.83}-NR, similar to the one obtained for Ir/CeO₂-NP.

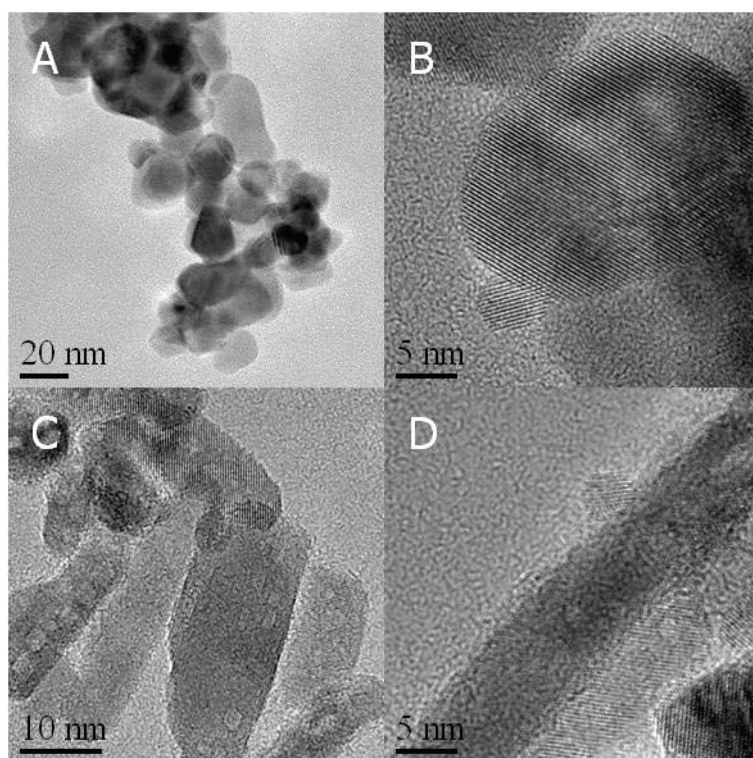


Figure VI-3 HRTEM images of the fresh Ir/CeO₂ catalysts (Ir/CeO₂-NP: A-B, Ir/CeO₂-NR: C-D).

TEM analysis. Figure VI-3 shows the HRTEM images of the Ir species on ceria shaped catalysts. For the Ir/CeO₂-NP sample (Figure VI-3 A-B), the ceria phase displayed polyhedral shape with an average size of 5-10 nm, in good accordance with the XRD result. The dominant plane of the ceria polyhedron was {111}, while with minor {110} [1]. The Ir particles displaying a size of 3-4 nm and a dispersion of 30% were homogeneously dispersed on the surface of the CeO₂-NP. For the Ir/CeO₂-NR sample (Figure VI-3 C-D), the ceria rods presented an average diameter of ca. 9 nm and an average length of ca. 14-30 nm. The main

exposed planes were {110} and {100}, as analyzed in [3]. The Ir particles attached to the rods presented a size of 3-4 nm and a dispersion of 30%.

The HRTEM analysis further demonstrated that the precipitation of the Ir precursors and the subsequent heat treatments did not result in visible changes of the shape of the ceria supports.

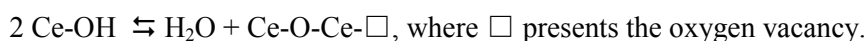
Water adsorption/desorption. Since the water activation is a key step of steam reforming, we have followed the adsorption and desorption of water on fresh materials.

Figure VI-4 shows the water desorption curves of the fresh ceria supports and Ir/CeO₂ catalysts after adsorption saturation. On the Ir-free CeO₂ supports, the main part of adsorbed water was desorbed at 390 K, but the amount of water adsorbed on the CeO₂-NP was higher than that on the CeO₂-NR, as analyzed in Table VI-1.

On the Ir/CeO₂ catalyst, two peaks of water desorption were detected at 390 and 505 K, and more water was adsorbed on the Ir/CeO₂-NP catalyst.

Some important features can be underlined:

i) Only one type of water desorption process occurs on the non-promoted ceria surface, likely corresponding to weakly adsorbed water, possibly under a non-dissociated form. A second mode of water desorption is made possible in the presence of Ir particles. Here we may reasonably assume that OH groups on the ceria surface can recombine at the ceria/Ir interface. This process would involve either a reverse spillover of OH groups towards the metal surface, or more likely a dehydroxylation of the ceria surface assisted by the metal particles, as follows:



ii) The second feature is that the amount of water on NP is larger than on the NR systems. This is quite in line with the fact that NP ceria displays more dense {111} planes, and therefore more potential O vacancies which are required for water activation, surface mobility and desorption.

iii) Finally, these water desorption results confirm that water is essentially adsorbed on the ceria support, but may require the metal interface to provide surface oxygen which will react with adsorbed ethanol intermediates [25]. Hence the higher water activation ability over the Ir/CeO₂-NP catalyst was beneficial for higher conversion of ethanol, thus the Ir/CeO₂-NP catalyst exhibited the better activity and stability, as will be seen later on.

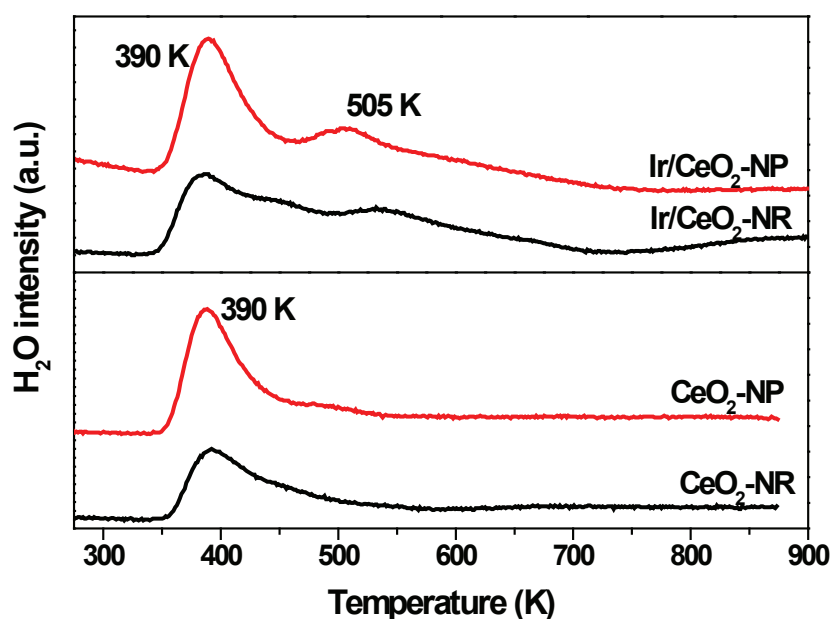


Figure VI-4 Water desorption curves of fresh CeO₂ nanomaterials and the calcined Ir/CeO₂ catalysts.

Table VI-6 The comparison of water desorption over the fresh ceria nanomaterials and the calcined Ir/CeO₂ catalysts.

Samples	Mass of sample (g)	BET (m ² /g)	Water desorption area (a.u.)	Water desorption per unit (/(m ² ·g))
CeO ₂ -NP	0.02	24	1.2 x 10 ⁻¹⁰	1.25 x 10 ⁻⁸
CeO ₂ -NR	0.02	84	7.7 x 10 ⁻¹¹	2.29 x 10 ⁻⁹
Ir/CeO ₂ -NP	0.02	20	2.2 x 10 ⁻⁸	2.75 x 10 ⁻⁶
Ir/CeO ₂ -NR	0.02	84	1.8 x 10 ⁻⁸	5.36 x 10 ⁻⁷

VI.2. Steam reforming of ethanol over the nano-shaped Ir/CeO₂ catalysts

VI.2.1. Effects of reaction temperature

Figure VI-5 illustrates the temperature-dependence of ethanol conversion and product selectivity in steam reforming of ethanol over the Ir/CeO₂ catalysts. In line with the previous catalytic results, both the conversion of ethanol and the selectivity of H₂ increased progressively as the temperature increased. For the Ir/CeO₂-NP catalyst, H₂, CH₃CHO, CO and CH₄ were the main products below 773 K, indicating that ethanol dehydrogenation to H₂

and CH₃CHO, further decomposed into CO and CH₄ were the main reactions. At 873 K, the selectivity of CO and CH₄ was decreased, while the one of CO₂ was increased, as expected from the reverse water gas shift equilibrium and methane SR. At 923 K, the selectivity of H₂, CO, CO₂ and CH₄ was 60%, 4%, 18% and 6%, respectively, and the conversion of ethanol reached 94%, in line with composition predicted by thermodynamics.

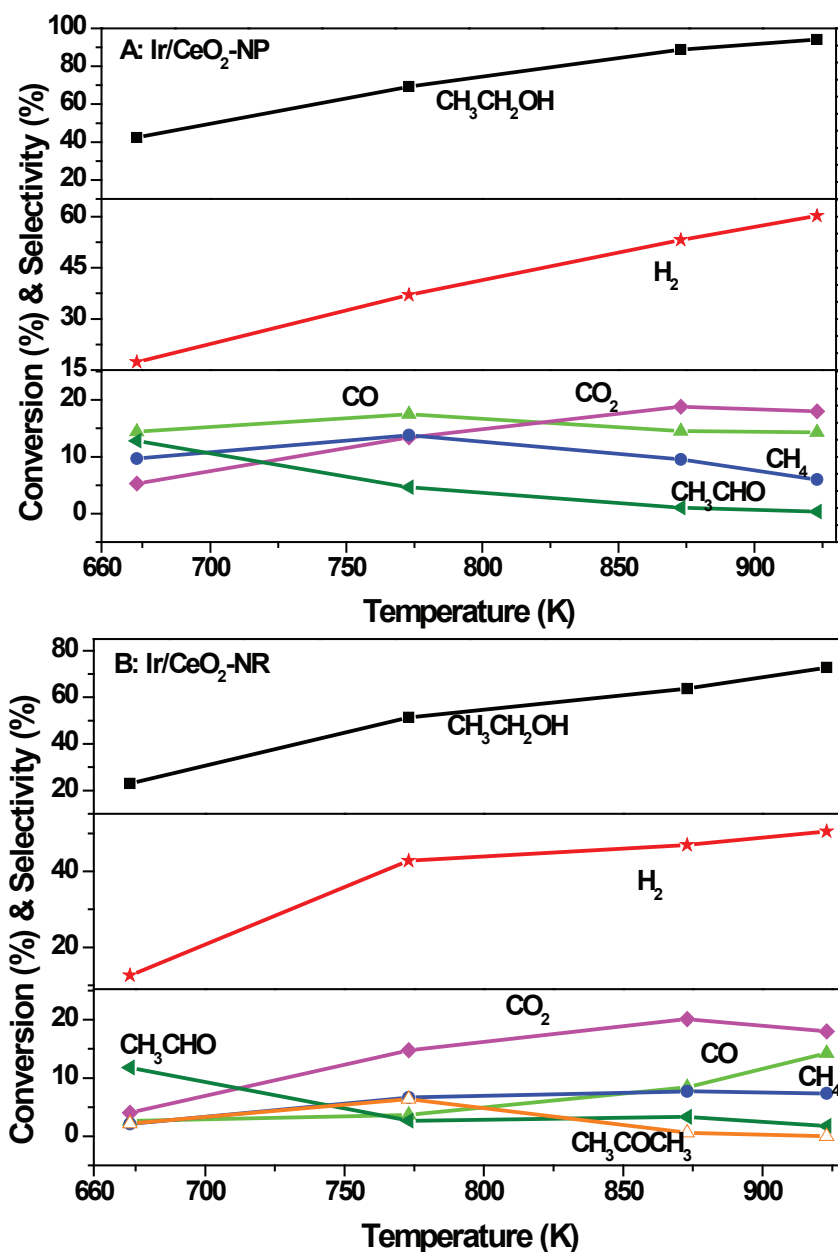


Figure VI-5 Effects of reaction temperature on ethanol conversion and product selectivity for steam reforming of ethanol over the Ir/CeO₂-NP (A) and the Ir/CeO₂-NR (B) catalysts. Reaction conditions: 100 mg catalyst, C₂H₅OH/H₂O = 1:3 (molar ratio), GHSV = 18,000 mL/(g·h) and P = 0.1 MPa.

For the Ir/CeO₂-NR catalyst, CH₃CHO and H₂ were the main products at 673 K, indicating that only the primary dehydrogenation of ethanol to CH₃CHO occurred, but without further cracking into C₁ products at the ceria/metal interface. At 773 K, H₂, CH₄ and CO₂ were the main product, in addition to CH₃COCH₃, indicating that acetaldehyde was partly cracked into C₁ products and partly condensed to acetone [26], as already seen for poorly active systems. At 873 K, the selectivity of CO increased, while the one of CH₄ and CO₂ decreased, as also expected from the reverse water gas shift equilibrium (WGS/RWGS) and methane SR. At 923 K, the gas selectivity of H₂, CO, CO₂ and CH₄ was 50%, 14%, 18% and 7%, respectively, getting closer to the predicted equilibrium, but with a lower conversion of ethanol as compared to the previous case (at 923 K, 73% vs 94 %, respectively).

The above results demonstrated that not only the catalytic activity, but also the reaction pattern was significantly dependent on the shape and therefore on the structure of the ceria support. The conversion of ethanol and selectivity of hydrogen was slightly higher over the Ir/CeO₂-NP catalyst. Ethanol dehydrogenation, acetaldehyde decomposition and WGS were the main reactions over the Ir/CeO₂-NP catalyst; while ethanol dehydrogenation was dominant over the Ir/CeO₂-NR catalyst at 673 K. Above 773 K, WGS/RWGS and methane SR were mainly involved in the two catalyst systems, but the activity of WGS/RWGS were slightly higher over the Ir/CeO₂-NR catalyst.

VI.2.2. Origin of the differences in activity and product selectivity for ethanol steam reforming between the Ir/CeO₂ nano-shaped catalysts

In the above analysis of the catalytic performance over the two nano-shaped catalysts, it was clearly evidenced that the catalytic activity and product selectivity were different, especially at low temperature such as 673 K.

At low temperature, the ethanol conversion was around 20% over the Ir/CeO₂-NR catalyst, while it was 40% over the Ir/CeO₂-NP catalyst. Considering the BET surface areas of the Ir/CeO₂-NR and Ir/CeO₂-NP catalyst (84 vs 24 m²/g), it can be derived that the specific activity per surface area of the Ir/CeO₂-NP catalyst was eight times higher than that of the Ir/CeO₂-NR catalyst.

From both literature and XRD/TEM analysis, we have seen previously that the CeO₂-NP support would present essentially dense (111) planes, while less dense (100) and (110) planes are privileged over the exposed surface of CeO₂-NR support. As commonly agreed, the surface energy of (100) and (110) planes can be considered as slightly higher than for the (111) planes. Therefore the activation of ethanol over the NR surface presenting higher concentration of (100) and (110) planes should be slightly easier, but leading to a stronger bonding between ethoxy/acetate species and the ceria surface. Accordingly, the mobility of ethoxy and acetate species along the NR ceria surface is expected to be much hindered, which would explain the poor performances observed on the NR based catalysts, especially at low temperature.

The difference in product selectivity at low temperature between the two selected shaped catalysts could also be analyzed from a structural point of view. From our mechanistic analysis, the syngas and methane formation originates from the decomposition of intermediates like acetate, occurring at the Ir-ceria interface, followed by desorption from the Ir nanoparticles, as demonstrated in [24] for oxy-steam reforming. Assuming that the higher density of low index planes on the ceria surface for Ir/CeO₂-NP would make easier the transfer of C₂ adspecies from ceria to Ir particles to undergo the cracking step, it can be speculated a higher capacity in acetate decomposition, resulting in a higher selectivity into syngas and methane over the Ir/CeO₂-NP catalyst, as observed experimentally. Following that reasoning, the higher selectivity to carbon dioxide observed for the NR catalyst at low temperature might come from a more difficult water activation (observed experimentally) due to a lower concentration of oxygen defects, leading to a lower activity in WGS allowing the oxidation of CO into CO₂ and H₂.

VI.3. Summary

The shape and therefore the structure of two types of ceria materials (either nanorods or nanoparticle shaped) were found to influence significantly the catalytic performances of the Ir/ceria systems for steam reforming of ethanol. At low reaction temperature, the Ir/nanorods displayed a lower conversion of ethanol, together with a higher selectivity to the partial conversion of ethanol to acetaldehyde and to CO₂. In contrast, the nanoparticle-based system

was more efficient to transform the ethanol to CO₂ and H₂, indicating a deeper cracking of the C₂ ethanol intermediates and an equilibrated WGS activity. These major differences in catalytic performances were also supported by a better ability of nanoparticles to activate water into hydroxyl groups. The differences in catalytic performances between the two nano-shaped catalysts, especially at low temperature, were tentatively assigned to the differences in exposed crystallographic planes on the ceria supports. Ethanol would be more easily activated on the (100) and (110) planes of the CeO₂-NR support, but the migration of ethoxy and acetate species over the surface which strongly control the overall reaction rate would be hindered due to a stronger bonding of ethoxy and acetate species with the ceria surface. The difference in Ir-ceria interaction at their interface would also result in different capacity in acetate decomposition, and therefore explain the different product selectivity observed essentially at low temperature.

References

- [1] H. X. Mai, L. D. Sun, Y. W. Zhang, R. Si, W. Feng, H. P. Zhang, H. C. Liu, C. H. Yan, *J. Phys. Chem. B* 109 (2005) 24380-24385.
- [2] X. S. Huang, H. Sun, L. C. Wang, Y. M. Liu, K. N. Fan, Y. Cao, *Appl. Catal. B: Environ.* 90 (2009) 224-232.
- [3] N. Ta, M. Zhang, J. Li, H. Li, Y. Li, W. Shen, *Catal. Today* 148 (2009) 179-183.
- [4] Z. Shao, S. M. Haile, J. Ahn, P. D. Ronney, Z. L. Zhan, S. A. Barnett, *Nature* 435 (2005) 795-798.
- [5] Z. L. Wang, *Adv. Mater.* 15 (2003) 432-436.
- [6] S. Kuiry, S. Deshpande, S. Seal, *J. Phys. Chem. B* 109 (2005) 6936-6939.
- [7] H. I. Chen, H. Y. Chang, *Solid State Commun.* 133 (2005) 593-598.
- [8] S. Carrettin, P. Concepcion, A. Corma, J. M. L. Nieto, V. F. Puntes, *Angew. Chem. Int. Ed.* 43 (2004) 2538-2540.
- [9] W. Q. Han, L. Wu, Y. Zhu, *J. Am. Chem. Soc.* 127 (2005) 12814-12815.
- [10] K. Zhou, X. Wang, X. Sun, Q. Peng, Y. Li, *J. Catal.* 229 (2005) 206-212.
- [11] P. X. Huang, F. Wu, B. L. Zhu, X. P. Gao, H. Y. Zhu, T. Y. Yan, W. P. Huang, S. H. Wu, D. Y. Song, *J. Phys. Chem. B* 109 (2005) 19169-19174.
- [12] P. Gawade, B. Mirkelamoglu, U. S. Ozkan, *J. Phys. Chem. C* 114 (2010) 18173-18181.
- [13] W. Cai, B. Zhang, Y. Li, Y. Xu, W. Shen, *Catal. Commun.* 8 (2007) 1588-1594.
- [14] L. Yan, R. Yu, J. Chen, X. Xing, *Cryst. Growth Des.* 8 (2008) 474-477.
- [15] R. Si, M. F. Stephanopoulos, *Angew. Chem. Int. Ed.* 47 (2008) 2884-2887.
- [16] G. Yi, H. Yang, B. Li, H. Lin, K. Tanaka, Y. Yuan, *Catal. Today* 157 (2010) 83-88.
- [17] M. Baudin, M. Mojcik, K. Hermansson, *Surf. Sci.* 468 (2000) 51-61.
- [18] D. C. Sayle, S. A. Maicaneanu, G. W. Watson, *J. Am. Chem. Soc.* 124 (2002) 11429-11439.
- [19] Z. P. Liu, S. J. Jenkins, D. A. King, *Phys. Rev. Lett.* 94 (2005) 196102-1~4.
- [20] G. Yi, Z. Xu, G. Guo, K. Tanaka, Y. Yuan, *Chem. Phys. Lett.* 479 (2009) 128-132.
- [21] C. Ho, J. C. Yu, T. Kwong, A. C. Mak, S. Lai, *Chem. Mater.* 17 (2005) 4514-4522.
- [22] W. Hsiao, Y. Lin, Y. Chen, C. Lee, *Chem. Phys. Lett.* 441 (2007) 294-299.
- [23] J. Sun, Y. Wang, J. Li, G. Xiao et al., *Int. J. Hydrogen Energy* 35 (2010) 3087-3091.
- [24] W. Cai, F. Wang, C. Daniel, A. C. van Veen, Y. Schuurman, C. Descorme, H. Provendier, W. Shen, C. Mirodatos, *J. Catal.* 286 (2012) 137-152.
- [25] F. Can, A. le Valant, N. Bion, F. Epron, D. Duprez, *J. Phys. Chem. C* 112 (2008) 14145-4153.
- [26] T. Nishiguchi, T. Matsumoto, H. Kanai, K. Utani, Y. Matsumura, W. Shen, S. Imamura, *Appl. Catal. A: Gen.* 279 (2005) 273-277.

Chapter VII General conclusions and perspectives

As mentioned in the introduction part, the main objective of that work was dealing with catalytic processes for producing renewable hydrogen as a clean energy source for an efficient generation of electricity through fuel cells. Among the various feedstocks able to produce chemically hydrogen, bio-ethanol was selected as a promising source since its hydrogen content is high and it can be obtained from renewable biomass sources. This gives ethanol a key advantage over fossil fuels, because its reforming can be considered as a quasi carbon neutral process towards CO₂ emissions.

By comparing the numerous systems potentially suitable for hydrogen production by ethanol reforming, catalytic steam reforming was selected since offering the highest hydrogen yield with a relatively low CO concentration.

Starting from previous works performed within the frame of a French-Chinese joint program, a model Ir/CeO₂ catalyst was selected for studying that reaction of steam reforming of ethanol, on the basis of preliminary relationships established between the catalytic performance (activity and stability) and the characteristics (properties and structures) of the catalyst. However, an advanced literature analysis led us to state that a number of challenges were still to overcome to reach the minimum knowledge required for developing a commercial process. These challenges formed the basis of this thesis work, presented in the introduction section as four main requirements (written in italic) in terms of activity, stability, selectivity and mechanism. The main answers brought by this work to these requirements are presented below, eventually merged for the consistency of the reasoning.

(I) *Activity and stability: the challenge in the steam reforming of ethanol reaction is to develop a highly active and stable catalyst, which could achieve full conversion of ethanol with a minimum production of undesired by-products for long term testing periods and at the lowest possible temperature.*

The former model catalyst Ir/CeO₂ showed a good performance in terms of activity for the reaction of steam reforming of ethanol. However, its activity tended to decrease with time on stream. A thorough deactivation study was performed on this model catalyst in order to understand the ageing process, providing guidelines on how to improve its stability.

Various causes of deactivation were identified, depending on reaction temperature and time on stream. The initial, fast and but rather limited deactivation process was ascribed essentially to a loss of ceria surface (smoothing by loss of micro-porosity and/or roughness in the presence of steam), coinciding with an active phase build-up formed by a monolayer of carbonaceous reacting intermediates. In addition, a progressive and long-term deactivation was found to superimpose, originating from structural changes at the ceria/Ir interface, linked to the Ir particles sintering and the ceria restructuring. The continuous build-up of an encapsulating layer of carbon at moderate temperature, coming from C₂ intermediate polymerization, was found not to contribute significantly to the catalyst deactivation, at least under the operating conditions investigated in this study. This rather stable graphite like layer formed progressively on stream might be suppressed by simple catalyst reoxidation from time to time to avoid potential diffusion limitations.

On the basis of this ageing study, it could be concluded that the catalyst structure and texture were key parameters for any stability gain. In addition, the main mechanistic features of the proper SR reaction were established, based on former studies of close reactions such as the oxidative steam reforming.

Thus, it was proposed that the ethanol reforming proceeded essentially via a bi-functional way, involving that the active surface (metal and support) was covered with reacting intermediates considered as precursors of the reaction products. As such, ethoxy species and acetates were accumulating on the ceria while CH_x and carbonyls were adsorbed on the Ir particles. The transfer of the C₂ adspecies accumulated on ceria towards the metal particles to undergo the cracking steps was strongly monitored by the state of the ceria surface and of the interface between metal and ceria. Again these two parameters were found to be related to the structure (e.g., the density of surface defects on the ceria and the size of the metal particles) and the texture of the catalyst (microporosity and BET surface of the ceria).

All these key statements offered us strong guidelines for improving both the activity and stability of the reforming model catalyst. Accordingly, two ways for modifying our reference catalyst have been explored: the ceria shaping as nanorods and the ceria doping with PrO_x.

The shape/structure of ceria material (nanorods NR or nanoparticles NP) was effectively found to influence significantly the catalytic performances of the Ir/ceria systems for steam reforming of ethanol. At low temperature, ethanol dehydrogenation into acetaldehyde was dominant over the Ir/CeO₂-NR catalyst, while the reaction was more oriented towards the WGS and the syngas production over the Ir/CeO₂-NP catalyst, indicating that the nanoparticle-based system was more efficient both to activate water and to crack the adsorbed C₂ intermediates. These major differences were also supported by a poorer structure stability of the nanorods under the reaction conditions.

Following the other route for improving activity and stability of the reference catalyst, a new formula has been developed through ceria doping with Pr. It was revealed that Pr-doping significantly promotes the oxygen storage capacity and thermal stability of the catalyst by incorporating structural defects into the ceria lattice. Ethanol is readily converted to hydrogen, methane and carbon oxides at 773 K over the Ir/Ce_{0.9}Pr_{0.1}O₂ catalyst, being 100 K lower than that on the Ir/CeO₂ catalyst.

To sum up, the Pr-doping of ceria was demonstrated to greatly improve the catalytic activity and also decrease the by-products CH₄ and CH₃CHO in comparison with the initial Ir/CeO₂ catalyst. In contrast, the shaping of the catalyst into nanorods was found to lead to rather unfavourable performances.

Considering more precisely the catalyst stability, let us first remind the second objective of the work proposed in the introduction section:

(II) *Stability: the developed catalysts also need to be stable at industrial level. This requires to understand and control the two main ageing factors : (a) the coke formation on the surface of the catalyst, and (b) the sintering of the supports and/or the active phase..*

The stability test of the PrO_x-doped catalysts evidenced that the ethanol conversion was decreased from 100% to 60% in the operating conditions with Ir/CeO₂ catalyst, the ethanol conversion on the Ir/Ce_{0.9}Pr_{0.1}O₂ catalyst only slightly decreased from 100% to 98% during the first 60 h time on-stream and was kept constant at 95% up to the end of the test. So the

PrO_x-doped catalyst was found rather stable for 300 h on steam reforming of ethanol stream at 923 K without apparent changes in ethanol conversion and product distribution. In contrast, severe aggregation of ceria particles and heavy coke deposition were observed on the undoped Ir/CeO₂ catalyst, explaining its significant deactivation observed under the same reaction conditions.

Such a beneficial Pr doping effect was related to improved redox properties of the ceria, due to a higher density of oxygen vacancies. These vacancies are thought to increase the surface density of reactive oxygen species and/or hydroxyl groups, not only accelerating the transformation and migration of the reacting intermediates but also limiting the deposition of toxic carbon, possibly via stronger Ir-ceria interactions. In addition, this PrO_x-doping also improved the structural/textural stability of the mixed oxide, limiting the sintering of the Ir particles and the sintering/reshaping of the oxide support. All these features are proposed for explaining the greatly enhanced stability of the Ir/Ce_{0.9}Pr_{0.1}O₂ catalysts in the steam reforming of ethanol.

(III) *Selectivity: hydrogen selectivity has to be maximized, within the thermodynamic constraints, by playing on the general reaction scheme including key steps like WGS and methane steam reforming. The challenge is to minimize the production of CO and CH₄.*

As pointed out by the thermodynamics calculation reported in chapter I, the hydrogen yield increases and the methane yield decreases with reaction temperature, which unfortunately also favors the formation of CO, a potential poison for the fuel cell electrodes. The challenge was therefore to maximize the hydrogen yield but keeping the CO and CH₄ production as low as possible.

The present work demonstrated that the structure and texture of the catalysts were, at least partly, also controlling the product distribution calculated on a dry gas basis (considered as the reaction selectivity in this study).

While the selectivity into CO was almost the same with both catalysts Ir/CeO₂ and Ir/Ce_{0.9}Pr_{0.1}O₂, the CH₄ selectivity was decreased with the PrO_x-doped catalyst. The lower selectivity into methane and the higher hydrogen selectivity over the Ir/Ce_{0.9}Pr_{0.1}O₂ catalyst implied an enhanced activity in the methane steam reforming reaction due to PrO_x doping of ceria.

Below 900 K, the selectivity into CO was lower with the nanorods catalyst than with the reference Ir/CeO₂ catalyst, but it must be stated that it was the only positive feature of the nanorods catalyst in terms of selectivity. Indeed, even if the CO₂ selectivity was almost the same for both catalysts, the selectivity into hydrogen was slightly higher over the Ir/CeO₂ than over the nanorods catalyst.

Moreover, some undesirable by-products like acetone were formed with the nanorods catalyst.

To summarize this part, the PrO_x doping of ceria was found to be a favorable factor as regard to the product selectivity, reinforcing the advantages already stressed for activity and selectivity. In contrast, the shaping as nanorods was found not efficient for these properties.

(IV) Mechanism and kinetics: an advanced knowledge of the mechanistic pathways supporting a kinetic modeling, which may be specific of the catalyst and the operating conditions, is required for any further improvement of the catalytic performances and engineering design.

On the basis of the mechanistic knowledge acquired from the literature and all along the present work, a preliminary kinetic study was performed by checking the influence of the main operating parameters (temperature, molar ratio of water to ethanol and partial pressure of products) on the ethanol conversion and selectivity. The apparent activation energy of the ESR reaction was measured to be ca 58 kJ/mol, which is in line with the literature data for other types of catalysts. A power law rate equation was found to correctly describe the main kinetic trends, from which the reaction orders of the reactants, ethanol and water and of the main products, CO, CO₂, H₂, CH₄ were derived. The values obtained for these apparent partial orders were tentatively related to some aspects of the reaction mechanism.

The positive partial orders for ethanol and water, estimated to be 0.6 and 0.5, respectively, are thought to indicate that the ethanol and water adsorption steps are not determining, but participate to the overall rate of conversion, probably by ensuring a ceria surface occupancy by intermediates arising from these two adsorption steps, i.e., ethoxy and hydroxyls active intermediates. In turn, it was found that the conversion of ethanol was significantly inhibited by the addition of the main gas products in the inlet feed (negative apparent orders). It was

proposed that i) the CO₂ addition would inhibit the ethoxy and acetate migration from ceria to Ir particles upon increasing the carbonate concentration on the ceria, ii) the CO addition would increase the carbonyl concentration at the Ir-ceria interface, thus inhibiting the decomposition of acetate and methyl fragments into CO and iii) the CH₄ addition would favor its steam reforming at the expenses of the fragments coming from the ethanol decomposition.

Indeed, despite the interesting guidelines provided by this preliminary kinetic study for optimizing process conditions, much more work is required to progress significantly towards more robust models in view of being used for any further process development.

As a global conclusion, the general objectives of this work, centered around a better knowledge of the steam reforming of ethanol reaction on a model Ir/ceria catalyst, in order to propose new systems displaying improved catalytic activity, stability and selectivity, were satisfactorily reached.

From the ageing analysis of the Ir/CeO₂ catalyst, it was inferred that any marked improvement in catalyst stability would require the stabilization of both the ceria surface area and the metal dispersion. While the shaping of ceria was found not efficient, the ceria doping with Pr was found to induce a favorable effect on all the main catalytic properties in steam reforming of ethanol. Thus, the originally designed Ir/Ce_{0.9}Pr_{0.1}O₂ catalyst showed significantly improved activity, long term stability and selectivity, as required for any further industrial application.

Proposed further work

On the basis of this work carried out within the frame of a collaborative program, further studies on catalyst formulation and process optimization could be proposed as perspective for further work:

(I): Screening on catalyst formula might be continued by ceria doping with promoters like Zr or other lanthanides (La, et al.) for improving the redox and stability properties of the support. In parallel, alloying Ir with another metal (e.g., Cu or Ni) would favor the water gas shift reaction, thus enhancing the productivity of hydrogen while lowering the CO concentration.

(II): From the demonstrated structure/texture sensitivity of the reaction, other strategies for shaping Ce-Pr oxides could be explored, which would favor specific and selective crystalline planes at the expenses of less selective surface structure.

(III): All these improved formulas might be used for more advanced engineering studies, e.g., on micro-structured reactors, allowing a better heat management of this highly endothermic reaction. They would indeed beneficiate of a more robust kinetic model for optimizing the process conditions.

Annex 1: Hydrogen production from steam reforming of ethanol over Ni and Ni-Cu catalysts

Chapter VIII Hydrogen production from steam reforming of ethanol over Ni and Ni-Cu catalysts

Hydrogen production by steam reforming (SR) of ethanol has attracted wide attention because of the increasing concern in effective utilization of bio-ethanol and the potential application to fuel cells. To date, most studies have been focused on supported Ni [1-4], Co [5-7], Ir [8], and Rh [9] catalysts for SR of ethanol, operated at relative higher temperatures, typically 873-1073 K. Among them, Ir and Rh catalysts showed the most effective and promising performance with respect to ethanol conversion and hydrogen selectivity. However, the high cost of noble metals limits their practical applications.

Among the non-precious metals, Ni catalyst is the most favorable candidate in SR of ethanol, which exhibits adequate activity through the strong capability of breaking the C–C bond in ethanol, but it usually results in low-hydrogen yield because of the formation of significant amounts of methane [1–4,10]. Meanwhile, the Ni catalyst also suffers severe deactivation caused by the sintering of Ni particles and the heavy coke deposition during the course of reaction. The sintering of Ni particles rapidly decreases the activity, but it can be partially inhibited by adding the second metals such as Ag [11], Rh [12], and Cu [13,14-16] through the formation of metal alloys. For example, the combination of Ni and Cu showed higher activity and longer stability for SR of ethanol. The formation of Ni–Cu alloy resulted in the preferential elimination of large Ni ensembles necessary for carbon deposition [15]. On the other hand, coke deposition was found to be the major reason for the deactivation of Ni catalysts during steam reforming of ethanol [3, 4, 10]. The Ni catalysts reported so far for steam reforming of ethanol use metal oxides as supports to disperse the fine Ni particles and to prevent their sintering under reaction conditions. But the acidic and/or basic nature of the metal oxides usually favors the dehydration of ethanol to ethylene and its oligomerization

[4,10], leading to the formation of carbon in steam reforming of ethanol. Reforming of methane, formed by the decomposition of ethanol, was also proposed as an alternative route for carbon deposition, especially at temperatures above 673 K [17,18]. Additionally, the Boudouard reaction that is thermodynamically favored below 973 K may convert the produced CO into carbon and CO₂ as well [19]. Although not all of the deposited carbon causes the loss of activity, like filamentous carbon [10], it is generally acknowledged that the encapsulating carbon would cause significant deactivation. Therefore, carbon deposition remains a challenge to develop long-term stable and coke resistant Ni catalysts.

We have previously reported that unsupported fibrous nickel is very active for methane decomposition to produce hydrogen and carbon nanofiber [20]. In this work, we examined unsupported Ni and Ni-Cu catalysts for steam reforming of ethanol where the formation of coke through ethylene dehydro-condensation might be eliminated due to the absence of acidic or basic metal oxides supports [4,10].

VIII.1. Experimental

VIII.1.1. Catalyst preparation

The nickel hydroxide was prepared by precipitation of nickel acetate dissolved in ethylene glycol with sodium carbonate aqueous solution at 393 K, as described elsewhere [20]. A mixture containing 0.05 mol of nickel acetate (Ni(OAc)₂·4H₂O) and 150 mL of ethylene glycol (EG) was heated to 393 K under stirring and maintained at the same temperature for 30 min. 500 mL of 0.2 M aqueous Na₂CO₃ solution were then slowly added to the Ni-EG solution with a final pH value of about 10. The precipitate was aged in the mother liquid for 1 h. After being filtered and washed thoroughly with distilled water, the nickel hydroxide precipitate was dried at 100 °C overnight and finally calcined in air at 973 K for 6 h, giving NiO.

The Ni_{0.99}Cu_{0.01}O sample was prepared with the same procedure as that of the NiO, but a mixture of nickel and copper acetates with a proper Ni/Cu ratio was used.

VIII.1.2. Catalyst characterization

N₂ adsorption–desorption isotherms were recorded at 77 K using ASAP V2.02 instrument. Before the measurement, the sample was degassed at 573 K for 2 h. The surface area of the sample was calculated by a multipoint BET analysis of the nitrogen adsorption isotherm.

X-ray power diffraction (XRD) patterns were recorded using a Rigaku D/MAX-RB diffractor with a Ni-filtered Cu Ka radiation operated at 40 kV and 200 mA. The spectra were taken in the 2theta range of 10–80° at a scan speed of 5°/min with a step interval of 0.02°. In situ XRD measurements for the reductions of the NiO and Ni_{0.99}Cu_{0.01}O samples were performed in a high-temperature chamber. The sample was heated 923 K under N₂ flow, and a 5% H₂/N₂ mixture was introduced into the chamber and kept at 923 K for 3 h, after which the XRD patterns were recorded. The mean crystalline sizes of NiO and Ni were calculated according to the Scherrer equation.

Transmission electron microscopy (TEM) images were taken on Philips Tecnai G² Spirit microscope operated at 120 kV. Specimens were prepared by ultrasonically suspending the sample in ethanol. A drop of the suspension was deposited on a thin carbon film supported on a standard copper grid and dried in air.

Temperature-programmed reduction (TPR) measurement was performed with a conventional setup equipped with a thermal conductivity detector. 50 mg (40–60 mesh) samples were pretreated at 573 K for 1 h under N₂ flow (40 mL/min). After cooling to room temperature and introducing the reduction agent of a 5% H₂/N₂ mixture (40 mL/min), the temperature was then programmed to 973 K at a rate of 10 K/min.

Temperature-programmed hydrogenation (TPH) and oxidation (TPO) of the deposited carbon on the catalyst were performed in U-type quartz tubular reactor equipped with a mass spectrometer. 20 mg of the used catalysts were loaded and the sample was heated from room temperature to 973 K at a rate of 10 K/min under the flow of a 20% H₂/He mixture (30 mL/min for TPH) or a 20% O₂/He mixture (30 mL/min for TPO). The m/e intensities of 16 (CH₄), 18 (H₂O), 28 (CO), 28 (C₂H₄), 30 (C₂H₆), and 44 (CO₂) were monitored by the mass spectrometer. The amount of carbon deposited on the catalyst was calculated according to the intensities of carbon oxides.

VIII.1.3. Catalytic evaluation

Steam reforming of ethanol was conducted in a continuous-flow fixed bed quartz reactor at atmospheric pressure. 100 mg of catalyst (40–60 mesh) was loaded and sandwiched by two layers of quartz wool. Before the reaction, the catalyst was reduced with a 5% H₂/He (20 mL/min) mixture at 923 K for 3 h. Then, the temperature was set to 673–923 K under N₂ flow and a 50% ethanol aqueous solution (water/ethanol molar ratio of 3/1) was fed by a micro-pump with a gas hourly space velocity (GHSV) of 6000 mL/(gh). The effluent was analyzed by on-line gas chromatography equipped with a thermal conductivity detector (TCD) and a flame ionization detector (FID). The conversion of ethanol and the selectivity of the products were calculated according to the method in chapter II.

VIII.2. Results and discussion

VIII.2.1. Physical and chemical properties of the Ni catalysts

Figure VIII-1 shows the XRD patterns of the NiO and Ni_{0.99}Cu_{0.01}O samples. Only the diffraction peaks of nickel oxide with cubic structure (JCPDS# 4-835) were observed, and the average crystalline sizes of NiO were about 4 nm in both cases. There were no diffraction peaks of CuO in the Ni_{0.99}Cu_{0.01}O sample probably because of the very low content. Figure VIII-2 shows the TEM images of the two samples. Clearly, the nickel oxides exhibited inter-layered structure, and the addition of copper oxide did not alter the fibrous shape of the NiO. The specific surface areas of the NiO and Ni_{0.99}Cu_{0.01}O samples were 126 and 129 m²/g, respectively.

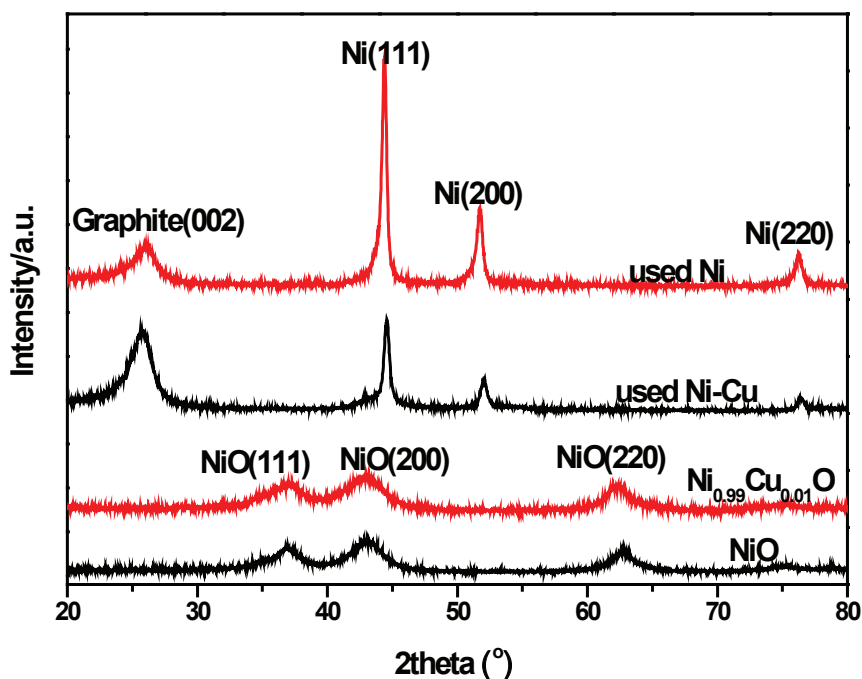


Figure VIII-1 XRD patterns of the NiO and Ni_{0.99}Cu_{0.01}O samples and the used Ni and Ni-Cu catalysts.

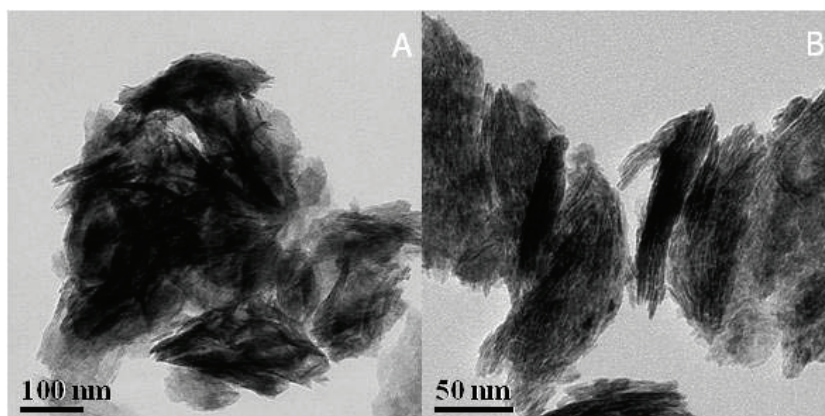


Figure VIII-2 TEM images of the NiO (A) and Ni_{0.99}Cu_{0.01}O (B) samples.

Figure VIII-3 shows the H₂-TPR profiles of the oxides. The reduction of NiO occurred at about 923 K with a small shoulder at 593 K, characteristic of fibrous nickel oxide [20]. The Ni_{0.99}Cu_{0.01}O sample exhibited two hydrogen consumptions at 633 and 973 K, respectively. The former is due to the reduction of copper oxide, which probably has a strong interaction with nickel oxide [21], while the latter is attributed to the reduction of nickel oxide. This implies that the addition of small amounts of copper oxide does not appreciably change the reduction feature of the fibrous nickel oxide.

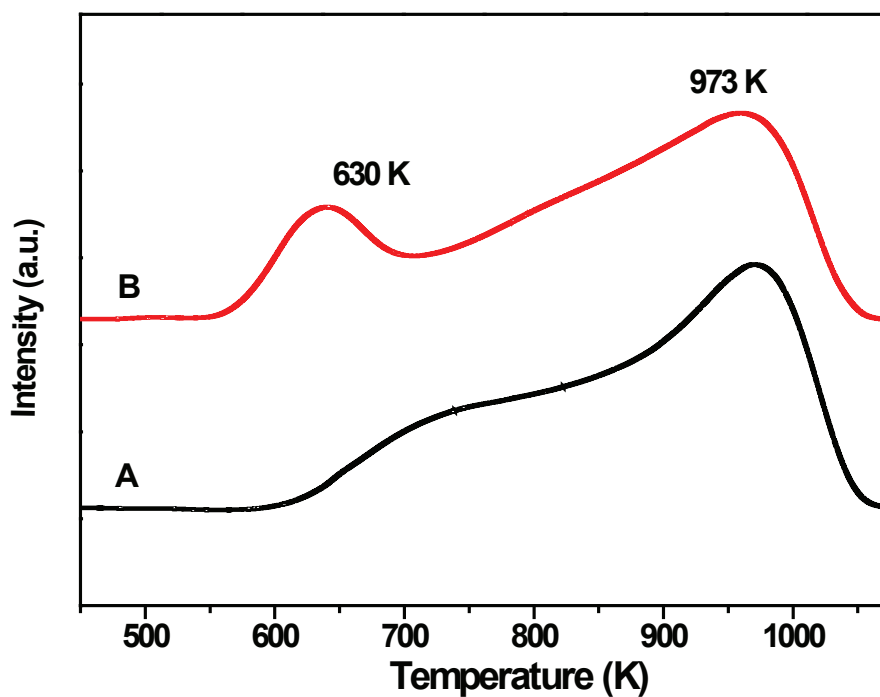


Figure VIII-3 TPR profiles of the NiO (A) and Ni_{0.99}Cu_{0.01}O (B) samples.

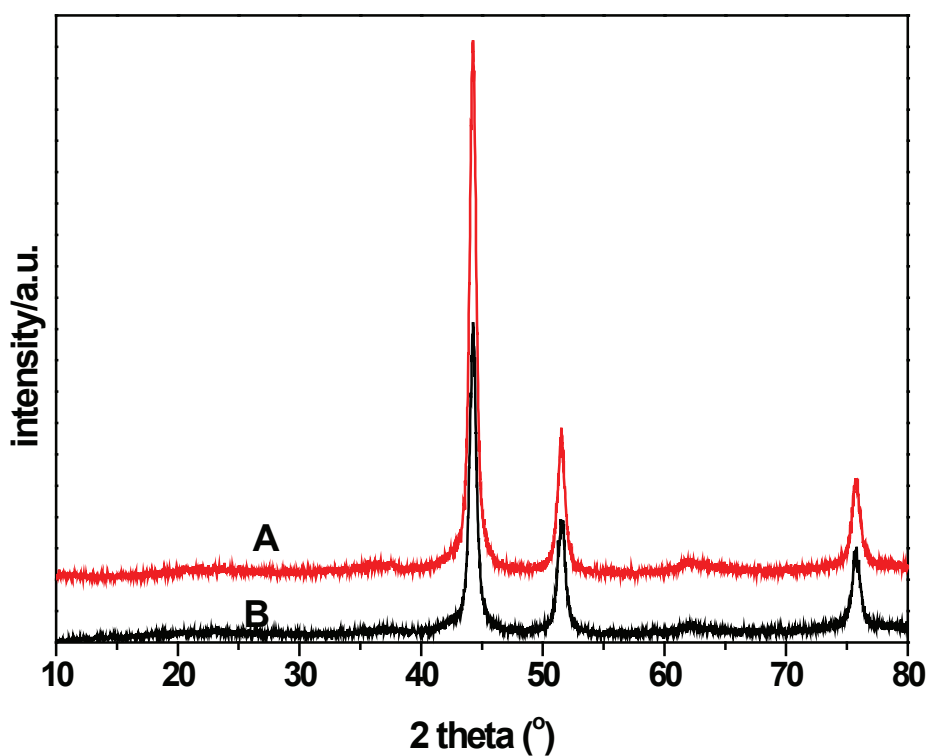


Figure VIII-4 XRD patterns of the *in-situ* reduced Ni (A) and Ni-Cu (B) catalysts.

Figure VIII-4 illustrates the XRD patterns of the Ni catalysts obtained by reducing the NiO and Ni_{0.99}Cu_{0.01}O samples with hydrogen at 923 K. Both NiO and Ni_{0.99}Cu_{0.01}O were fully

reduced to metallic nickel with a similar crystallite size of 11 nm. There were no diffraction peaks of copper mainly due to the very low content and the possible formation of Ni-Cu alloy. This phenomenon is accord with the observation in the TPR profiles that the presence of copper oxide does not apparently modify the reduction feature of the fibrous nickel oxide.

VIII.2.2. Steam reforming of ethanol

Figure VIII-6 shows the temperature dependence of the product distribution during steam reforming of ethanol over the Ni and Ni-Cu catalyts. Ethanol and the reaction intermediates like acetaldehyde and acetone were entirely converted to hydrogen and C1 products over the 673-972 K range, essentially due to the rather low contact time used for these experiments. Note however that these Ni catalyts can be considered as quite active since most supported Ni catalyts could give 100% ethanol conversion only above 773 K [3,4,22-24]. The concentration of hydrogen increased progressively with temperature, whereas the concentration of CH₄ and CO₂ decreased gradually, as expected from the thermodynamics equilibrium reported in the next figure (taken from chapter IV).

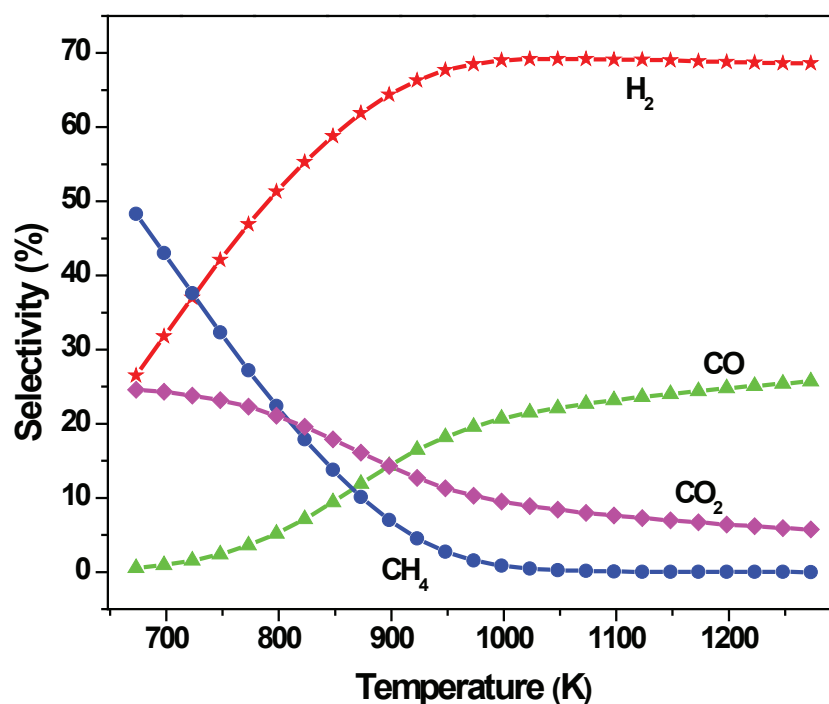


Figure VIII-5 Thermodynamic equilibrium selectivity for the steam reforming of ethanol as a function of temperature (EtOH/H₂O=1/3, pressure: 1atm).

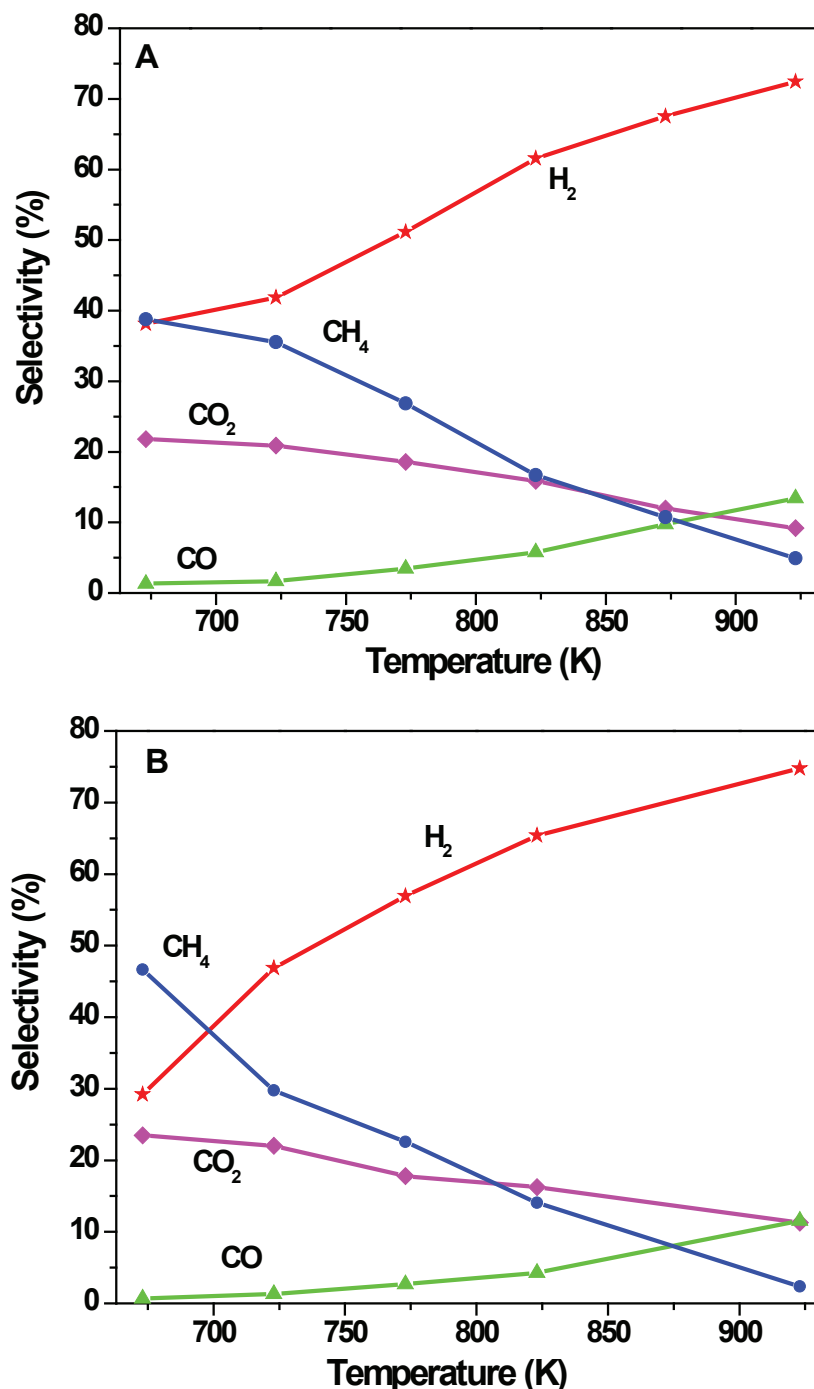


Figure VIII-6 Effect of reaction temperature on the product selectivity for steam reforming of ethanol over the Ni (A) and Ni-Cu (B) catalysts. Reaction conditions: C₂H₅OH/H₂O=1:3 (molar ratio), GHSV=6000 mL/(gh).

This can be formalized by assuming steam reforming of methane and reverse water as shift (WGS) reactions as the major reactions. At 923 K, methane was almost completely reformed, while the concentration ratio of CO/CO₂/H₂ reached the equilibrium of the WGS reaction. The very similar reaction patterns between the Ni and the Ni-Cu catalysts confirm that the

product distribution is only controlled by thermodynamics and not by the catalyst composition in this temperature range and at full ethanol conversion.

As seen in Figure VIII-6 from a more quantitative point of view, the outlet stream for both catalysts consisted at 923 K of 72% H₂, 13% CO, 10% CO₂ and 4% CH₄. From the thermodynamic analysis reported in Figure VII-5, the equilibrium gas composition is 66.3% H₂, 4.5% CH₄, 16.5% CO and 12.7% CO₂, which is rather close to the experimental values, though some deviations may come from non equilibrated side reactions like the decomposition of methane into hydrogen and carbon (which was not considered in our thermodynamic calculations, being unfavored at these high temperatures).

Note also that it has been reported that the addition of copper (2%) to a 7% Ni/SBA-15 catalyst could promote the WGS reaction, especially at lower temperatures [16]. However, such a promotional effect is not observed for the present Ni-Cu catalyst due to the above reported thermodynamic control.

VIII.2.3. Ageing analysis

Figure VIII-7 compares the selectivity of H₂, CO, CO₂ and CH₄ in the outlet streams as a function of time-on-stream at 923 K over the Ni and Ni-Cu catalysts. The Ni catalyst showed relatively stable performance at the initial 8 h, and then the selectivity of hydrogen tended to decrease slightly while the selectivity of CO and CH₄ increased significantly. The pressure of the reactor was also increased, indicating the occurrence of heavy coke deposition on the surface of the catalyst. Though the trends observed with the Ni-Cu catalyst were close to the unpromoted Ni system, it can be observed a slightly higher stability of that former Cu promoted system with time on stream. This effect of copper addition might be caused by the formation of Ni-Cu alloy, as shown in [13,16].

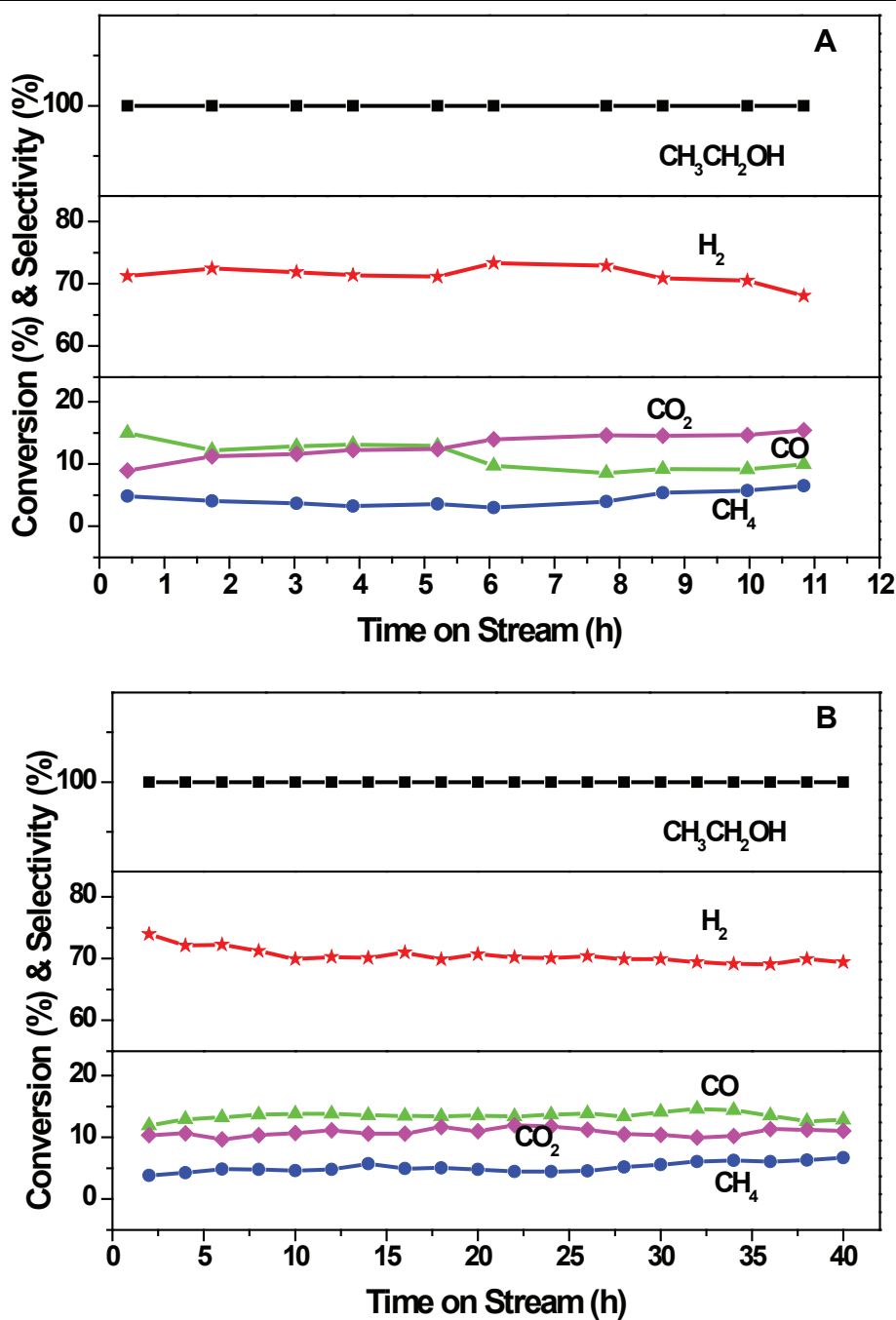


Figure VIII-7 Outlet gas selectivity at full ethanol conversion for steam reforming of ethanol over the Ni (A) and Ni-Cu (B) catalysts. Reaction conditions: $T = 923$ K, $C_2H_5OH/H_2O = 1:3$, GHSV = 6000 mL/(gh).

To understand stability vs ageing features, the used catalysts were characterized by several techniques.

Figure VIII-1 shows the XRD patterns of the used Ni and Ni-Cu catalysts. In addition to the typical diffraction peaks of metallic nickel, a broad diffraction peak at $2\theta = 26^\circ$ was observed, representing the deposited carbon. As already stated, the initial crystallite size of nickel was

11 nm for the two catalysts. After 12 h on stream, the Ni particles were sintered to a mean time of 30 nm, whereas the size of Ni crystallite was 45 nm in the Ni-Cu catalyst after 40 h on stream.

Two features deserve to be underlined here:

- i) A significant sintering of the Ni phase occurs under the present operating conditions, which will have to be considered for explaining the ageing processes.
- ii) Assuming a quasi constant sintering rate, it comes that in all cases, the sintering is slower on Cu-promoted Ni than that for Ni alone. Again the Ni-Cu alloying should be considered to account for this sintering inhibition by Cu promotion.

Note finally on the XRD reflexes a very minor diffraction peak of NiO appeared at around $2\theta = 43^\circ$, which might be caused by the exposure to air during the sample handling or the possible oxidation of Ni under the reaction conditions.

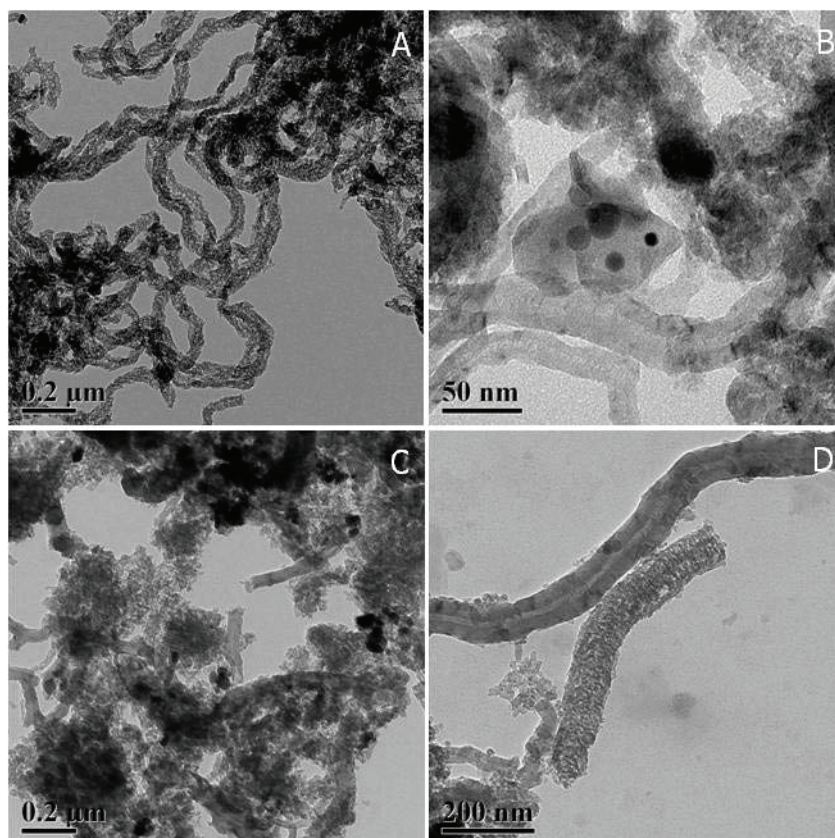


Figure VIII-8 TEM images of the used Ni (A-B) and Ni-Cu (C-D) catalysts.

Figure VIII-8 shows the TEM images of the used Ni and Ni-Cu catalysts. For the Ni catalyst, filament carbon with rough surface was formed and most of the Ni particles with size of 10–40 nm were encapsulated by the deposited carbon. In the case of the Ni-Cu catalyst, however, mainly condensed carbon was produced, which is similar to the carbon deposited on the Ni/MgO catalyst [25, 26]. Most of the Ni particles having size of 20–60 nm were dispersed on the deposited carbon, instead of being encapsulated. It seems that the presence of Ni-Cu alloy inhibits the formation of encapsulating coke through the efficient hydrogen mobility of copper [15, 27]. This is similar to the previous observation that the addition of copper to Ni catalysts could change the morphology of the deposited carbon by adjusting the electronic feature and the affinity with carbon of nickel particle [28].

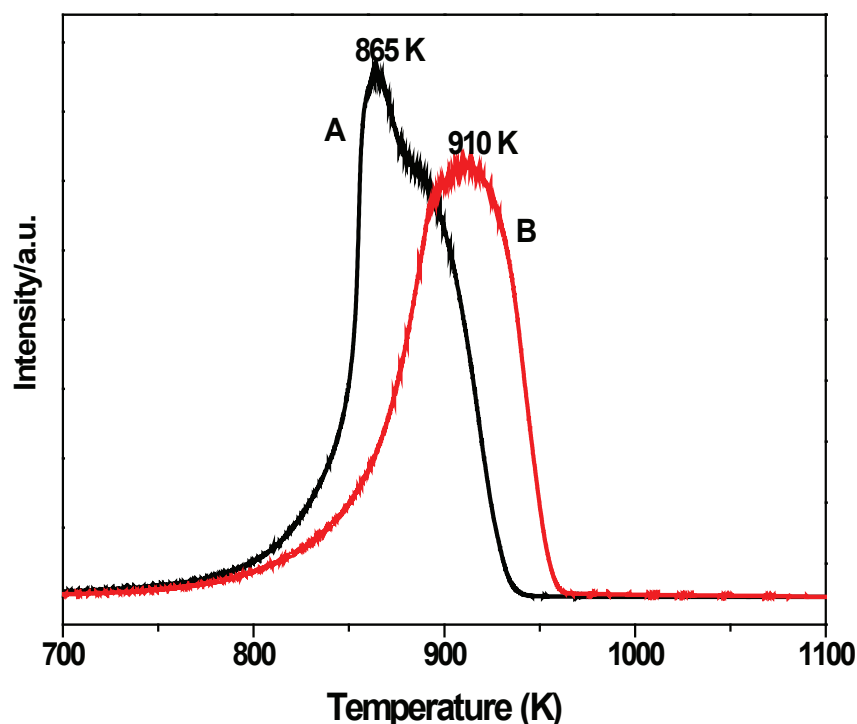


Figure VIII-9 TPO profiles of the used Ni (A) and Ni-Cu (B) catalysts.

Figure VIII-9 shows the TPO profiles of the used Ni and Ni-Cu catalysts. The evolution of CO₂ over the Ni catalyst occurred at a relatively lower temperature than that over the Ni-Cu catalyst, suggesting that that the carbon species deposited on the Ni catalyst is slightly reactive than that on the Ni-Cu catalyst. The total amount of deposited carbon was almost the same in both cases, 21–22 mg/g, but the deposition rate of carbon on the Ni-Cu catalyst (0.53

mg C/h) was much less than that on the Ni catalyst (1.83 mg C/h). This demonstrates that the Ni-Cu catalyst has a better resistance towards carbon deposition during the course of steam reforming of ethanol. This promotional effect has also been observed on SiO₂, SBA-15 and Al₂O₃ supported Ni-Cu catalysts, which was ascribed to the preferential elimination of larger ensembles of Ni atoms necessary for carbon deposition with the addition of copper [29].

Figure VIII-10 presents the TPH profiles of the used Ni and Ni-Cu catalysts. Two main peaks of methane were observed at about 690 and 880 K on the two catalysts, demonstrating that the carbon formed during the course of steam reforming of ethanol is of various nature and structure. The low temperature TPH peak is generally assigned to the carbon filaments, more easily hydrogenated due to the tight contact with the Ni particles able to activate the hydrogen during the TPH. The higher temperature TPH peak is more related to graphitic coke formed above and around the catalyst particles, probably from the ethylene dehydrocondensation into coke aromatic precursors. The presence of ethylene detected during the TPH is probably a good indication of this process of condensation to make graphitic carbon. Other possible routes for coke formation like Boudouard reaction might be considered as well but would require further experiments (possibly by labelling the ethanol).

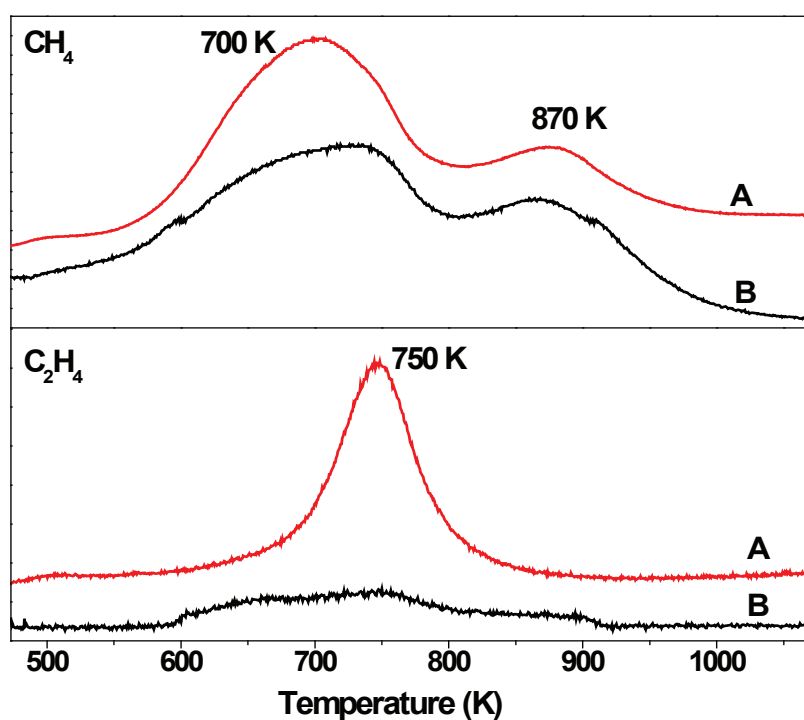


Figure VIII-10 TPH profiles of the used Ni (A) and Ni-Cu (B) catalysts.

VIII.3. Summary

The Ni–Cu catalyst was found relatively active and stable for steam reforming of ethanol even with a stoichiometric feed composition. Ethanol was entirely reformed into hydrogen and C1 products at 673 K, while methane steam reforming and reversible water gas shift became the major reactions at higher temperatures. The Ni–Cu catalyst exhibited stable performance during 40 h on-stream at 923 K without apparent deactivation, evidenced by the consistent composition of the outlet stream. Condensed carbon was deposited on the Ni–Cu catalyst, probably through the decomposition of methane formed during steam reforming of ethanol.

References

- [1] J. W. C. Liberatori, R. U. Ribeiro, D. Zanchet, F. B. Noronha, J. M. C. Bueno, *Appl. Catal. A: Gen.* 327 (2007) 197-204.
- [2] F. Frusteri, S. Freni, *J. Power Sources* 173 (2007) 200-209.
- [3] M. Ni, D. Y. C. Leung, M. K. H. Leung, *Int. J. Hydrogen Energy* 32 (2007) 3238-3247.
- [4] A. N. Fatsikostas, X. E. Verykios, *J. Catal.* 225 (2004) 439-452.
- [5] J. Llorca, N. Homs, J. Sales, P. Ramirez de la Piscina, *J. Catal.* 209 (2002) 306-317.
- [6] M. S. Batista, R. K. S. Santos, E. M. Assaf, J. M. Assaf, E. A. Ticianelli, *J. Power Sources* 134 (2004) 27-32.
- [7] S. Tuti, F. Pepe, *Catal. Lett.* 122 (2008) 196-203.
- [8] W. J. Cai, F. G. Wang, E. S. Zhan, A. C. Van Veen, C. Mirodatos, W. J. Shen, *J. Catal.* 257 (2008) 96-107.
- [9] G. A. Deluga, J. R. Salge, L. D. Schmidt, X. E. Verykios, *Science* 303 (2004) 993-997.
- [10] A. L. Alberton, M. M. V. M. Souza, M. Schmal, *Catal. Today* 123 (2007) 257-264.
- [11] N. V. Parizotto, K. O. Rocha, S. Damyanova, F. B. Passos, D. Zanchet, C. M. P. Marques, J. M. C. Bueno, *Appl. Catal. A: Gen.* 330 (2007) 12-22.
- [12] J. Kugai, V. Subramani, C. Song, M. H. Engelhard, Y. H. Chin, *J. Catal.* 238 (2006) 430-440.
- [13] V. Klouz, V. Fierro, P. Denton, H. Katz, J. P. Lisse, S. Bouvot-Mauduit, C. Mirodatos, *J. Power Sources*, 105 (2002) 26-34.
- [14] F. Marino, M. Boveri, G. Baronetti, M. Laborde, *Int. J. Hydrogen Energy* 29 (2004) 67-71.
- [15] A. J. Vizcaino, A. Carrero, J. A. Calles, *Int. J. Hydrogen Energy* 32 (2007) 1450-1461.
- [16] A. Carrero, J. A. Calles, A. J. Vizcaino, *Appl. Catal. A: Gen.* 327 (2007) 82-94.
- [17] C. H. Bartholomew, *Appl. Catal. A: Gen.* 212 (2001) 17-60.
- [18] Y. H. Hu, E. Ruckenstein, *Adv. Catal.* 48 (2004) 297-345.
- [19] J. R. Rostrup-Nielsen, *Adv. Catal.* 47 (2002) 65-139.

- [20] Y. Li, B.C. Zhang, X. W. Xie, J. L. Liu, Y. D. Xu, W. J. Shen, *J. Catal.* 238 (2006) 412-424.
- [21] L. Dussault, J. C. Dupin, C. Guimon, M. Monthieux, N. Latorre, T. Ubieta, E. Romeo, C. Royo, A. Monzon, *J. Catal.* 251 (2007) 223-232.
- [22] S. Freni, S. Cavallaro, N. Mondello, L. Spadaro, F. Frusteri, *Catal. Commun.* 4 (2003) 259-268.
- [23] Y. Yang, J. Ma, F. Wu, *Int. J. Hydrogen Energy* 31 (2006) 877-882.
- [24] P. Biswas, D. Kunzru, *Chem. Eng. J.* 36 (2008) 41-49.
- [25] F. Frusteri, S. Freni, V. Chiodo, L. Spadaro, O. Di Blasi, G. Bonura, S. Cavallaro, *Appl. Catal. A: Gen.* 270 (2004) 1-7.
- [26] F. Frusteri, S. Freni, V. Chiodo, L. Spadaro, G. Bonura, S. Cavallaro, *J. Power Sources* 132 (2004) 139-144.
- [27] Y. Nishiyama, Y. Tamai, *J. Catal.* 33 (1974) 98-107.
- [28] J. L. Chen, Y. D. Li, Y. M. Ma, Y. N. Qin, L. Chang, *Carbon* 39 (2001) 1467-1475.
- [29] H. W. Chen, C. Y. Wang, L. T. Tseng, P. H. Liao, *Catal. Today* 97 (2004) 173-180.

List of Publications

1. **Fagen Wang**, Yong Li, Weijie Cai, Ensheng Zhan, Xiaoling Mu, Wenjie Shen. Steam reforming of ethanol over Ni and Ni–Cu catalysts. *Catalysis Today* 146 (2009) 31-36.
2. **Fagen Wang**, Weijie Cai, H el ene Provendier, Claude Descorme, Yves Schuurman, Claude Mirodatos, Wenjie Shen. Hydrogen production from steam reforming of ethanol over Ir/CeO₂ catalysts: Enhanced stability by PrOx Promotion. *International Journal of Hydrogen Energy* 36 (2011) 13566-13574.
3. **Fagen Wang**, Weijie Cai, Na Ta, H el ene Provendier, Yves Schuurman, Claude Descorme, Claude Mirodatos, Wenjie Shen. Ageing analysis of a model Ir/CeO₂ catalyst in steam reforming of ethanol. *Applied Catalysis B: Environmental* 125 (2012) 546-555.
4. Na Ta, **Fagen Wang**, Huaju Li, Wenjie Shen. Influence of Au particle size on Au/CeO₂ catalysts for CO oxidation. *Catalysis Today* 175 (2011) 541-545.
5. Weijie Cai, **Fagen Wang**, Ceciel Daniel, Andrew C. Veen, Yves Schuurman, Claude Descorme, Helene Provendier, Wenjie Shen, Claude Mirodatos. Oxidative steam reforming of ethanol over Ir/CeO₂ catalysts: a structure sensitivity analysis. *Journal of Catalysis* 286 (2012) 137-152.
6. Weijie Cai, **Fagen Wang**, Andrew. C. Veen, Claude Descorme, Yves Schuurman, Wenjie Shen, Claude Mirodatos. Hydrogen production from steam reforming of ethanol in a micro-channel reactor. *International Journal of Hydrogen Energy* 35 (2010) 1152-1159.
7. Weijie Cai, **Fagen Wang**, Ensheng Zhan, Andrew C. Veen, Claude Mirodatos, Wenjie Shen. Hydrogen production from ethanol over Ir/CeO₂ catalysts: A comparative study of steam reforming, partial oxidation and oxidative steam reforming. *Journal of Catalysis* 257 (2008) 96-107.

8. Weijie Cai, **Fagen Wang**, Andrew C. Veen, H el ene Provendier, Claude Mirodatos, Wenjie Shen. Autothermal reforming of ethanol for hydrogen production over an Rh/CeO₂ catalyst.

Catalysis Today 138 (2008) 152-156.

9. **Fagen Wang**, Weijie Cai, H el ene Provendier, Claude Descorme, Yves Schuurman, Claude Mirodatos, Wenjie Shen. Hydrogen production from steam reforming of ethanol over iridium/ceria catalyst: enhanced stability after praseodymium promotion.

Poster (PT-62), EuropaCat X, Glasgow, UK, 2011.

10. Na Ta, **Fagen Wang**, Juan Li, Wenjie Shen. Influence of CeO₂ morphology on Au nanoparticles for CO oxidation.

Oral (C-O25), 6th ICEC, Beijing, China, 2010.

11. Weijie Cai, Baocai Zhang, **Fagen Wang**, Xiuming Huang, Wenjie Shen. Hydrogen production by reforming of bio-ethanol over Ir/CeO₂ catalysts.

Oral, Post-conference of 14th ICC, Gyeongju, Korea, 2008.

12. Na Ta, **Fagen Wang**, Juan Li, Wenjie Shen. Influence of CeO₂ morphology on Au nanoparticles for CO oxidation.

Oral, TOCAT6/APCAT5, Tokoy, Japan, 2010.

13. Weijie Cai, **Fagen Wang**, Ensheng Zhan, Wenjie Shen, Claude Mirodatos, Andrew C. Veen, H el ene Provendier. Hydrogen production via oxidative steam reforming over Ir/CeO₂ catalysts: influence of particle sizes.

Poster (P106), NGCS-9, Lyon, France, 2010.

14. **Fagen Wang**, Weijie Cai, Ta Na, Wenjie Shen, Claude Mirodatos, H el ene Provendier. Hydrogen production from steam reforming of ethanol over Ir supported on CeO₂ nanorods catalyst.

Poster (PC-005), 15NCC, Guangzhou, China, 2010.

15. **Fagen Wang**, Weijie Cai, Ensheng Zhan, Wenjie Shen. Hydrogen production from steam reforming of ethanol over unsupported Ni catalyst.

Poster (P396), 14NCC, Nanjing, China, 2008.

Acknowledgements

As the thesis is finally finished, I would like to give my honest appreciation to all the people who helped me made the success of this scientific project and give me wonderful and unforgettable memory. This work has been started from September 2008 to June 2012 in the French and Chinese collaborating laboratories of Institut de Recherches sur la Catalyse et l'Environnement de Lyon (IRCELYON/CNRS, Villeurbanne, France) and Dalian Institute of Chemical Physics, Chinese Academy of Sciences (DICP/CAS, Dalian, China).

Professor Claude Mirodatos, Director of Engineering and Process Intensification Group at IRCELYON, Dr. Yves Schuurman, Dr. Claude Descorme and Dr. H el ene Provendier welcomed me warmly and supported me so much during my stay in France. Professor C. Mirodatos designed all the work and reviewed the whole thesis, giving much meaningful suggestions. Dr. Yves Schuurman, Dr. Claude Descorme and Dr. H el ene Provendier revised the chapters of the thesis. I am eager to appreciate them for their intellectual support and valuable suggestions to make the thesis possible. Their kindness, hospitality, enthusiasm, guidance and suggestion were inevitable for the thesis.

Professor Wenjie Shen, Director of Catalytic Reaction Chemistry Group at DICP, who led me into the world of catalysis chemistry, taught me the first view of research and introduced me the concept and method to how to make a successful research. His guidance, broad-mindedness and professional qualities have been of fundamentals for the whole thesis. I also gave my thankfulness to him to give me the opportunity to study abroad, which widens my field of vision.

I also express my deepest gratitude and thanks to my colleagues who are in DICP of China and IRCELYON of France. They gave me a lot of instructions and technique support during my experiments, and we became friends in daily lives.

I also wish to express my appreciation to all the facilities in the IRCELYON, Claude Bernard University in France and in DICP in China for the catalyst characterizations.

I gratefully acknowledge the Embassy of France in Beijing and the French government for the joint PhD scholarship to support me study in France, without which the thesis is impossible.

Acknowledgements

Finally, I would like to give my deepest thanking to my wife Yan Xu, who supports my study during the PhD candidate period and encouraged me all the time. I am willing to give her my promise that I would love her forever.

Thanks all, and may the happy lives with you all!

RESUME en français

Ce travail rapporte l'étude des processus de désactivation et des modifications d'un catalyseur Ir supporté sur cérine en vaporeformage de l'éthanol. Différentes causes de désactivation ont été identifiées selon les conditions opératoires : température, temps de contact et temps de réaction. La désactivation initiale, rapide mais limitée a été attribuée à la restructuration de surface de la cérine et à la formation d'une monocouche d'intermédiaires de type acetate, carbonate et hydroxylys. En parallèle, une désactivation lente et progressive a été mise en évidence, ayant pour origine les changements structurels de l'interface entre la cérine et l'iridium, liés au frittage des particules d'iridium et à la restructuration profonde de la cérine. Par contre, la formation continue, à température modérée, d'une couche de carbone encapsulant issu de la polymérisation d'intermédiaires C2 n'a pas semblé contribuer significativement à la désactivation du catalyseur dans nos conditions opératoires. Pour limiter ce phénomène de désactivation, des modifications ont été apportées au catalyseur. Le dopage du catalyseur par PrO_x a permis de fortement améliorer la capacité de stockage de l'oxygène et la stabilité thermique du catalyseur, entraînant une augmentation de son activité et de sa stabilité en vaporeformage de l'éthanol. Le catalyseur Ir/ CeO_2 a ensuite subi une mise en forme de la cérine (nano-tubes), avec une influence significative sur l'activité et la stabilité en vaporeformage de l'éthanol, liée à des effets structuraux. Une modélisation simplifiée de ces divers phénomènes a également contribué à soutenir les propositions originales de ce travail.

TITRE en anglais : "Hydrogen production from steam reforming of ethanol over an Ir/ceria-based catalyst: catalyst ageing analysis and performance improvement upon ceria doping"

RESUME en anglais

The objective of the thesis was to analyze the ageing processes and the modifications of an Ir/ CeO_2 catalyst for steam reforming of ethanol. Over a model Ir/ CeO_2 catalyst, the initial and fast deactivation was ascribed to ceria surface restructuring and the build-up of intermediates monolayer (acetate, carbonate and hydroxyl groups). In parallel, a progressive and slow deactivation was found to come from the structural changes at the ceria/Ir interface linked to Ir sintering and ceria restructuring. The encapsulating carbon, coming from C_2 intermediates polymerization, did not seem too detrimental to the activity in the investigated operating conditions. By doping ceria with PrO_x , the oxygen storage capacity and thermal stability were greatly promoted, resulting in the enhanced activity and stability. The Ir/ CeO_2 catalyst was then modified by changing the shape of ceria. It was found that the shape and therefore the structure of ceria influenced the activity and stability significantly. A simplified modeling of these processes has contributed to support the new proposals of this work.

DISCIPLINE : Catalyse

MOTS-CLES : Vaporeformage de l'éthanol, Ir/ CeO_2 , désactivation catalytique, frittage des particules d'Ir, restructuration de la cérine

Steam reforming of ethanol, catalyst deactivation, Ir sintering, ceria restructuring, carbon deposition

INTITULE ET ADRESSE DE L'U.F.R. OU DU LABORATOIRE :

IRCELYON, 2 avenue Albert Einstein, 69626 Villeurbanne Cedex